In silico insights into the effect of mutation on peramivir resistance against influenza H7N9 virus and the development of potential inhibitors

by

Sphamandla Enock Mtambo

Dissertation in fulfilment of the requirement for the degree

Doctor of Philosophy

in

Pharmaceutics

at

University of KwaZulu-Natal
Discipline of Pharmaceutical Sciences
Collage of Health Sciences

Supervisor: Dr. H.M. Kumalo

2022

In silico insights into the effect of mutation on peramivir resistance against influenza H7N9 virus and the development of potential inhibitors

by

Sphamandla Enock Mtambo

209505023

2022

A thesis submitted to the College of Health Sciences, University of KwaZulu-Natal, Westville, in fulfilment of the requirements of the degree of

Doctor of Philosophy

in

Pharmaceutical Chemistry

This is the thesis in which the chapters are written as a set of discrete submitted manuscripts, with an overall introduction and final summary. In most cases, these chapters will have been published in reputable, internationally recognized, peer-reviewed journals.

This is to certify that the contents of this thesis are the original research work of **Sphamandla Enock Mtambo**. As the candidate's supervisor, I have approved this thesis for submission.

Signed: Name: Dr. H.M. Kumalo Date: 03/10/22

DECLARATIONS

DECLARATION 1 - PLAGIARISM

I, **Mr Sphamandla Enock Mtambo** declare that

1. The research reported in this thesis, except where otherwise indicated, is my original research.
2. This thesis has not been submitted for any degree or examination at any other university.
3. This thesis does not contain other persons' data, pictures, graphs, or other information, unless specifically acknowledged as being sourced from other persons.
4. This thesis does not contain other persons' writing, unless specifically acknowledged as being sourced from other researchers. Where other written sources have been quoted, then:
   a. Their words have been re-written, but the general information attributed to them has been referenced
   b. Where their exact words have been used, then their writing has been placed in italics and inside quotation marks and referenced.
5. This thesis does not contain text, graphics or tables copied and pasted from the Internet, unless specifically acknowledged, and the source being detailed in the thesis and in the References sections.

Signed:  Name: Mr. S.E. Mtambo Date: 28/10/22

DECLARATIONS

DECLARATION 2 - PUBLICATIONS

Publicaion 1

Mtambo, S.E.; Amoako, D.G.; Somboro, A.M.; Agoni, C.; Lawal, M.M.; Gumede, N.S.; Khan, R.B.; Kumalo, H.M. Influenza Viruses: Harnessing the Crucial Role of the M2 Ion-Channel and Neuraminidase toward Inhibitor Design. *Molecules* **2021**, 26, 880, https://doi.org/10.3390/molecules26040880.

Contributions:
Mtambo, S.E: Conceptualization, data curation, formal analysis, investigation, project administration, visualization, original draft writing, review, and editing.
Amoako, D.G: Assisted in data curation, review, and editing.
Somboro, A.M: Assisted in data curation, review, and editing.
Agoni, C: Contributed to the manuscript writing and proof reading.
Lawal, M.M: Assisted in data curation, review, and editing.
Gumede, N.S: Assisted in review, and editing.
Khan, R.B: Assisted in review, and editing.
Kumalo, H.M: Supervision.

Publication 2

Mtambo, S.E.; Ugbaja,S.C.; Kumalo, H.M. Impact of the R292K Mutation on Influenza A (H7N9) Virus Resistance Towards Peramivir: A Molecular Dynamics Perspective. *Molecules* **2022**, 27, 1645, https://doi.org/10.3390/molecules27051645.

Contributions:
Mtambo, S.E: Conceptualization, data curation, formal analysis, investigation, project administration, visualization, original draft writing, review, and editing.
Ugbaja,S.C: Assisted in conceptualization, review, and editing.
Kumalo, H.M: Supervision.

Publication 3

Mtambo, S.E.; Ugbaja,S.C.; Mushebenge, A.G.; Abubakar, B.H.; Ntuli, M.L.; Kumalo, H.M. Intermolecular Mechanism and Dynamic Investigation of Avian Influenza H7N9 Virus Susceptibility to E119V Substituted Peramivir-Neuraminidase Complex. *Molecules,* **2022**, 27, 1640; https://doi.org/10.3390/molecules27051640.

Contributions:
Mtambo, S.E: Conceptualization, data curation, formal analysis, investigation, project administration, visualization, original draft writing, review, and editing.
Ugbaja,S.C: Assisted in conceptualization, review, and editing.
Mushebenge, A.G: Assisted in data curation, review, and editing.
Abubakar, B.H: Assisted in review, and editing.
Ntuli, M.L: Assisted in data curation, review, and editing.
Kumalo, H.M: Supervision.

Publication 4

Mtambo, S.E.; Kumalo, H.M. *In silico* drug repurposing of FDA-approved drugs highlighting promacta as a potential inhibitor of H7N9 influenza virus. *Molecules* **2022**, 27, x, https://doi.org/10.3390/xxxxx.

Contributions:
Mtambo, S.E: Conceptualization, data curation, formal analysis, investigation, project administration, visualization, original draft writing, review, and editing.
Kumalo, H.M: Supervision.

Signed: [redacted] Name: Mr. S.E. Mtambo Date: 28/10/22

DEDICATION

This dissertation is dedicated to my family.

ACKNOWLEDGEMENTS

I wish to express my sincere gratitude and appreciation to the following persons and institutions:

All thanks to the creator of the universe for giving me the strength and courage to successfully finish this journey.

Sincere gratitude to my supervisor, **Dr. H.M. Kumalo**, who has believed in me for his support, guidance, and patience throughout this journey. You have granted me the opportunity to learn many skills and equipped me with valuable tools I will need as a young researcher, I will forever be grateful.

My appreciation also goes to Drug Research and Innovation Unit (DRIU) for their support.

Profound gratitude goes to Centre for High Performance Computing, South Africa for their resources and technical support.

My beloved family, thank you.

To the friends **(Njabulo Nene, Khulekani Khumalo, Lethukuthula Ngobese, Gcinokwakhe Ngcobo, Sifiso Makhathini, Ramesh Ganimani, Siyabonga Sibiya, Samuel Ugbaja**) I made along this journey that have positively contributed to my progress at one stage or another, I am eternally grateful.

ABSTRACT

Influenza A virus infections causes substantial population illness with consequent healthcare and economic problems. There has been an outbreak of novel influenza A (H7N9) virus strains on the Chinese mainland as of March 2013. As a result of their fast geographical spread and genomic variety, the ongoing circulation of H7N9 virus poses a pandemic threat. At present, available anti-influenza drugs are mainly directed at the viral M2 ion-channel (amantadine and rimantadine), neuraminidase (oseltamivir, zanamivir, laninamivir, and peramivir), or polymerase (baloxavir marboxil), and emerging anti-viral resistance against these inhibitors is a concern. The development of safe and effective anti-influenza drugs is essential to a balanced strategy against seasonal influenza. The use of computational approaches for designing and developing new anti-influenza drugs has proven beneficial in response to resistance to current therapies.

The use of computer-aided drug design (CADD) is crucial to the development of novel drugs. It has been shown over the years that CADD plays a vital role in the drug design process, accelerating the discovery of possible drug candidates at a lower cost. CADD approaches are able to investigate protein-ligand interactions at the atomic level, which provides insights that can be used to improve drug design. As a result, the studies presented in this thesis employed CADD approaches in order to explore molecular mechanisms of action of new therapeutic approaches designed to combat H7N9 viral infections. The aim of this study was to offer an in-depth understanding of the effect of H7N9 mutation on neuraminidase inhibitor resistance and discover the fundamentals for the design and development of more potent anti-viral drugs.

Clinical studies demonstrated that the peramivir resistance to extremely pathogenic influenza H7N9 viruses is caused R292K mutation. As such, we used numerous molecular dynamics methods to assess the effect of neuraminidase-R292K mutation towards peramivir resistance in influenza H7N9 viruses. We found that a R292K mutation caused peramivir orientation to be altered in the binding site of the peramivir-R292 mutant complex, consequently hampering the mutant's ability to bind peramivir. In contrast to its wildtype counterpart, R292K mutant decreased the interaction between neighboring amino acid residues, as evidenced by a high degree of flexibility in the radius of gyration. The mutation altered hydrogen bond-mediated interactions with peramivir and resulted in a greater accessibility of water molecules nearby the K292 mutated amino acid residue. Based on the energy binding calculations, it was determined that the R292K mutation caused a reduction of 17.28 kcal/mol in the peramivir binding affinity compared to the peramivir-wildtype complex. As a result, the peramivir was oriented differently in the binding site and the overall conformation of the peramivir-mutant complex changed.

Experimental investigations have been conducted into the mutation of E119 in neuraminidase. Contrary to this, there is insufficient information regarding the impact of E119V mutation towards peramivir at the intermolecular level. Therefore, a thorough understanding of the protein-ligand intermolecular interactions is crucial to understanding its inhibition. In the present study, we explored the intermolecular mechanism and dynamics associated with the susceptibility of peramivir to influenza H7N9 virus containing E119V mutation. We utilized molecular dynamic simulations and a wide range of post-molecular dynamic analysis for comprehensive insights into the impact of the E119V mutation and the conformational of the peramivir-E119V mutant complex. Based on the post-molecular dynamic analysis, the peramivir-E119V mutant complex showed relative stability. For the peramivir-wildtype complex, the calculated binding free energy (ΔG_{bind}) is -49.09 ± 0.13 kcal/mol, while for E119V mutant it is -58.55 ± 0.15 kcal/mol. The increase in binding free energy by 9.46 kcal / mol is in accordance with other post-molecular dynamic analyses, which found that the E119V mutation increases protein stability. These findings could play a crucial role in developing new anti-influenza drugs and controlling the avian influenza H7N9 virus.

New and re-emerging diseases like influenza are challenging to treat due to the lengthy development process and high failure rate. To develop potential therapies against the H7N9 virus, we repurposed FDA-approved drugs using an *in silico* drug repurposing method. A total of 2,568 drugs were screened for potential inhibitors. A DrugBank database virtual screening identified the compounds promacta, tucitanib, and lurasidone as promising hits. The calculations of MM-GBSA suggest that tucitanib (-54.1 kcal/mol) and promacta (-56.2 kcal/mol) occupy the active site of neuraminidase with a higher binding affinity than the standard drug peramivir (-49.09 kcal/ mol). Based on the results of Molecular dynamics (MD) simulation, the C-α atom backbones of the complexes of tucatinib and promacta neuraminidase remained stable during the simulation time. Absorption, distribution, metabolism, and excretion (ADME) analysis revealed that the hit compounds have a high gastrointestinal absorption (GI) and lack properties that allow them to cross the blood-brain barrier (BBB). Based on the *in silico* toxicity prediction, promacta is not cardiotoxic, while lurasidone and tucatinib are only weakly inhibitory. We, therefore, propose to test these compounds experimentally against influenza H7N9. To bring these compounds to clinical settings, further investigation, and validation of these potential H7N9 inhibitors are necessary.

In summary, this study has established that the R292K mutation decreases peramivir binding affinity and distorts peramivir optimum position in the binding site of neuraminidase. In contrast, the E119V mutation contributed to relative stability of the peramivir-neuraminidase complex. Promacta and tucatinib could be used as lead compounds to combat the H7N9 influenza virus. Insights gained from this study will enhance future drug development and help in combating the avian influenza H7N9 virus. Nonetheless, the concept of multi-target drugs, quantum mechanics (QM) method such as density functional theory (DFT) and hybrid quantum mechanics/molecular mechanics (QM/MM) for effective design of neuraminidase inhibitors should be widely explored.

PREFACE

This dissertation is presented as a compilation of 7 chapters.

Chapter 1	**Introduction**
Chapter 2	**Influenza Viruses: Harnessing the Crucial Role of The M2 Ion-Channel and Neuraminidase toward Inhibitor Design**
Chapter 3	**Computational Methods**
Chapter 4	**Impact of the R292K Mutation on Influenza A (H7N9) Virus Resistance Towards Peramivir: Molecular Dynamics Perspective**
Chapter 5	**Intermolecular Mechanism and Dynamic Investigation of Avian Influenza H7N9 Virus Susceptibility to E119V Substituted Peramivir-Neuraminidase Complex**
Chapter 6	***In silico* drug repurposing of FDA-approved drugs highlighting promacta as a potential inhibitor of H7N9 influenza virus**
Chapter 7	**Conclusion**

CONTENTS

LIST OF ABBREVIATIONS

3D	Three dimensional
Å	Angstrom (10^{-10} m)
ADMET	Absorption, distribution, metabolism, and excretion
AM2	Influenza A M2
BBB	Blood-brain barrier
CADD	Computer assisted drug discovery
cRNA	Complementary ribonucleic acid
DANA	Dehydrodeoxy-N-acetylneuraminic acid
ER	Endoplasmic reticulum
FDA	Food and drug administration
GAFF	General Amber force Field
GI	Gastrointestinal absorption
HA	Haemagglutinin
HEF	Hemagglutinin-esterase-fusion
IV	Influenza virus
IAV	Influenza A virus
IBV	Influenza B virus
ICV	Influenza C virus
LBHB	Low-barrier hydrogen bond
M1	Matrix protein 1
M2	Matrix protein 2
MD	Molecular dynamics
MM/GBSA	Molecular Mechanics/Generalized Born Surface Area
NA	Neuraminidase
MTOC	Microtubule-organizing centre
NEP	Nuclear export protein
NMR	Nuclear Magnetic Resonance Spectroscopy
NS1	Non-structural protein 1
PA	polymerase A protein
PB1	polymerase B1 protein
PB2	polymerase B2 protein
PCA	Principal Component Analysis
PDB	Protein Data Bank
QM	Quantum Mechanics
QM/MM	Hybrid Quantum Mechanics/Molecular Mechanics

RoG	Radius of gyration
RMSD	Root mean square deviation
RMSF	Root mean square fluctuation
RNA	Ribonucleic acid
RNP	Ribonucleoprotein
RdRp	RNA-dependent RNA polymerase
SASA	Solvent Accessible Solvent Area
TM	Transmembrane
TMD	Transmembrane domain
vRNP	Ribonucleoprotein
VDW	van der Waals

LIST OF FIGURES

LIST OF TABLES

Chapter 1

INTRODUCTION

1. INTRODUCTION

1.1 PREFACE

This chapter provides a brief background to the study and highlights the status of the influenza virus, limitations associated with anti-influenza therapy, and the emergence of anti-viral resistance. Furthermore, it provides details on alternative strategic solutions to enhance anti-influenza therapy, which resulted in the proposed aims and objectives of the study.

1.2 BACKGROUND TO THE STUDY

The influenza virus is notoriously recognised for its exclusive capability to cause recurring epidemics and pandemics where people of all ages suffer acute respiratory illness [1–3]. The ability of the virus to emerge and circulate in reservoirs such as an avian or porcine species through genetic reassortment or direct transmission and then irregularly spread to humans accounts for the epidemiological spread of the virus [4–6]. The fast and random antigenic change and immune invasion as soon as a human has become infected by the virus also contribute to the spread of influenza [7].

The influenza virus has infected human population as of the 16th century causing repeated epidemics of respiratory illness [8]. The emergence of a new virus that the general population is not immune to may also result in rapid pandemic spread to all parts of the globe [9,10]. The features of pandemics incorporate prevalence separate of the typical season, tremendously fast transmission with simultaneous outbreaks worldwide, and high attack rates across all ages with high death rates even in young, healthy individuals [1].

The years 1889, 1918, 1957, and 1968 saw four global pandemics during the 19th and 20th centuries. Informally classified as Russian, Spanish, Asian, and Hong Kong influenzas, respectively. They are, respectively, H1N1, H2N2, H3N2, and H1N1, three distinct antigenic subtypes of the influenza A virus [11]. In 2009, an epidemic was brought on by a strain of swine influenza A related to domestic swine influenza [12]. Coronavirus, the primary culprit behind the current pandemic, was discovered to be the source of severe acute respiratory syndrome Coronavirus 2 (SARS-CoV-2) in 2019 [13].

The human influenza virus is part of the *Orthomyxoviridae* family [5]. It includes influenza A, B, and C viruses. Among human influenza viruses, only influenza A and B cause acute infection and immense seasonal epidemics because they spread and cause acute infection [5]. In contrast, the influenza C virus is associated with mild illnesses. Haemagglutinin (HA) and neuraminidase (NA) glycoproteins are the primary influenza A and B virus epitopes [7,14].

New influenza A and B virus strains emerge through a mechanism called an antigenic alteration of HA and NA antigens. Influenza A and B viruses exhibit smaller alterations in antigenic composition called antigenic drift that cause epidemics [5,7]. A pandemic of influenza occurs irregularly and unpredictably and is due to a major antigenic alteration occurring only in influenza A, called antigenic shift (Figure 1). Influenza viruses can be spread by aquatic birds because they host several subtypes of the influenza A virus [14].

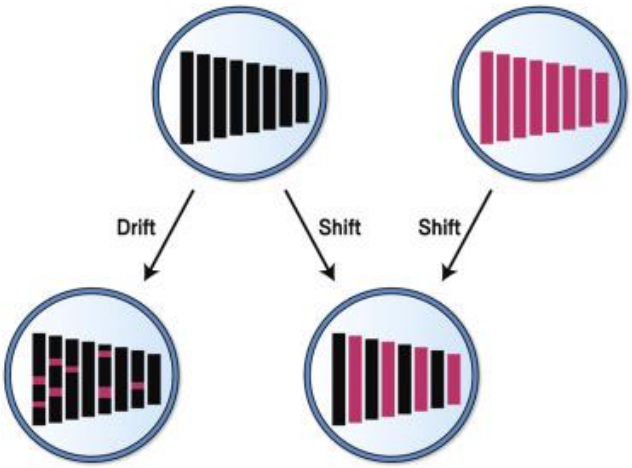

Figure1: Antigenic drift and antigenic shift. Antigenic drift: the pink color highlights mutations in the RNA genome. Antigenic shift: different colours represent antigenic differences between two strains [15].

An antigenic shift arises when a new influenza A virus evolves by encoding a different haemagglutinin gene from that which is present in an avian influenza. It might be achieved by adapting an avian virus to make it transmittable among humans [2,16]. Humans are more likely to be infected by the H5 and H7 subtypes of avian influenza if they are introduced into domestic poultry [17,18].

Avian influenza A (H7N9) virus infection in the human population emerged in East China in March 2013 [19]. Since that time, it has infected a total of 1565 humans and killed approximately 39 percent of people infected with Asian H7N9 virus [19,20]. Influenza A (H7N9) virus infection in humans has been linked with pneumonia and acute respiratory distress syndrome with high mortality rates [21,22]. NA catalyzes the breakage of α-(2-3 or 2-6)-ketosidic connection amongst terminal sialic acid and adjacent surface glycoprotein. Moreover, this promotes the budding of relatively new viral particles from the infected cell. Consequently, progeny viruses are released, infecting uninfected host cells and spreading infection to respiratory tract mucins [7,23].

The influenza virus attaches to the sialic acid found on the surface glycoprotein of the host cell by using HA. The HA proteins of avian viruses are specifically designed to recognize an α-2,3-linkage found on epithelial cells of duck intestines. Whereas the HA proteins of human viruses have an affinity for the sialic acid connected to galactose through an α-2,6-linkage found on the surface of human respiratory epithelial cells [24–28]. The A (H7N9) virus demonstrates a greater affinity for the human α-2,6-linked sialic acid host cell receptor, whilst demonstrating a reduced affinity for the avian α-2,3-linked sialic acid host cell receptor [29]. Serological studies indicate that no human population has pre-existing immunity towards H7 subtype influenza viruses [25,30]. Thus, the A (H7N9) virus is concerning as a probable pandemic source and should continue to be monitored, and more potent anti-influenza drugs should be developed.

The number of existing anti-influenza drugs is restricted to those targeting the M2 ion-channel (amantadine and rimantadine), neuraminidase (oseltamivir, zanamivir, laninamivir, and peramivir), or polymerase (baloxavir marboxil), and emerging anti-viral resistance against these

inhibitors is a problem [7,16]. It is therefore important to develop safe and effective anti-viral drugs as a component of the balanced strategy to dealing seasonal influenza and is vital in response to new outbreaks of strains caused by seasonal and pandemic influenza. The active site of NA forms a pocket composed of 19 highly conserved amino acid residues [7,23,31]. If amino acid residues at the conserved amino acid sites of the NA active site are mutated, the susceptibility to NA inhibitors may be altered, affecting the therapeutic properties of the inhibitors.

Computer-aided drug design (CADD) is very important in the exploration of potential novel drugs. CADD forms an integral portion of the research approach known as structure-based design, which is a composition of experimental and computational approaches [32,33]. CADD has gained substantial attention as a complementary tool for finding new drug leads, understanding disease mechanisms, and drug-target interaction. Computational approaches critically reduce the costs of preclinical and clinical studies by reducing the time and resources required for chemical synthesis and biological testing [34].

The application of computational methods in the development of probable novel therapeutic agents has proven to possess the ability to significantly address the anti-influenza drug resistance [34]. Understanding the binding interactions of a ligand and a receptor is of high interest since it can provide critical information to study structural changes in the binding site. The study of antiviral resistance to peramivir by mutants such as R292K and E119V using computational tools is paramount to effectively understand the mechanisms of drug resistance and to further predict potential drug resistance.

1.3 NOVELTY AND SIGNIFICANCE OF THE STUDY

Both influenza A and B viruses are susceptible to NA inhibitors. They inhibit NA from breaking down the sialic acid, allowing budding viral particles to stay connected to the surface of the infected cell. As a result, an infection is suppressed to just one replication cycle. The active site forms a pocket composed of 19 highly conserved amino acid residues in IAV and IBV. The inner cavity contains 8 highly conserved enzymatic residues (Arg118, Asp151, Arg152, Arg224, Glu276, Arg292, Arg371, and Tyr406) (N2 numbering) that interact directly with sialic acids responsible for the enzymatic activity. In addition, the rim comprises of 11 extremely conserved framework residues (Glu119, Arg156, Trp178, Ser179, Asp (or Asn in N7 and N9) 198, Ile222, Glu227, His274, Glu277, Asp294, and Glu425) that stabilizes the enzymatic binding pocket [7,23,31]. A nucleotide alteration in the NA gene confers resistance to NA inhibitors in the enzyme's binding site.

In this study, key insights will be gained into the mechanisms of resistance and the susceptibilities of pathogenic H7N9 virus to current anti-viral treatment such as peramivir. The employment of computational approaches might provide a clear outlook to understand R292K and E119V mutant resistance to peramivir against H7N9 virus. With the use CADD techniques, an impact of a single point mutation on pathogenic H7N9 in influenza neuraminidase to NA inhibitors is offered. Understanding the molecular mechanism behind mutation-induced drug resistance in neuraminidase N9 subtype is critical for the optimal design of anti-influenza agents. Virtual screening is one of the most promising *in silico* approaches for drug design and

development. The use of a molecular docking-based virtual screening approach to perform in silico repurposing of FDA-approved drugs against the influenza A (H7N9) virus is beneficial for reducing drug development costs and time. The study will characterize amino acid residues involved in protein-ligand interactions. A detailed understanding of the binding landscape will facilitate the development of unique and selective inhibitors with critical pharmacophore features.

1.4 STUDY AIMS AND OBJECTIVES

The main aim of this study was to provide an extensive understanding of the impact of pathogenic H7N9 mutation on the resistance of neuraminidase inhibitors and explore the basis for the design of more effective anti-influenza drugs. The specific aims and objectives of this study are highlighted below.

1. The aim was to provide an extensive review on the vital function of the M2 ion-channel and neuraminidase protein for inhibitor design. The main objectives are as follows:
   1.1 Highlight the latest studies on the bio-molecular fundaments of influenza viruses, with emphasis on the structure, function, and mechanisms of action of the M2-ion channel and neuraminidase as possible targets for anti-viral drugs.
   1.2 Outline the progress made in the development of anti-viral treatments that target M2-ion channel and neuraminidase as alternatives to current anti-viral drugs.
   1.3 Identify possible therapeutic approaches for designing new anti-viral inhibitors that would be able to inhibit resistant strains of influenza.

2. The aim was to provide an extensive and detailed understanding of the impact of R292K mutation on peramivir resistance towards H7N9 and provide additional dimensions to the existing experimental work. The main objectives of this study are as follows:
   2.1 Investigate the intermolecular dynamics on the susceptibility of peramivir to R292K mutant.
   2.2 Evaluate the effect of R292K mutation on peramivir binding affinity and the conformation of peramivir-R292K mutant complex.
   2.3 Identify and characterize amino acid residues responsible for the impact on the active site.

3. The aim of this study was to computationally investigate the intermolecular mechanisms of E119V substituted NA on peramivir. The main objectives of this research study are as follows:
   3.1 Investigate the effects of this mutation on the binding affinity and the conformational terrain of peramivir-neuraminidase E119V mutation.
   3.2 Examine the mechanism and dynamism of the susceptibility of the E119V mutation on the peramivir-neuraminidase complex relative to the wild-type complex at the intermolecular level.
   3.3 To offer contributory insight and additional knowledge that would enhance future drug designs and help in the fight targeted at controlling the avian influenza H7N9 virus.

4. The aim of this study was to conduct a virtual screening investigation using molecular docking to perform repurposing of FDA-approved drugs against influenza A (H7N9) virus. The main objectives of this study are as follows:
   4.1 Perform an *in silico*-based drug repurposing method to repurpose FDA-approved drugs to find potential influenza H7N9 virus inhibitors.
   4.2 Investigate the stability of hit compounds complexed with viral NA using molecular dynamics simulation.
   4.3 Predict the pharmacokinetic and toxicological properties of the hit compounds.

1.5 THESIS OVERVIEW

This dissertation encompasses six chapters, including this one:

Chapter 1, Introduction:
Outlines the background to the study, aims and objectives of the study, the impact of the research and structure of the thesis.

Chapter 2, Literature Review:
Presents the importance of M2 ion-channel and neuraminidase with regards to anti-influenza drug design. The paper is titled "Influenza Viruses: Harnessing the Crucial Role of the M2 Ion-Channel and Neuraminidase toward Inhibitor Design". Published in Molecules (Impact Factor 4.412).

Chapter 3, Computational Methods:
Highlights the specific principles of computer simulations employed in this study.

Chapter 4, Research Article:
Studies the impact of R292K mutation on peramivir resistance towards H7N9. The paper is titled "The impact of R292K mutation on peramivir resistance towards influenza A (H7N9) virus: molecular dynamics perspective". Published in Molecules (Impact Factor 4.412).

Chapter 5, Research Article:
Reports on the effect of E119V mutation on peramivir resistance on pathogenic influenza A (H7N9). The paper is title "Intermolecular mechanism and dynamic investigation of avian influenza H7N9 virus susceptibility to E119V substituted peramivir-neuraminidase complex". Published in Molecules (Impact Factor 4.412).

Chapter 6, Research Article:
Reports on the *in silico* repurposing of FDA-approved drugs against the H7N9 influenza virus. The paper is title "*In silico* drug repurposing of FDA-approved drugs highlighting promacta as a potential inhibitor of H7N9 influenza virus" Submitted for Publication in Molecules (Impact Factor 4.412).

Chapter 6, Conclusion:
Comprises of general conclusion as well as recommendations.

1.6 REFERENCES

1. Knobler, S.L.; Mack, A.; Mahmoud, A.; Lemon, S.M. *The Threat of Pandemic Influenza: Are We Ready?*; 2005; ISBN 0-309-54685-0.

2. Peiris, J.S.M.; De Jong, M.D.; Guan, Y. Avian influenza virus (H5N1): A threat to human health. *Clin. Microbiol. Rev.* **2007**, *20*, 243–267, doi:10.1128/CMR.00037-06/ASSET/DA9595D2-D46A-41D9-98E1-1FCF84E42BDA/ASSETS/GRAPHIC/ZCM0020722060004.JPEG.

3. Harrington, W.N.; Kackos, C.M.; Webby, R.J. The evolution and future of influenza pandemic preparedness. *Exp. Mol. Med. 2021 535* **2021**, *53*, 737–749, doi:10.1038/s12276-021-00603-0.

4. Ma, W.; Kahn, R.E.; Richt, J.A. The pig as a mixing vessel for influenza viruses: Human and veterinary implications. *J. Mol. Genet. Med.* **2009**, *3*, 158–166.

5. Horimoto, T.; Kawaoka, Y. Influenza: Lessons from the past pandemics, warnings from current incidents. *Nat. Rev. Microbiol. Vol.* **2005**, *3*, 591–600, doi:10.1038/nrmicro1208.

6. Priyadarsini, S.L.; Suresh, M.; Huisingh, D. What can we learn from previous pandemics to reduce the frequency of emerging infectious diseases like COVID-19? *Glob. Transitions* **2020**, *2*, 202–220, doi:10.1016/J.GLT.2020.09.003.

7. Mtambo, S.E.; Amoako, D.G.; Somboro, A.M.; Agoni, C.; Lawal, M.M.; Gumede, N.S.; Khan, R.B.; Kumalo, H.M. Influenza Viruses: Harnessing the Crucial Role of the M2 Ion-Channel and Neuraminidase toward Inhibitor Design. *Molecules* **2021**, *26*, 880, doi:10.3390/molecules26040880.

8. Taubenberger, J.K.; Morens, D.M. 1918 Influenza: the Mother of All Pandemics. *Emerg. Infect. Dis.* **2006**, *12*, 15, doi:10.3201/EID1201.050979.

9. Potter, C.W. A history of influenza. *J. Appl. Microbiol.* **2001**, *91*, 572–579, doi:10.1046/J.1365-2672.2001.01492.X.

10. Piret, J.; Boivin, G. Pandemics Throughout History. *Front. Microbiol.* **2021**, *11*, 3594, doi:10.3389/FMICB.2020.631736/BIBTEX.

11. Kilbourne, E.D. Influenza Pandemics of the 20th Century. *Emerg. Infect. Dis.* **2006**, *12*, 9, doi:10.3201/EID1201.051254.

12. Girard, M.P.; Tam, J.S.; Assossou, O.M.; Kieny, M.P. The 2009 A (H1N1) influenza virus pandemic: A review. *Vaccine* **2010**, *28*, 4895–4902, doi:10.1016/J.VACCINE.2010.05.031.

13. Adil, T.; Rahman, R.; Whitelaw, D.; Jain, V.; Al-Taan, O.; Rashid, F.; Munasinghe, A.; Jambulingam, P. SARS-CoV-2 and the pandemic of COVID-19. *Postgrad. Med. J.* **2021**, *97*, 110–116, doi:10.1136/POSTGRADMEDJ-2020-138386.

14. Long, J.S.; Mistry, B.; Haslam, S.M.; Barclay, W.S. Host and viral determinants of influenza A virus species specificity. *Nat. Rev. Microbiol.* **2019**, *17*, 67–81, doi:10.1038/s41579-018-0115-z.

15. Ryu, W.-S. *Molecular Virology of Human Pathogenic Viruses*; First Edit.; Elsevier, 2016; ISBN 9780128008386.

16. Shao, W.; Li, X.; Ullah Goraya, M.; Wang, S.; Chen, J.-L. Molecular Sciences Evolution of Influenza A Virus by Mutation and Re-Assortment. *Int. J. Mol. Sci.* **2018**, *18*, 1650, doi:10.3390/ijms18081650.

17. Proença-Módena, J.L.; Macedo, I.S.; Arruda, E. H5N1 avian influenza virus: an overview. *Brazilian J. Infect. Dis.* **2007**, *11*, 125–133, doi:10.1590/S1413-86702007000100027.

18. Li, Y.T.; Linster, M.; Mendenhall, I.H.; Su, Y.C.F.; Smith, G.J.D. Avian influenza viruses in humans: lessons from past outbreaks. *Br. Med. Bull.* **2019**, *132*, 81, doi:10.1093/BMB/LDZ036.

19. World Health Organisation (WHO) Analysis of recent scientific information on avian influenza A(H7N9) virus. *https://www.who.int/influenza/human_animal_interface/avian_influenza/riskassessment_AH7N9_201702/en/* **2021**.

20. Gao, R.; Cao, B.; Hu, Y.; Feng, Z.; Wang, D.; Hu, W.; Chen, J.; Jie, Z.; Qiu, H.; Xu, K.; et al. Human Infection with a Novel Avian-Origin Influenza A (H7N9) Virus. *N. Engl. J. Med.* **2013**, *368*, 1888–1897, doi:10.1056/nejmoa1304459.

21. Gao, H.-N.; Lu, H.-Z.; Cao, B.; Du, B.; Shang, H.; Gan, J.-H.; Lu, S.-H.; Yang, Y.-D.; Fang, Q.; Shen, Y.-Z.; et al. Clinical Findings in 111 Cases of Influenza A (H7N9) Virus Infection. *N. Engl. J. Med.* **2013**, *368*, 2277–2285, doi:10.1056/nejmoa1305584.

22. Xiang, N.; Li, X.; Ren, R.; Wang, D.; Zhou, S.; Greene, C.M.; Song, Y.; Zhou, L.; Yang, L.; Davis, C.T.; et al. Assessing Change in Avian Influenza A(H7N9) Virus Infections During the Fourth Epidemic — China, September 2015–August 2016. *MMWR. Morb. Mortal. Wkly. Rep.* **2016**, *65*, 1390–1394, doi:10.15585/mmwr.mm6549a2.

23. Colman, P.M.; Varghese, J.N.; Laver, W.G. Structure of the catalytic and antigenic sites in influenza virus neuraminidase. *Nature* **1983**, *303*, 41–44, doi:10.1038/303041a0.

24. Watanabe, T.; Kiso, M.; Fukuyama, S.; Nakajima, N.; Imai, M.; Yamada, S.; Murakami, S.; Yamayoshi, S.; Iwatsuki-Horimoto, K.; Sakoda, Y.; et al. Characterization of H7N9 influenza A viruses isolated from humans. *Nature* **2013**, *501*, 551–555, doi:10.1038/nature12392.

25. Zhou, J.; Wang, D.; Gao, R.; Zhao, B.; Song, J.; Qi, X.; Zhang, Y.; Shi, Y.; Yang, L.; Zhu, W.; et al. Biological features of novel avian influenza A (H7N9) virus. *Nature* **2013**, *499*, 500–503, doi:10.1038/nature12379.

26. Tharakaraman, K.; Jayaraman, A.; Raman, R.; Viswanathan, K.; Stebbins, N.W.; Johnson, D.; Shriver, Z.; Sasisekharan, V.; Sasisekharan, R. Glycan-Receptor Binding of the Influenza A Virus H7N9 Hemagglutinin. *NIH Public Access* **2013**, *153*, 1486–93, doi:10.1016/j.cell.2013.05.034.

27. Pitera, J. Expected distributions of root-mean-square positional deviations in proteins. *J. Phys. Chem. B* **2014**, *118*, 6526–6530, doi:10.1021/JP412776D.

28. Wu, L.; Mitake, H.; Kiso, M.; Ito, M.; Iwatsuki-Hirimoto, K.; Yamayoshi, S.; Lopes, T.J.S.; Feng, H.; Sumiyoshi, R.; Shibata, A.; et al. Characterization of H7N9 avian influenza viruses isolated from duck meat products. *Transbound. Emerg. Dis.* **2020**, *67*, 792–798, doi:10.1111/TBED.13398.

29. Xiong, X.; McCauley, J.; Steinhauer, D. Receptor binding properties of the influenza virus hemagglutinin as a determinant of host range. *Curr. Top. Microbiol. Immunol.* **2014**, *385*, 63–91, doi:10.1007/82_2014_423.

30. Bai, T.; Zhou, J.; Shu, Y. Serologic Study for Influenza A (H7N9) among High-Risk Groups in China. *N. Engl. J. Med.* **2013**, *368*, 2339–2340, doi:10.1056/NEJMC1305865.

31. Varghese, J.N.; Colman, P.M. Three-dimensional Structure of the Negraminidase of Influenza Virus A / Tokyo / 3 / 67 at 2-2 A Resolution receptor. *J. Mol. Biol.* **1991**, *221*,

473–486, doi:10.1016/0022-2836(91)80068-6.

32. Usha, T.; Shanmugarajan, D.; Goyal, A.K.; Kumar, C.S.; Middha, S.K. Recent Updates on Computer-aided Drug Discovery: Time for a Paradigm Shift. *Curr. Top. Med. Chem.* **2017**, *17*, 3296–3307, doi:10.2174/1568026618666180101163651.

33. Batool, M.; Ahmad, B.; Choi, S. A Structure-Based Drug Discovery Paradigm. *Int. J. Mol. Sci.* **2019**, *20*, 2783, doi:10.3390/IJMS20112783.

34. Honarparvar, B.; Govender, T.; Maguire, G.E.M.; Soliman, M.E.S.; Kruger, H.G. Integrated approach to structure-based enzymatic drug design: Molecular modeling, spectroscopy, and experimental bioactivity. *Chem. Rev.* **2014**, *114*, 493–537, doi:10.1021/cr300314q.

Chapter 2

LITERATURE REVIEW

molecules

MDPI

Review

Influenza Viruses: Harnessing the Crucial Role of the M2 Ion-Channel and Neuraminidase toward Inhibitor Design

Sphamadla E. Mtambo [1], Daniel G. Amoako [1,2,*], Anou M. Somboro [1,2], Clement Agoni [1], Monsurat M. Lawal [1], Nelisiwe S. Gumede [1], Rene B. Khan [1] and Hezekiel M. Kumalo [1,*]

[1] Drug Research and Innovation Unit, Discipline of Medical Biochemistry, School of Laboratory Medicine and Medical Science, University of KwaZulu-Natal, Durban 4000, South Africa; sphamtambo@gmail.com (S.E.M.); anou.somboro@gmail.com (A.M.S.); clegoni@gmail.com (C.A.); lawalmonsurat635@gmail.com (M.M.L.); gumedenelly0@gmail.com (N.S.G.); myburgr@ukzn.ac.za (R.B.K.)

[2] Centre for Respiratory Diseases and Meningitis, National Institute for Communicable Diseases, Johannesburg 2131, South Africa

* Correspondence: amoakodg@gmail.com (D.G.A.); kumaloh@ukzn.ac.za (H.M.K.); Tel.: +27-084-330-8957 (D.G.A.); +27-031-260-4940 (H.M.K.)

Abstract: As a member of the *Orthomyxoviridae* family of viruses, influenza viruses (IVs) are known causative agents of respiratory infection in vertebrates. They remain a major global threat responsible for the most virulent diseases and global pandemics in humans. The virulence of IVs and the consequential high morbidity and mortality of IV infections are primarily attributed to the high mutation rates in the IVs' genome coupled with the numerous genomic segments, which give rise to antiviral resistant and vaccine evading strains. Current therapeutic options include vaccines and small molecule inhibitors, which therapeutically target various catalytic processes in IVs. However, the periodic emergence of new IV strains necessitates the continuous development of novel anti-influenza therapeutic options. The crux of this review highlights the recent studies on the biology of influenza viruses, focusing on the structure, function, and mechanism of action of the M2 channel and neuraminidase as therapeutic targets. We further provide an update on the development of new M2 channel and neuraminidase inhibitors as an alternative to existing anti-influenza therapy. We conclude by highlighting therapeutic strategies that could be explored further towards the design of novel anti-influenza inhibitors with the ability to inhibit resistant strains.

Keywords: influenza virus; influenza; neuraminidase; M2 channel; antiviral drugs

Citation: Mtambo, S.E.; Amoako, D.G.; Somboro, A.M.; Agoni, C.; Lawal, M.M.; Gumede, N.S.; Khan, R.B.; Kumalo, H.M. Influenza Viruses: Harnessing the Crucial Role of the M2 Ion-Channel and Neuraminidase toward Inhibitor Design. *Molecules* **2021**, *26*, 880. https://doi.org/10.3390/molecules26040880

Academic Editor: Kyoko Nakagawa-Goto

Received: 1 January 2021
Accepted: 1 February 2021
Published: 7 February 2021

1. Introduction

Influenza is a major cause of high morbidity and mortality through seasonal flu and global pandemics [1,2]. Seasonal influenza has resulted in 9–45 million illnesses and 12,000–61,000 deaths annually since 2010 [2,3]. Vaccination and anti-influenza drugs are the main current strategies used to prevent and treat influenza infections [4–7]. Antigenic drift or shift of human influenza viruses can result in new, highly virulent influenza strains that arise unexpectedly to cause new epidemics or worldwide pandemics [8,9]. The influenza virus mutates rapidly, which renders efforts to control the spread of the virus by vaccination inadequate [10,11].

These evolutionary mechanisms of viruses lead to the development of a variety of hybrid influenza viruses with different characteristics when compared to the parental viruses [12,13]. These variations make it difficult to control human influenza outbreaks through vaccination alone, since humans will not have immunity to this new virus subtype, thus increasing the possibilities of seasonal and sporadic pandemics [12–14].

The great Spanish 1918 H1N1 influenza pandemic with genes of avian origin resulted in approximately 50 million deaths in two years [15,16]. During that period, there were no effective vaccines or anti-influenza drugs. Thus, seasonal updates of influenza vaccines

are essential to countermeasure changes in circulating influenza viruses. Even though vaccination is the primary strategy for prevention, in some seasons, protection cannot be rapid enough [17]. As such, the development of effective and safe anti-viral agents forms a significant component in the balanced approach of managing seasonal influenza and is critical for responding to new outbreaks of seasonal and pandemic strains.

Two major classes of anti-viral agents are currently available for treatment or prevention of influenza infections: M2 channel inhibitors, and neuraminidase inhibitors [18,19]. M2 channel inhibitors are only effective against influenza A viruses and are also associated with severe side effects and the emergence of drug resistance [20–22]. Neuraminidase inhibitors are a newer class of anti-influenza agents and they are effective against both influenza A and B viruses. Contrary to M2 channel inhibitors, they are associated with little toxicity and less drug resistance [23,24].

Currently no drug has been discovered that is effective against all influenza virus strains. This review will focus on the recent studies on the biology of influenza viruses as well as the structure, function, and mechanism of action of both M2 channel and neuraminidase influenza viruses. We also address the progress made in developing new M2 channel and neuraminidase inhibitors to offer more insights into possible therapeutic options.

2. Influenza Viruses

The human influenza viruses A (IAV), B (IBV), and C (ICV) belong to the *Orthomyxoviridae* family and have many common biological properties [25]. IAVs and IBVs are of epidemiological interest since they circulate and cause severe disease and major seasonal epidemics in the human population. On the other hand, ICV is associated with mild illnesses [5,26].

IAV and IBV are stabbed with two major surface glycoproteins (antigens) that dominate the virus surface: hemagglutinin (HA), and neuraminidase (NA) [27]. Both HA and NA perform complementary functions in the life cycle of the influenza virus. HA is responsible for the attachment of the virus to the host cell surface that is being infected. In contrast, NA is involved in the release of a progeny virion from an infected cell [27–29]. Conversely, ICV has a single major surface glycoprotein, the hemagglutinin-esterase-fusion (HEF) protein, which combines functions of both HA and NA [30,31].

IAVs and IBVs are conventionally named according to their species (if non-human), the location where isolated, the isolate number, a year of isolation, and lastly, the HA and NA virus subtypes in brackets. For example, A/Wisconsin/67/05(H3N2) was isolate number 67 of a human influenza A virus isolated in the state of Wisconsin in 2005, and it has an HA subtype 3 and an NA subtype 2 [32].

IAVs are classified based on the antigenic properties of HA and NA glycoproteins [33,34]. To date, 16 HA and 9 NA IAV subtypes, designated H1–H16 and N1–N9, have been discovered circulating in a wide range of aquatic birds [35,36]. These are expressed in several combinations of viruses isolated from aquatic avian species. An additional two combinations, H17N10 and H18N11, have been discovered in bats [37,38].

IBVs are instead divided into two antigenically distinct phylogenetic lineages, the B/Victoria/2/87 (B/Victoria) and B/Yamagata/16/88 (B/Yamagata) found circulating in seals [32,39]. ICVs have been isolated from humans and pigs. IAVs are more varied than IBVs, which are fundamentally exclusive to humans due to their capability to adapt to several species. IBV epidemics happen on average three weeks later than IAV epidemics [40–42].

New IAV and IBV strains arise regularly in a process referred to as antigenic variation (antigenic drift and antigenic shift) of HA and NA antigens [8,9]. This process inhibits the binding of neutralizing antibodies against common circulating strains, thereby allowing a new subtype of viral strains to avoid host immune response acquired through vaccination. These variations cause yearly outbreaks of influenza in the human population [43,44].

Antigenic drift is caused by intense selection pressure by the neutralizing antibodies of host immune systems, resulting in point mutations in the genes encoding NA and HA antigens. This drift leads to amino acid sequence changes in the antibody binding sites on these viral proteins. It occurs in both IAVs and IBVs [10]. The antigenic shift is due to the re-assortment of virus genomic segments when a cell is infected by two different strains of influenza viruses of different subtypes. It occurs only in IAV. This shift contributes to the replacement of genes encoding one or both surface antigens during replication, resulting in genome exchange [14,44].

2.1. Structure of Influenza Viruses

By electron microscopy, IAVs and IBVs are both pleomorphic (spheres or very long filaments), with an average size of 100 nm in diameter for spheres and 300 nm in length for filaments. HA and NA glycoproteins project from the membrane surface as spikes. The two spikes differ in morphology—HA is triangular rod-shaped, while NA is mushroom-shaped (Figure 1). Each virion has an average of 500 HA and 100 NA spikes [45–47].

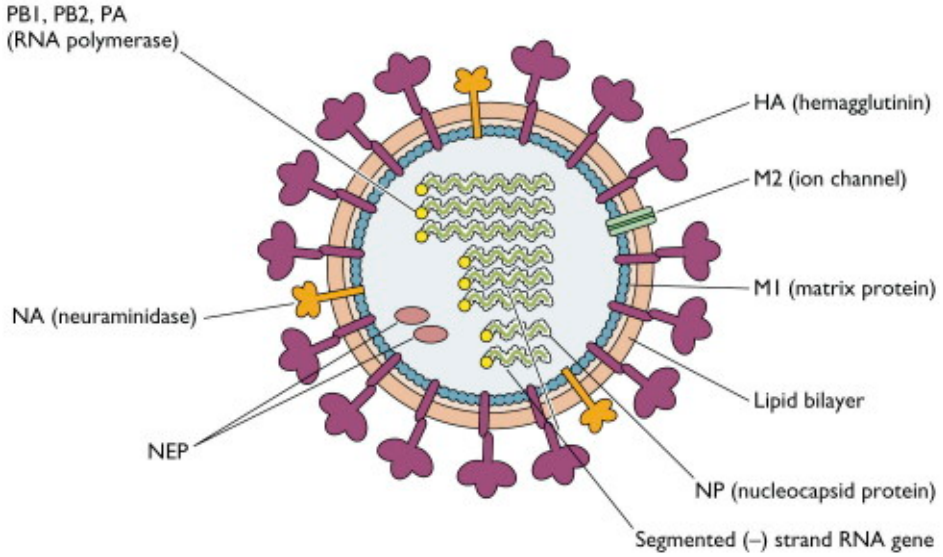

Figure 1. Structure of influenza A virus showing the two major surface glycoproteins (hemagglutinin (HA) and neuraminidase (NA)), the nucleocapsid and polymerase proteins (NP, PB1, PB2, and PA), the matrix proteins (M1 and M2), the non-structural proteins (nuclear export protein (NEP)), lipid bilayer and segmented negative-strand RNA genes [48].

IAVs and IBVs contain eight negative-sense, single-stranded RNA genome segments and are encapsidated by nucleocapsid proteins to form ribonucleoprotein (RNP) [29,49]. They encode transcripts for 10 essential virus proteins categorized into four groups: (1) the nucleocapsid and polymerase proteins—nucleocapsid protein (NP), polymerase B1 protein (PB1), polymerase B2 protein (PB2), and polymerase A protein (PA); (2) the envelope proteins—HA and NA; (3) the non-glycosylated matrix proteins—matrix protein 1 (M1) and matrix protein 2 (M2) (NB and BM2 for IBV); and (4) the non-structural proteins—non-structural protein 1 (NS1) and nuclear export protein (NEP) [50–55].

In contrast, ICV only consists of seven RNA genome segments, and a single major surface glycoprotein, the HEF protein [30,31]. The lipid core interior of the virus particle is enclosed by the matrix protein (M1), covering the three integral membrane proteins: HA, NA, and CM2. A virus particle must contain each of all unique RNA segments to be fully infectious [56,57].

2.2. Replication Cycle of Influenza Virus

Human influenza viruses infect cells of the upper respiratory epithelium [58]. They are assumed to be transmitted from an infected person predominantly by aerosol or droplet

infection, which is created while talking, coughing, or sneezing, thus contaminating the mucosa of the respiratory tract. Transmission can also occur via direct contact with virus-contaminated surfaces and successive mouth–nose contact. Following infection, the viruses replicate in the nasal and laryngeal mucosa [5,59].

Influenza virus replication can be divided into seven distinct phases (Figure 2): (1) virus attachment; (2) endocytosis; (3) uncoating and membrane fusion; (4) transcription of the viral RNA; (5) translation of viral proteins; (6) replication of the viral RNA; (7) virion budding and release.

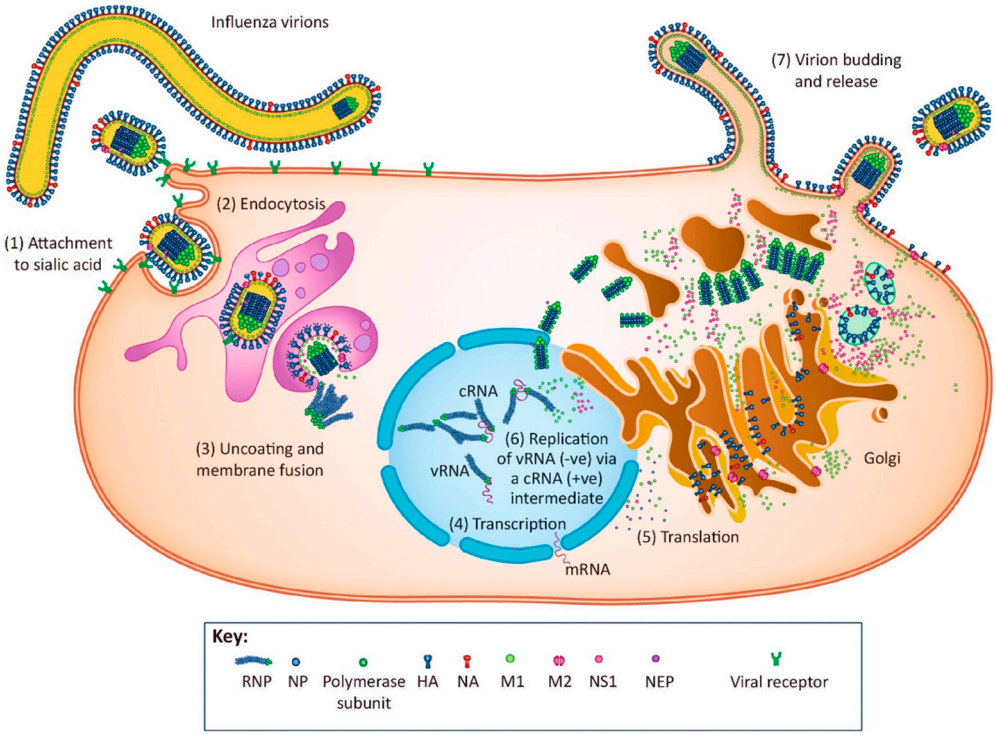

Figure 2. The replication cycle of influenza virus, illustrating seven discernible phases: (1) attachment; (2) endocytosis; (3) uncoating and membrane fusion; (4) transcription of the viral RNA; (5) translation of viral proteins; (6) replication of the viral RNA; and (7) virion budding and release [60].

2.2.1. Virus Attachment

This is the first step in viral replication, where the virus binds to the host cell. Viral HA binds the influenza virus to the sialic acid of the cell surface glycoprotein or glycolipid that is being infected [26,61]. The sialic acid termini have two unique steric configurations, the α-2,3- and α-2,6- linkages. The HA proteins of human viruses prefer to bind sialic acid linked to galactose via an α-2,6-linkage (Siaα2,6Gal), which is predominantly found in human respiratory epithelial cells [62,63]. In contrast, HA proteins of avian viruses preferentially recognize an α-2,3- linkage (Siaα2,3Gal) that is predominant on the epithelial cells of duck intestines [64–66].

2.2.2. Endocytosis

Following HA protein (or HEF in ICV) virus attachment to sialic acid-containing receptors on the host cell, virus particles enter the cell by clathrin-mediated endocytosis via clathrin-coated pits—a process by which receptors on the cell surface mediate an inward budding of the plasma membrane. This leads to the formation of endocytic vesicles (endosomes) containing the absorbed substances [67–69].

2.2.3. Uncoating and Membrane Fusion

The acidity of the endosomal membrane influences the uncoating of the influenza virus. Low pH (~5) of the late endosome triggers host cell protease (trypsin-like) to cleave HA into two subunits (fusion peptide), HA1 and HA2 [70–72].

After cleavage, the hydrophobic free N terminus of the HA2 subunit (exposed fusion peptide) inserts into the endosomal membrane of the host cell. Fusion leads to the incorporation of the virus envelope with the endosomal membrane; this result in the opening of a pore through which Influenza A viral ribonucleoproteins (vRNPs) are released into the cellular cytoplasm. Uncleaved HA of influenza viruses can attach to, but not enter, the host cell and is consequently not infectious [73,74].

Additionally, in IAVs, protons influx through the M2 ion channel from the late endosome into the virus particle [75,76]. This influx leads to acidification of the interior of the virus particle leading to disruption of M1-RNP complexes, consequently enabling the release of vRNPs into cellular cytoplasm [77,78]. The M2 ion channel is also believed to prevent the premature activation of HA after cleavage by equilibrating the acidic pH of the Golgi apparatus [79,80].

Following release from the virion, cytoplasmic vRNPs are trafficked into the host cell nucleus by cellular import factors (nuclear localization signals), importin-α (karyopherin-α) and importin-β (karyopherin-β). The M1 protein, on the other hand, following separation from the vRNP complexes, is separately trafficked into the nucleus, where all vRNA synthesis takes place [77,81–83].

2.2.4. Transcription of the Viral RNA

Inside the nucleus, viral RNA transcription is carried out by the viral RNA-dependent RNA polymerase (RdRp) complex (PB1, PB2, and PA subunits), whereby it binds to and cleaves the vRNA and concurrently leads to elongation [84,85]. The RdRp complex primes the vRNA template via a mechanism called "cap snatching" to increase initiation efficiency [86].

For cap snatching, the PB2 subunit binds to the 5′caps of the host mRNA, while the endonuclease activity of the PA subunit "snatches" (cleaves) 10–13 nucleotides downstream of the 5′cap. The produced 10–13 nucleotides with the cap serve as a primer for viral mRNA synthesis [54,87,88]. Synthesis is carried out by the polymerase activity of the PB1 subunit. Transcription finalizes by polyadenylation of the viral mRNA encoded by polyadenylation signal, an oligo-U sequence (5 to 7 Uracil residues) located close to the 5′-end of the template [87–89].

2.2.5. Translation of Viral Proteins

Synthesis of viral mRNA also occurs in the nucleus of the cell catalyzed by the same polymerase complex used for mRNA transcription, but without the requirement of a capped primer [90,91]. The viral polymerase uses the negative-sense vRNA as a template to synthesize a positive-sense copy of the vRNA termed complementary RNA (cRNA). The viral RNA polymerase subsequently transcribes this cRNA to produce more copies of vRNA [92,93].

The viral mRNA (vRNP segments) is exported from the cellular nucleus into the cytosol by the nuclear export proteins (M1 and NS2) for translation by the cytoplasmic ribosomes. The mRNAs transcribed by the RdRp complex are spliced by host cell machinery regulated by interferon-antagonist (NS1) protein to yield M and NS proteins. M1 is thought to form complexes with vRNPs, and NS2 mediates the export of the M1-RNP complex into the cytosol via nucleoporins [90,91].

2.2.6. Replication of the Viral RNA

In the cytosol, the influenza virus protein synthesis is directly mediated by the host cell translation machinery. Viral RNA replication occurs in two steps: the first vRNA is replicated into cRNA, and then cRNA is copied into vRNA. Newly synthesized nucleoprotein

(NP) and viral polymerase subunits (PA, PB1, and PB2) are imported back into the nucleus. These newly synthesized proteins are known to assist in viral mRNA transcription and vRNA replication [91]. Progeny vRNPs associate with nuclear export proteins and form a M1-RNP complex for trafficking towards the cell surface using microtubule-organizing centers (MTOCs) [94–96].

HA, NA and M2 membrane proteins are synthesized by ribosomes associated with the endoplasmic reticulum (ER). Following synthesis, they are trafficked into the Golgi apparatus for post-translational modifications (glycosylation of HA and NA, and palmitoylation of HA and M2) and subsequently directed to the cell membrane. HA, NA, and M2 integrate with vRNPs in the cell membrane and stick in the lipid bilayer for packaging [85,90]. The mechanism of packaging the eight vRNPs (seven for ICV) is currently not fully understood but is thought to be facilitated by segment-specific packaging signals. Influenza viruses with incomplete vRNPs are known to be not fully infectious [97,98].

2.2.7. Virion Budding and Release

Influenza virus budding occurs in the lipid raft, a plasma membrane region known to be rich in sphingolipid and cholesterol [99,100]. The RNPs and M1 proteins aggregate in this membrane region, and when they reach high concentrations, they concentrate to create a virus particle. Budding is believed to be initiated by an accumulation of M1 matrix protein at the cytoplasmic side of the plasma membrane [20,101]. M2 has also been shown to accumulate at the boundaries of the budding sites and contribute to the scission of the virus particles [20,46].

The release of the newly assembled influenza virus bud is exceptionally dependent on the sialidase activity of NA to catalyze the cleavage of sialic acid from the host cell and virus glycoprotein [28,102]. As a result, HA is prohibited from binding to the cell surface, and the progeny viruses are released from the infected cell to spread the infection to uninfected cells [29,103].

3. The AM2 Ion Channel

Influenza A M2 (AM2) membrane protein is a type III integral membrane protein that is very selective for protons versus sodium and potassium ions. It forms a homotetrameric pH-regulated proton-selective channel located in the viral envelope [104–107]. Ion channel activity has been detected in *Xenopus oocytes* [106,107], mammalian cells [107,108], and yeast [109,110] expression systems. In the early stages of viral replication, the AM2 channel permits influx of protons from endosomes into the virus interior, leading to virus uncoating and the subsequent release of free RNPs into the host cell cytoplasm such that the viral genetic material can replicate [108,111].

The AM2 ion channel also plays a crucial role in the late stages of the viral replication cycle by working as a proton channel and equilibrating the pH of the Golgi apparatus with the cytoplasm. Thus, this prevents premature conformation change of the newly synthesized viral HA while they are transported to the plasma membrane of the infected cells [112,113]. The critical requirement for this viral protein makes it a good target for antiinfluenza drugs [114]. Evidence as to its functions has been mainly from studies of the action of drug-resistant mutants [110].

3.1. Structure and Function of the AM2 Ion Channel

The structure, mechanism of proton conductance, and inhibition of the AM2 ion channel were broadly studied by electrophysiology [22,115], site-directed mutagenesis [116,117], and molecular dynamics (MD) simulations [118,119]. However, the studies only established the overall topology and location of sidechains. Studies that employ high-resolution techniques such as solution NMR, crystallographic structures and solid-state NMR (SSNMR) have provided an elevated understanding of the proton channel to the atomic level [120–123].

These studies determined that the three-dimensional structures of the AM2 ion channel (97 residues single-pass membrane) comprise three structural domains, which perform multiple functions (Figure 3). The *N*-terminal 23 residues ectodomain is responsible for the integration of AM2 into the virion [124,125]. Succeeding this region is a single transmembrane (TM) domain (19 residues), which is imperative for proton conductance, tetramerization of the protein, and drug binding [108,110]. Finally, the *C*-terminal cytoplasmic tail endodomain (54 residues) is critical for membrane localization, budding, scission, and binding to matrix protein M1, which is essential for the assembly and production of infectious virus particles [20].

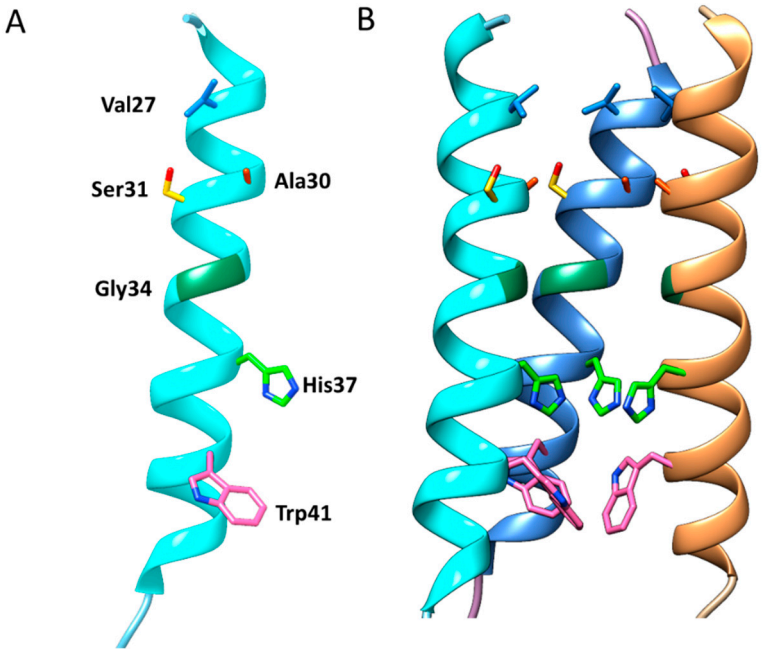

Figure 3. Three-dimensional structure of the influenza A M2 (AM2) ion channel. (**A**) A monomer of the AM2 protein transmembrane domain (TMD) displaying channel facing amino acid residues; (**B**) Organization of four TMDs, and the alignment of pore-lining residues. For clarity, three AM2 monomers are shown to expose the sidechains of the pore-lining residues. The NMR structure with PDB ID 2RLF was used (prepared by authors).

The active site of the channel was established to be in the TM domain. The TM helices assemble into a four identical α-helix bundle with a left-handed twist angle of ~23° and a well-defined water-filled pore through which protons must pass to gain access to the viral interior [122,126,127]. Water molecules within the channel pore form a hydrogen-bonded water network known as the Grotthuss mechanism along the 17 Å stretch between the Val27 valve and His37 box.

The continuous highly structured network of water molecules is only observed in low pH conditions, compared to the intermediate pH 6.5 conditions, which shows less ordered waters [126,127]. Functional studies and crystallographic structures indicate that the ion channel pore is lined by Gly34, Ser31, Ala30, and Val27 sidechains with a tilt angle of ~25°.

The helices are firmly packed at the N terminus, and they are marginally spread-out toward the C terminus. At the *N*-terminal end, the ion channel pore entrance is narrowed to 2 Å by the hydrophobic sidechain of the Val27 valve and restricts water molecules from penetrating the channel [126]. The channel pore size progressively expands to an inner diameter of ~9 Å until Gly34. The channel then narrows at the half of the channel towards the C terminus, and the His37 and Trp41 sidechains form the narrowest points—too small to allow anything to pass. Trp41 obstructs the *C*-terminal end of the pore to a pore size of 1.4 Å in diameter [125,127].

His37 and Trp41 residues are located near the center of the TM domain. Four His37 sidechains are packed into a box-like structure (His-box) and individual imidazoles are connected by a structured network of water molecules via a low-barrier hydrogen bond (LBHB) [122]. The His-box needs to expand only slightly (1–2 Å) to permit the passage of water molecules [126]. The His37 sidechain acts as a proton sensor and conducts protons by protonation or deprotonation of its imidazole sidechain. The Trp41 sidechain forms a Trp-basket that acts as a pH-dependent gate of the channel [76,123,126].

This two-state gating mechanism has a structurally rigid closed state and loses the quaternary structure open state [128]. Cross-linking studies indicated that the four parallel TM helices are bound at one end of the N-terminus by intermolecular disulfide bridges at Cys17 and Cys19 [129,130]. Additionally, they are bound at the other end by C-terminal amphipathic (AP) helices (residues 51–59), ensuring that acid activation of the channel does not dissociate the tetramer [120].

In the closed conformation of the channel pore, the Val27 valve at the N-terminus and the Trp41 gate at the C-terminus effectively block water from freely diffusing into the pore from either side of the membrane. The four bulky Trp41 indole rings are at van der Waals (VDW) distance from each other, preventing the passage of water or ions [120,131]. Additionally, the Trp41 residue is suggested to form intermolecular hydrogen bonding with the carboxyl group of the adjacent Asp44 subunit to stabilize the closed Trp41 gate [126]. Mutating Asp44 to Asn triggered a significant increase in the activity of the AM2 channel, supposedly triggered by the disruption of Asp-Trp hydrogen bonding interaction [132,133].

Although IAV mutates and shuffles its genes, the coding regions for His37 and Trp41 residues are highly conserved in all known strains of avian, swine, equine, and human IAVs when compared with the other AM2 proteins encoded by the genome [134,135]. Mutagenesis studies have identified His37 and Trp41 residues as a function core of the channel. When His37 is replaced with either Gly, Ala, Glu, Lys, or Arg, the effectivity of the AM2 channel is reduced, indicating that His37 is essential for the proton selectivity of the channel [136,137]. Site-directed mutagenesis replacement of Trp41 with Ala, Cys, or Phe also results in the absence of the measurable pH-modulating activity of the channel at high pH, suggesting that Trp41 is the gate that blocks the fusion of protons from the inside but not from the outside of the virus [117].

A low pH medium destabilizes the TM helix–helix packing via electrostatic repulsion; this widens the pore to accept water molecules to enable His37 imidazole ring protonation [138]. This conformational change breaks the hydrogen bond between Trp41 and Asp44, enabling the Trp41 gate to flip open. The influx of protons goes through the channel into the virus interior to facilitate the separation of matrix protein and RNPs [117,123].

3.2. Catalytic Mechanism of the AM2 Ion Channel

The mechanism of AM2 ion channel activity has been thoroughly studied in oocytes, mammalian cells, and vesicles [106–110]. The interest in the ion channel stems from its proton selectivity since it has 10^6 to 10^7-fold more permeability to protons versus alkali metal ions such as sodium (Na^+) and potassium (K^+) under physiological conditions [111,121]. MD calculations, as well as functional studies, suggest that the channel responds solely to external pH. Low pH activates the channel and high pH closes the channel, irrespective of the interior pH. It conducts protons from the outside to the inside of the virus when the external pH is low, but does not as efficiently conduct protons outward when the pH gradient is reversed [139–141].

MD simulations and functional and spectroscopic studies of the AM2 proton transport mechanism have been extensively used to study the exact molecular mechanism of how protons are transported through the membrane, and they are still under debate. Two proton transport mechanisms have been proposed: an early model "water wire model" and the currently accepted model "proton relay model" [118,142–145].

According to the water wire model, protonation and deprotonation of His37 imidazole sidechains cause an electrostatic repulsion between charged histidine residues. This pushes

tightly packed transmembrane (TM) helices apart, thereby opening the "tryptophan" gate and exposing His37 to proton acceptors (water). This repulsion results in the formation of a continuous water wire that shuttles protons from one water molecule to another [76].

According to the proton relay model, the His37 imidazole sidechain serves as a "relay" molecule, binding protons from the outside of the channel and releasing them to the inside of the channel by dissociation. This mechanism is assisted by tautomerization or flipping of the imidazole ring [110,122].

It has been suggested that the channel is closed when the pH_{out} exceeds pH 7.5 and is opened when the pH_{out} is lower than pH 6.5. Proton exchange is at the highest level between pH 5 and 6 of the endosome, where the +2 and +3 protonation states dominate [146,147]. MD simulations suggest that conformation change between C_{closed} and C_{open} conformers is stimulated by pH_{out} and typically takes place at the +3-protonation state of His37 imidazole rings (Figure 4) [127,141].

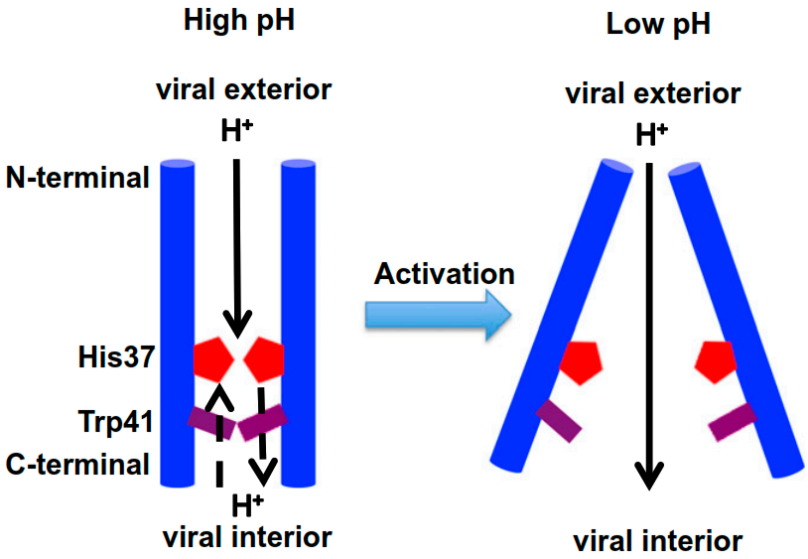

Figure 4. Model for AM2 channel acid activation and proton conductance displaying conformation change from closed to open conformers [148]. For clarity, only two helices and one protonation state are shown.

The relay model was further supported by solid-state NMR studies, which reported the first two protonation conduction steps of His37 residue occurring with pKa of 8.2, the third protonation at pKa of 6.3 and the fourth at pKa of $\leq$5 [147]. A different study reported the first two protonation steps of His37 tetrad to occur at pKa values of 7.6 and 6.8 [149]. These findings identified the shuttling of the third proton (conducting pKa) to occur near the midpoint of the conductance curve, suggesting that conduction transpires via the alternation of +2 and +3 states. Furthermore, MD simulations for possible protonation states were in agreement with the above studies [135,138].

Under a low protonation state of His37 (pH > 7.5), the Trp41 basket constricts the *C*-terminal pore below His37, forming a gate that blocks the influx of protons through the channel and dehydrates the His-box (the channel favors C_{closed} conformers) [76,138,149]. The NMR study indicated that lowering the pH from 7.5 to 6.0 caused immense broadening of most of the NMR resonances corresponding to the TM domain. The expansion was due to increased exchange between multiple TM domain conformations as the Trp gate opens and closes the channel [120,133].

A high His37 protonation state (pH < 6.5) favors the C_{open} conformers. As the pH decreases, the Trp-basket opens to expose protonated His37 molecules to the viral interior, able to enter primary proton conduction step, while the Val27 valve N terminal end of the bundle contracts [122,135,138]. When the highest protonation state is reached, the

positive charge on the His-box increases and the Trp-basket opens sufficiently due to electrostatic repulsion between the His-tetrad. The open Trp-basket hydrates the His-box to create an aqueous conduction path, allowing the release of protons into the viral interior [123,135,138]. Succeeding the dissociation of protons from the His-box and their discharge into the virus interior, the AM2 channel reverts to conformers resembling a neutral pH structure (C_{closed}) for a subsequent cycle of proton shuttle [126,127,129,136].

M2-blockers are thought to block virus replication after the influenza virus infection has taken place through the prohibition of proton influx from the endosomes into the virus interior, accordingly halting virus uncoating, such that the viral genetic material cannot replicate [22,150].

3.3. AM2 Channel Inhibitors

Amantadine (Symmetrel) was approved by the food and drugs board (FDA) in 1966, followed by rimantadine (Flumadine) in 1994 for both treatment and prevention of IAV. They are only effective against IAV, and their utility is limited by association with severe side effects on the central nervous system (CNS) as well as the emergence of drug-resistant viruses [106]. The drug-binding site has previously been predicted by mutagenesis and electrophysiological studies, which suggested that drug-resistant mutants (V27A, A30T, S31N, and G34E) bind to the *N*-terminal pore of the TM domain [22,151].

Recently, numerous NMR and X-ray crystal structures of the intracellular TM domain have been resolved [146]. They suggest that Adamantane fits into the central cavity of the AM2 channel above the His37 box to prevent the conformational change from C_{open} to C_{closed} conformers, thus obstructing the proton conductance [128,142].

Amantadine and rimantadine are amphiphilic, comprised of a hydrophilic amine and a hydrophobic adamantyl or adamantylethyl cage (Figure 5). Rimantadine has a chiral center and is clinically administered as a racemate. The solution NMR spectroscopy structure of the rimantadine–AM2 channel complex indicated that inhibition occurred by an allosteric mechanism. Four rimantadines were bound to the *C*-terminal on the lipid facing surface of the helices and tightly packed to block the *C*-terminal end of the channel [120]. R-rimantadine was found to exhibit full occupation of the *C*-terminal end, thus causing higher inhibition activity of the AM2 channel than S-rimantadine [152].

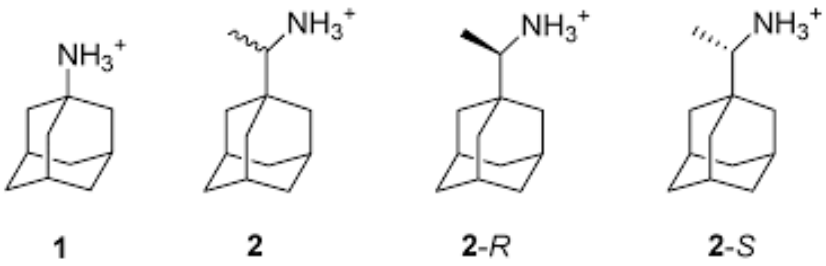

Figure 5. Adamantane and its amine analogues: amantadine (**1**), rimantadine (**2**), *R*-rimantadine (**2**-*R*) and *S*-rimantadine (**2**-*S*) (prepared by authors).

The X-ray crystallographic structure of the amantadine–AM2 channel complex showed that amantadine binds to the *N*-terminal domain. The large hydrophobic group comfortably fits into the center of the aqueous cavity and physically blocks the pore, thus interrupting highly structured water networks and disturbing the protonation equilibrium of His37. This blockage suggests a physical occlusion mechanism of inhibition [121]. The amantadine cage fits into the channel pore with exceptional geometric complementarity. Amantadine fits better in the inward configuration with its amine facing towards but not directly contacting His37. pKa of His37 is affected by amantadine binding [127].

This proposed binding model (physical occlusion mechanism) is consistent with the stoichiometry of binding and the location of drug-resistant mutants (V27A, A30T, S31N, and G34E) which bind to the *N*-terminal domain, suggesting a physical occlusion mechanism

for inhibition [22,153,154]. Physical occlusion is also coherent with indications that when the ammonium group of amantadine is replaced with a bulky secondary alkylamine, its effectiveness is retained [146]. The hydrophobic substituents can similarly replace the adamantine cage. Although, the positively charged primary ammonium group shows an optimal high-binding affinity when compared to tertiary amines, alcohols, and other neutral head groups, which tend to have a lower binding affinity [155–157].

The optimum binding affinity of primary amines suggested that the positively charged ammonium group may mimic positively charged hydronium ions produced as protons permeate through the channel to reach His37-box. The hydrated ammonium or hydronium ions are stabilized by water-mediated hydrogen-bonding [137,141,157].

The binding of amantadine to the channel causes structural and dynamical modifications to the channel by disrupting the continuous water networks that are vital for proton conductance [127,148]. The SSNMR structure of the adamantine–channel complex presented a significant decline in water–protein cross-peak by 47% compared to the open state upon drug binding, demonstrating channel dehydration, thereby preventing proton conductance. These findings indicate that amantadine binds into the pore instead of the surface, as suggested by the solution NMR study of AM2 [120,158].

These findings are in exceptional agreement with the high-resolution SSNMR structure of the amantadine–AM2 channel complex in lipid bilayers at high pH, which indicates that amantadine physically occludes the AM2 channel [122]. The crystallographic structures are also in excellent agreement with numerous functional and spectroscopic data and provide a basis for developing new anti-viral drugs against influenza viruses [22,136].

Vaccination provides the best method for the prevention and control of influenza and normally elicits a potent neutralizing antibody response [159]. The immunogenicity of M2e was first investigated in 1988 by Zebedee et al., in which to gain an understanding of the M2 protein function in the influenza virus' replicative pathway, their study produced and characterized a monoclonal antibody to M2 [160]. This monoclonal antibody (14c2) recognized the ectodomain of the protein, and it was able to spot M2 on the virions, thus reducing viral growth through the size reduction in lytic plaques [161]. Manzoor et al. in 2020 [162] examined the anti-viral activity of monoclonal antibody rM22223 and found that rM2ss23 inhibited A/Aichi/2/1968 (H3N2) (Aichi) but not A/PR/8/1934 (H1N1) (PR8) replication. Amino acid residues at positions 54 and 57 in the M2 cytoplasmic tail were also discovered to be important for the sensitivity to rM2ss23.

Employing the amino acid sequence of the rM2ss23 variable region, Okuya et al. constructed mouse–human chimeric rMss23 (ch-rM2ss23) IgA and IgG, which were presumed to identify the same epitope, and compared their inhibitory activities in vitro [163]. The results indicated that IgA restricts virus budding more proficiently than IgG and suggested a contribution of IgA in cross-protective immunity. More so, it has been discovered that M2e-specific IgGs mouse monoclonal antibodies inhibit the plaque growth and infectivity of A/Udorn/72 in vitro [164]. Filament formation was repressed by treatment of A/Udorn/72 infected cells with M2e-specific IgG2a and IgG1 monoclonal antibodies and resulted in the fragmentation of pre-existing filaments.

Peptides have also been studied for at least 40 decades, and a broad spectrum of biological activities has been described so far. The development of antiviral peptides has been attracting much attention in recent years due to their relative safety and lower development costs in comparison with those associated with small-molecule- or antibody-based antiviral drugs [165]. The derivative (M2 MH) of M2 AH has been established to instigate viral membrane distortion and it effectively eliminated the infectivity of influenza viruses, demonstrating its potential as an antiviral peptide [166]. Membrane distortion was caused by the deep introduction of the peptide into the membrane.

4. Neuraminidase (NA)

The activity of NA to remove influenza virus receptors adhered to erythrocytes was discovered by Hirst [153] in studies on hemagglutination. Influenza virus receptor studies

by Gottschalk [28] identified this enzyme as NA, which was eventually revealed to be involved in the spread of infection from cell to cell [167,168]. The receptor-destroying enzyme (RDE) from *Vibrio cholerae* culture fluid was found to be a source of NA [169].

Influenza virus NA (EC 3.2.1.18) catalyzes the cleavage of α-(2-3 or 2-6)-ketosidic linkage between terminal sialic acid (*N*-acetyl-neuraminic acid) and adjacent surface glycoprotein [28,168]. Cleavage facilitates the budding of the newly formed viral particles from the surface of the infected cell and prevents their aggregation on the host cell surface. The cleavage promotes the release of progeny virus to infect new host cells and spread infection in the respiratory tract mucins [154,170].

To date, 11 IAV subtypes of NA are recognized by the Centers for Diseases Control and Prevention. Of these, nine subtypes (N1–N9) are circulating in wild aquatic birds, and two more (N10 and N11) were recently found in bats [37]. N1–N9 subtypes are further divided into two phylogenic groups on the basis of their sequences and the sialic acid-binding pocket (150-loop) conformational differences. Group 1 NA *apo*-structures are in an open conformation, with a 150-cavity (residues 147 to 150) formed by the opening of the 150-loop (excluding N1 of the 2009 H1N1 pandemic), while all group 2 NA *apo*-structures lack this cavity. Group 1 comprises the N1, N4, N5, and N8 subtypes, while group 2 consists of the N2, N3, N6, N7, and N9 subtypes [171–173]. NA-like (N10 and N11) genes from bats are genetically distinct from NA molecules ascertained on established influenza A viruses (N1–N9), thereby creating a distinctive cluster, which is termed group 3.

4.1. Structure and Function of NA

High-resolution structures of NA have led to the successful design and worldwide approval of NAs. Crystal structures of all group 1 NAs (N1 [174,175], N4 [174], N5 [176], and N8 [174] and group 2 NAs (N2 [171] and N9 [177]) have been ascertained, except for N3 and N7, where attempts for crystallization have been unsuccessful. Influenza B NA crystal structures have also been established [71]. The structures of the nine N subtypes have a similar topology and share 50–70% amino acid sequence similarities [174].

NA is a type II integral membrane glycoprotein, assembling as a tetramer comprised of four identical disulfide-linked polypeptide chains. Each monomer has a molecular weight of 60 kDa and is made up of 470 amino acid residues [171,178]. NA exists as a mushroom-shaped homotetramer (240 kDa) on the virion surface, with the head atop a rod hydrophobic stalk anchoring it onto the viral surface (Figure 6). The head domain is box-shaped. Each monomer has a topologically identical six-bladed propeller-like structure. Each blade comprises four antiparallel strands of β-sheets [179,180]. The viral particle bears around 50 copies of tetramers that can form bundles on the viral surface [181].

The three-dimensional structure of NA shows that each monomer is folded into four unique structural domains. The cytoplasmic tail is critical for NA transport and incorporation into virions, while the transmembrane domain is responsible for attaching the NA to the viral envelope. The stalk domain is accountable for connecting the head to the transmembrane domain. Lastly, the catalytic head ectodomain attached to the C-terminus of the stalk carries the enzyme active site for sialic acid cleavage and other essential antigenic amino acids.

The structure of the tetrameric head domain has been determined for all nine NA subtypes by X-ray crystallography. The active site forms a shallow cavity at the surface and center of each monomer. It is positioned in a sideways conformation, which allows it to cleave sialic acids from adjacent membrane glycoproteins. This sialic acid binding site is well-formed, large and rigid, with an unusually large number of charged amino acid residues which cluster in the cavity and around its rim [34].

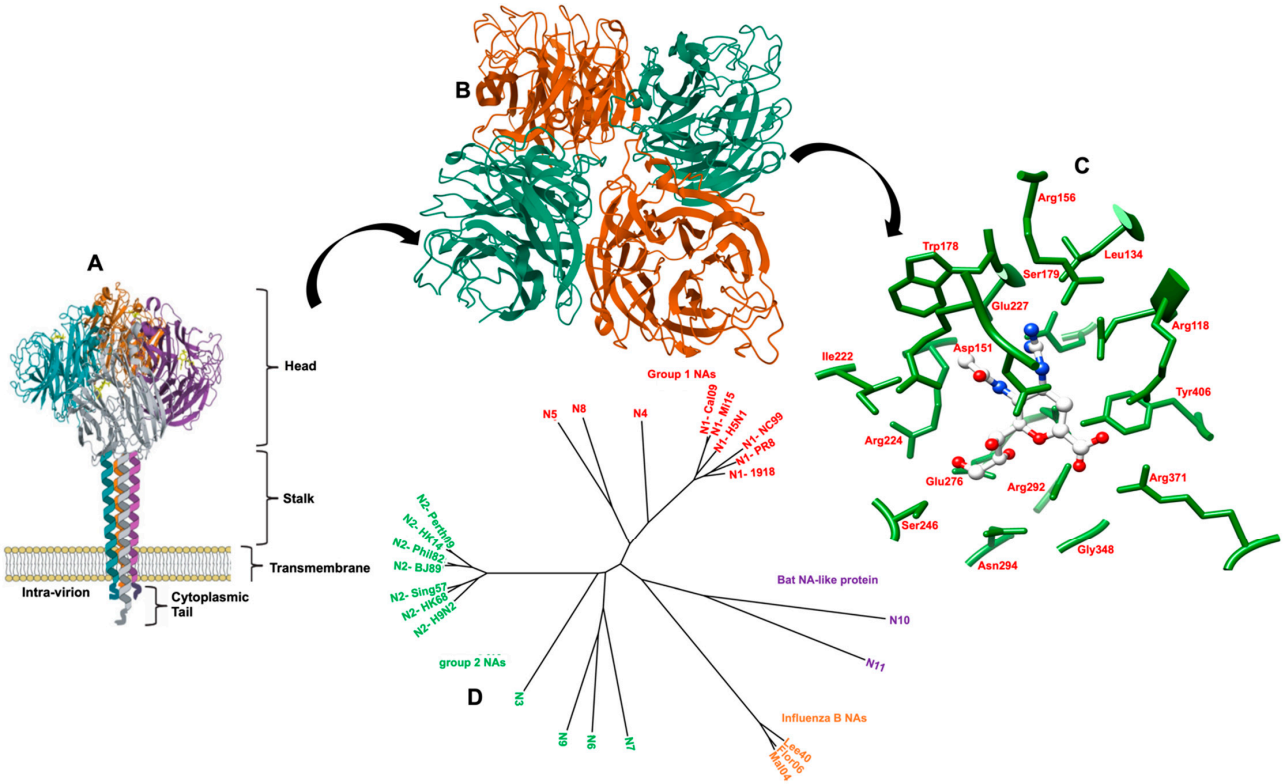

Figure 6. (**A**) The structure of NA as a tetramer of 4 identical monomers. Each monomer consists of 4 different structural domains called catalytic head, stalk, transmembrane and the cytoplasmic tail. The head domain structure was generated in Pymol using structural information from protein data bank code 4GZX [182]. (**B**) Top-down view of the NA tetramer. (**C**) The active site of NA in complex with Zanamivir is represented. Residues involved in catalysis are shown as green sticks (adapted with permission from ref. [183]). (**D**) Tree of known influenza virus NAs and NA-like proteins (N10 and N11). Influenza NAs cluster into group 1 (N1, N4, N5, N8) and group 2 NAs (N2, N3, N6, N7, N9). Influenza B NAs as well as the NA-like proteins (from sequences found in bats) form their own clusters (adapted with permission from ref. [184]).

The inner cavity is comprised of eight highly conserved catalytic residues that interact directly with sialic acids responsible for the catalytic activity of the enzyme (Arg118, Asp151, Arg152, Arg224, Glu276, Arg292, Arg371, and Tyr406) (N2 numbering) [170,181]. Additionally, the rim consists of 10 highly conserved structural residues (Glu119, Arg156, Trp178, Ser179, Asp (or Asn in N7 and N9) 198, Ile222, Glu227, Glu277, Asp293, and Glu425) responsible for the stabilization of the structure. Two calcium-binding sites located near the active site are responsible for the stabilization of the tetramer at low pH conditions [185–187].

The eight conserved catalytic residues are organized in a sequence of interlinked pockets that determine the mode in which the enzyme interacts with sialic acid. The active site is divided into five regions, termed subsites (S1 to S5), derived from the crystal structure of the substrate-based inhibitor DANA (dehydrodeoxy-*N*-acetylneuraminic acid) bound to the active site (Figure 7). Subsites S1, S2, S3, and S5 are occupied, while any portion of the DANA-based inhibitors does not occupy subsite S4.

Site S1 comprises a cluster of positively charged arginine triad residues: Arg118, Arg292, and Arg371. Site S2 forms a negatively charged region derived from Glu119 and Glu227 residues. Site S3 is a small hydrophobic region derived from Trp178 and Ile222 sidechains and a hydrophilic region provided by the Arg152 sidechain and a bound water molecule. Site S4 is primarily a hydrophobic region formed from the sidechains of Ile222, Ala246, and the hydrophobic face of Arg224. Site S5 creates an area of mixed polarity, derived from Glu276 and Ala246 residues.

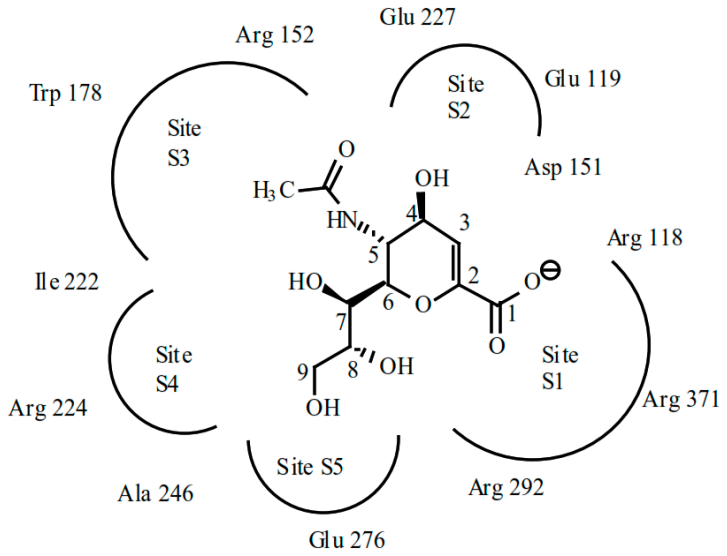

Figure 7. Diagram of NA active site with dehydrodeoxy-*N*-acetylneuraminic acid (DANA) inhibitor showing the five inhibitor binding sub-sites and nearby critical residues [188].

4.2. Catalytic Mechanism of NA

The catalytic mechanism of NA has been studied in some detail but is still not completely elucidated. Still, based on structural information and biochemical studies, it has been suggested that the catalytic mechanism for the cleavage of sialic acid from glycoconjugate has four major steps (Figure 8). The first step is the binding incidence. The substrate binds to the active site, resulting in salt-bridge formation between the carboxylate of the substrate and the triarginyl cluster of the active site. The binding of sialic acid to the catalytic site distorts the pyranose ring from the preferred chair conformation to a pseudoboat conformation. This is a result of a strong ionic, hydrogen bond and steric interactions [34,189]. The carboxylate group of the bound sialic acid adjusts from the axial into the pseudoequatorial position due to strong ionic interactions with the three arginine residues, 118, 292, and 371, resulting in the formation of a sialosyl cation (oxocarbenium ion) at the C2 atom of sialic acid.

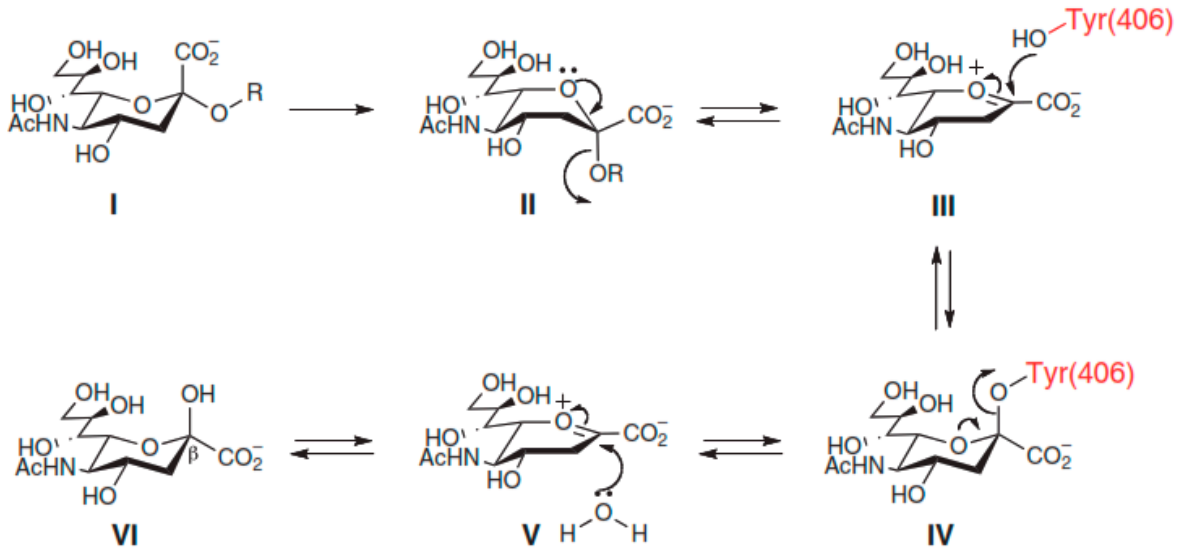

Figure 8. Catalytic Mechanism of NA showing four major steps of NA Inhibitors [190].

The second step of the catalytic reaction is the formation of the endocyclic sialosyl cation transition state intermediate. It requires proton donation from solvent aided by negatively charged amino acid residues. It is believed that the hydrogen-bonding network of water molecules and protein residues leading from a charged group on the protein surface to water molecules could facilitate proton donation [191]. Asp151, Arg152, and Glu277 residues are thought to stabilize the positive charge of the sialosyl cation. Covalent interaction of the sialosyl cation with the hydroxyl group of Tyr406 at the base of catalytic site is also believed to contribute to the stability of the cationic intermediate.

The final two steps of the enzymatic mechanism encompass the formation and release of sialic acid. Stable sialosyl cation intermediate favors the cleavage of the glycosidic bond, yielding sialic acid and the aglycon molecule. The release of sialic acid from the active site is favored by the mutarotation of β-anomer conformation to a thermodynamically more stable α-anomer conformation for sialic acid in solution. The aglycon molecule leaves the enzyme active site with the glycosidic oxygen [192,193].

The optimum NA activity was observed to occur at a pH range of 5.5–6.6 and a temperature of 37 °C. It has also been suggested that the presence of calcium ions adjacent to the active site is essential for both the activation and thermostability of NA [185]. Moreover, the existence of highly conserved amino acid residues in the active site makes it an attractive target for drug design as it accords the development of transition-state analogues that inhibit NA.

NA inhibitors are effective against both IAV and IBV. They prevent NA from cleaving the sialic acid, thus budding viral particles remain attached to the surface of the infected cell and each other. This results in the suppression of infection to one round of replication [168]. There are three classes of globally approved NA inhibitors (zanamivir, oseltamivir, and peramivir) for the treatment and prophylaxis of influenza infection (Figure 9). Their design is based on the transition state analogue of sialic acid (2-deoxy-2,3-dihydro-*N*-acetylneuraminic acid or DANA) developed in the 1970s, which displayed low binding affinity into the active site [179,194].

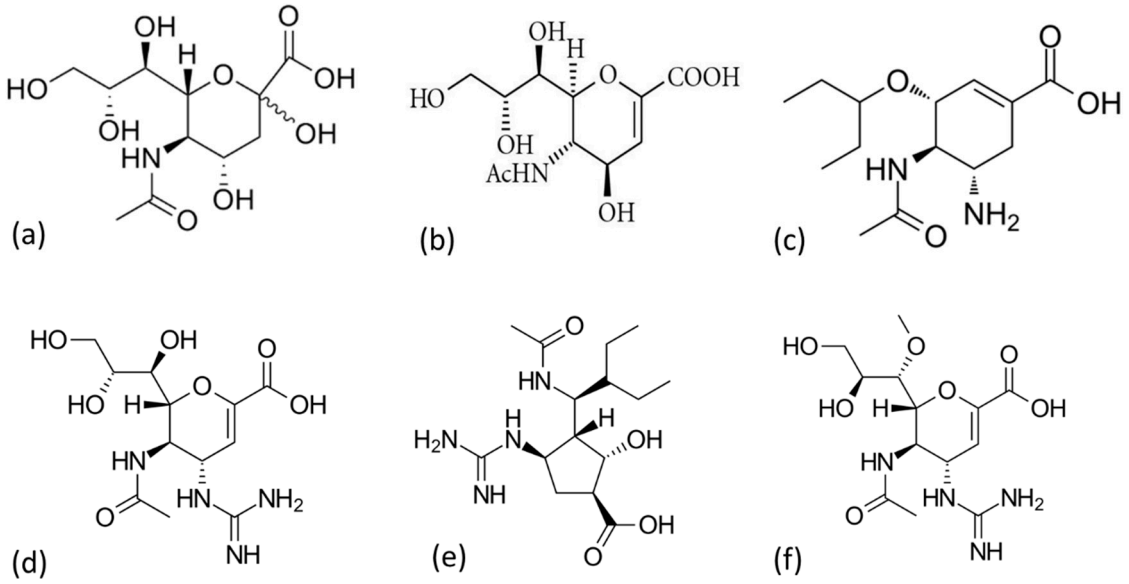

Figure 9. Chemical structure of sialic acid for treatment and prophylaxis of influenza infection (**a**), DANA (**b**), zanamivir (**c**), oseltamivir (**d**), peramivir (**e**), and laninamivir (**f**) (prepared by authors).

This critical finding paved the way for the design and development of drugs that closely mimic DANA and fit in the active site pocket to hinder NA activity. Further advances in technology and different techniques led to the discovery of high-resolution crystal structures of both NA and sialic acid [178,195]. Protein X-ray crystallographic study of the complex NA with DANA has aided the identification and characterization of the site

of enzyme catalysis. It displayed the presence of an empty positively charged cavity in the active site, which aligned with C4 of the bound sialic acid. The findings led to suggestions that the introduction of a positively charged group to the C4 of DANA might enhance binding affinity to the catalytic site [170,196–198].

Zanamivir (Relenza) was the first potent NA inhibitor to be approved by the FDA in 1999. DANA-based zanamivir synthesis involved the substitution of C4-OH with the 4-guanidino group, which showed a 1000-fold better binding affinity into the active site pocket over DANA. Zanamivir (4-guanidino-DANA) is administered via oral inhalation directly into the respiratory tract. However, it has low bioavailability due to the presence of the guanidino group [197].

The FDA subsequently approved oseltamivir (Tamiflu) in the year 1999 to address the low bioavailability limitation of zanamivir. The development of orally bioavailable oseltamivir involved two substitution mechanisms of the DANA cyclohexene ring: the substitution of the C6 glycerol sidechain of DANA with a bulky hydrophobic pentyl ether sidechain, and the C4-OH substitution with an amino group rather than guanidino. Oseltamivir is orally administered as a prodrug of oseltamivir phosphate and converted to an active metabolite, oseltamivir carboxylic acid, by endogenous esterase [199–201].

The FDA globally approved Peramivir (Rapivab/Rapiacta/Peramiflu) in the year 2010. Peramivir is also derived from DANA and contains a cyclopentane ring with features of both zanamivir and oseltamivir, the C4-guanidino group, and the bulky hydrophobic pentyl ether sidechain, respectively. Such features lead to multiple interactions (higher binding affinity) with the NA catalytic site. This drug is administered intravenously due to low oral bioavailability [202–205].

Laninamivir (Inavir) is currently licensed for use in Japan since the year 2014 and is undergoing Phase III clinical trials in other countries. It is a derivative of zanamivir, and it contains the C4-guanidino group and an additional 7-methoxy group. Laninamivir is administered as a prodrug (laninamivir octanoate) via nasal inhalation and converted to an active metabolite (laninamivir) by endogenous esterase. It has long-lasting anti-viral inhibition with activity against oseltamivir-resistant viruses [206–208].

With regards to new antivirals for targeting NA, acylhydrazone has been considered a fortunate structure capable of offering ligand points for more than one type of bio-receptor. Zhao et al. [209] discovered that some acylhydrazone derivatives exhibit better inhibition than oseltamivir carboxylate against NA. Furthermore, Yu et al. [210] also designed and synthesized benzoylhydrazone NA inhibitors with higher NA inhibitory activity to the positive control oseltamivir carboxylic acid. Li et al. [211] likewise designed and synthesized novel acylhydrazone NA inhibitors, with most of them exhibiting good inhibition activity with a significantly lower activity than that of the positive control oseltamivir carboxylic acid.

Modifications of oseltamivir that enable higher affinity binding at the amino acids forming the 150- or 430-cavity could yield novel NA inhibitors that are not sensitive to common mutations of NA [212]. Moreover, Ju et al. [213] designed and synthesized 27 oseltamivir analogues by modification at the C-1 position to research the chemical space around the 430-cavity. Compound 8b indicted the best inhibitory activity against H5N1 and H5N6 NAs. Xie et al. [214] also discovered group-1-specific NA inhibitors that are involved in fighting the H5N1 virus. Derivatives of oseltamivir were designed and synthesized by targeting the 150-cavity. Among the synthesized derivatives, compound 20l showed higher inhibitory efficacy against NAs from three H5N1 viruses. The inhibitory activity was better than that of oseltamivir carboxylate.

In 2019, Ji et al. [212] designed and synthesized oseltamivir derivatives by exploiting the 150-cavity in NAs. The compounds exhibited antiviral activities with higher potency (5- to 85-fold) than those of oseltamivir carboxylate against N1, N8, and N1-H274Y mutations. Jia and colleagues [212] also explored the chemical space of both 150-cavities in NAs, and oseltamivir derivatives were designed, synthesized and evaluated by modifying the C1 and C5 amino group of oseltamivir carboxylate. The most effective N1-selective inhibitor

exhibited 1.5- and 1.8-times greater activity than oseltamivir carboxylate against H5N1 and H5N1-H274Y.

5. Conclusions and Future Perspectives

The transmission of human influenza through inter-continental circulation makes surveillance a vital member in the global management of influenza. The broad host range of influenza virus and interspecies transmission are essential factors for its continual spread and genetic variation. The transitional reservoirs such as pigs, birds, ducks and horses play a critical function in keeping the influenza virus in nature and facilitating its transmission to humans. Thus, other than constant surveillance and developing a universal vaccine and potent antivirals, prolific global management of such reservoirs to limit the circulation and formation of new infectious influenza virus variants is necessary.

Although a considerable amount of biochemical and lower-resolution structural information has been attained for the AM2 proton channel, many rhetorical questions persist about this versatile protein. The present high-resolution structure offers a foundation for elucidating the mechanism of proton conduction through the AM2 channel. However, advancement in the discovery of new inhibitors targeting mutants of the AM2 channels has been sluggish. Recent developments in understating the structure and vital properties of the AM2 channel in a lipid bilayer, as well as the interaction of amantadine with the channel, have stimulated structure-based drug design and computer-aided drug design.

The resistance to NA inhibitors by influenza viruses is an emerging problem of high epidemiological and clinical impact. The emergence of drug resistance to inhibitors of NA, such as oseltamivir and zanamivir, qualifies a necessity for an alternative strategy. The alternative strategies are predominantly essential to recognize viable NA inhibitors which may not only have improved antiviral activity, but can also endure the threat of resistance.

There is advancement in the development of new NA inhibitors, but there has been slow progress with AM2 proton channel inhibitors. Modifications of the subunits bonded to its acyl and imine functions of acylhydrazone result in several derivatives, which confers diversity of molecular targets and provides more therapeutic properties. The 430-cavity widely exists in a variety of subtypes, including group-1 and group-2, and could provide greater chemical space for further modification. Approaches to broaden the availability of novel antiviral compounds include the development of synthetic peptides that disrupt the entry of viruses into cells. Although antibodies specific for M2 are unable to bind efficiently to free virus particles and thus do not neutralize virus infectivity, they can bind to M2e expressed on the surface of virus-infected cells and thus are a potential antiviral tool for preventing new virion release. Further studies on humans are needed to understand the protective role played by anti-influenza protein antibodies during infection or vaccination. That information will greatly enhance our understanding of how current influenza vaccines could be improved to provide cross-protective immunity in humans.

Author Contributions: Conceptualization, All; Methodology, All; Software, S.E.M., M.M.L., D.G.A., A.M.S., C.A., N.S.G. and H.M.K.; Validation, M.M.L., D.G.A., A.M.S., C.A., R.B.K., N.S.G. and H.M.K.; Formal Analysis, All; Investigation, S.E.M.; Resources, D.G.A., A.M.S. and H.M.K.; Data Curation, All; Writing—Original Draft Preparation, S.E.M.; Writing—Review and Editing, M.M.L., D.G.A., A.M.S., C.A., R.B.K., N.S.G., and H.M.K.; Visualization, All; Supervision, H.M.K., D.G.A., A.M.S.; Project Administration, D.G.A., A.M.S. and H.M.K.; Funding Acquisition, H.M.K. All authors have read and agreed to the published version of the manuscript.

Funding: This research received no external funding.

Figure Disclosure: The authors have appropriately referenced all images used in this report. Likewise, figures generated by the authors have been accordingly indicated.

Acknowledgments: We acknowledge the College of Health Sciences, University of Kwa-Zulu Natal, Durban, South Africa, South African National Research Financial Foundation for supporting this study, and The Centre for High-Performance Computing, South Africa (www.chpc.ac.za) is also appreciated for the computational resource.

Conflicts of Interest: The authors declare no conflict of interest.

References

1. Davidson, S. Treating influenza infection, from now and into the future. *Front. Immunol.* **2018**, *9*, 1946. [CrossRef] [PubMed]
2. Paget, J.; Spreeuwenberg, P.; Charu, V.; Taylor, R.J.; Iuliano, A.D.; Bresee, J.; Simonsen, L.; Viboud, C.; GSIMCN and GlCT. Global mortality associated with seasonal influenza epidemics: New burden estimates and predictors from the GLaMOR Project. *J. Glob. Health* **2019**, *9*, 20421. [CrossRef] [PubMed]
3. *Disease Burden of Influenza*; CDC: Atlanta, GA, USA, 2020.
4. Das, K. Antivirals targeting influenza A virus. *J. Med. Chem.* **2012**, *55*, 6263–6277. [CrossRef]
5. Hampson, A.W.; Mackenzie, J.S. The influenza viruses. *Med. J. Aust.* **2006**, *185*, S39–S43. [CrossRef] [PubMed]
6. Principi, N.; Camilloni, B.; Alunno, A.; Polinori, I.; Argentiero, A.; Esposito, S. Drugs for influenza treatment: Is there significant news? *Front. Med.* **2019**, *6*, 109. [CrossRef] [PubMed]
7. Syrjänen, R.K.; Jokinen, J.; Ziegler, T.; Sundman, J.; Lahdenkari, M.; Julkunen, I.; Kilpi, T.M. Effectiveness of pandemic and seasonal influenza vaccines in preventing laboratory-confirmed influenza in adults: A clinical cohort study during epidemic seasons 2009–2010 and 2010–2011 in Finland. *PLoS ONE* **2014**, *9*, e108538. [CrossRef]
8. Kim, H.; Webster, R.G.; Webby, R.J. Influenza virus: Dealing with a drifting and shifting pathogen. *Viral Immunol.* **2018**, *31*, 174–183. [CrossRef]
9. Wikramaratna, P.S.; Sandeman, M.; Recker, M.; Gupta, S. The antigenic evolution of influenza: Drift or thrift? *Philos. Trans. R. Soc. Lond. B. Biol. Sci.* **2013**, *368*, 20120200. [CrossRef]
10. Lowen, A.C. Constraints, drivers, and implications of influenza A virus reassortment. *Annu. Rev. Virol.* **2017**, *4*, 105–121. [CrossRef] [PubMed]
11. Shao, W.; Li, X.; Goraya, M.U.; Wang, S.; Chen, J.-L. Evolution of influenza a virus by mutation and re-assortment. *Int. J. Mol. Sci.* **2017**, *18*, 1650. [CrossRef]
12. Petrova, V.N.; Russell, C.A. The evolution of seasonal influenza viruses. *Nat. Rev. Microbiol.* **2018**, *16*, 47–60. [CrossRef] [PubMed]
13. Taubenberger, J.K.; Kash, J.C. Influenza virus evolution, host adaptation, and pandemic formation. *Cell Host Microbe* **2010**, *7*, 440–451. [CrossRef]
14. Morens, D.M.; Taubenberger, J.K.; Fauci, A. The persistent legacy of the 1918 influenza virus. *N. Engl. J. Med.* **2009**, *361*, 225–229. [CrossRef]
15. Taubenberger, J.K. The origin and virulence of the 1918 "Spanish" influenza virus. *Proc. Am. Philos. Soc.* **2006**, *150*, 86–112. [PubMed]
16. Taubenberger, J.K.; Morens, D.M. 1918 Influenza: The mother of all pandemics. *Emerg. Infect. Dis.* **2006**, *12*, 15–22. [CrossRef]
17. Wilson, I.A.; Cox, N.J. Structural basis of immune recognition of influenza virus hemagglutinin. *Annu. Rev. Immunol.* **1990**, *8*, 737–787. [CrossRef] [PubMed]
18. Farrukee, R.; Hurt, A.C. Antiviral drugs for the treatment and prevention of influenza. *Curr. Treat. Options Infect. Dis.* **2017**, *9*, 318–332. [CrossRef]
19. Tisdale, M. Influenza M2 ion-channel and neuraminidase inhibitors. In *Antimicrobial Drug Resistance*; Mayers, D.L., Ed.; Humana Press: Totowa, NJ, USA, 2009.
20. Rossman, J.S.; Jing, X.; Leser, G.P.; Balannik, V.; Pinto, L.H.; Lamb, R.A. Influenza virus M2 ion channel protein is necessary for filamentous virion formation. *J. Virol.* **2010**, *84*, 5078–5088. [CrossRef] [PubMed]
21. Jalily, P.H.; Duncan, M.C.; Fedida, D.; Wang, J.; Tietjen, I. Put a cork in it: Plugging the M2 viral ion channel to sink influenza. *Antivir. Res.* **2020**, *178*, 104780. [CrossRef] [PubMed]
22. Wang, C.; Takeuchi, K.; Pinto, L.H.; Lamb, R.A. Ion channel activity of influenza A virus M2 protein: Characterization of the amantadine block. *J. Virol.* **1993**, *67*, 5585–5594. [CrossRef] [PubMed]
23. Mckimm-Breschkin, J.L. Influenza neuraminidase inhibitors: Anti-viral action and mechanisms of resistance. *Influenza Other Respi. Viruses* **2013**, *7*, 25–36. [CrossRef]
24. Takashita, E.; Daniels, R.S.; Fujisaki, S.; Gregory, V.; Gubareva, L.V.; Huang, W.; Hurt, A.C.; Lackenby, A.; Nguyen, H.T.; Pereyaslov, D.; et al. Global update on the susceptibilities of human influenza viruses to neuraminidase inhibitors and the cap-dependent endonuclease inhibitor baloxavir, 2017–2018. *Antivir. Res.* **2020**, *175*, 104718. [CrossRef]
25. Palese, P.; Shaw, M.L. Orthomyxoviridae: The viruses and their replication. In *Fields' Virology*; Knipe, D.M., Howley, P.M., Eds.; Lippincott Williams & Wilkins: Philadelphia, PA, USA, 2007; pp. 1647–1689.
26. Horimoto, T.; Kawaoka, Y. Influenza: Lessons from past pandemics, warnings from current incidents. *Nat. Rev. Microbiol.* **2005**, *3*, 591–600. [CrossRef]
27. Kosik, I.; Yewdell, J.W. Influenza hemagglutinin and neuraminidase: Yin-Yang proteins coevolving to thwart immunity. *Viruses* **2019**, *11*, 346. [CrossRef]
28. Gottschalk, A. Neuraminidase: The specific enzyme of influenza virus and Vibrio cholerae. *Biochim. Biophys. Acta* **1957**, *23*, 645–646. [CrossRef]
29. Palese, P.; Schulman, J.L. Mapping of the influenza virus genome: Identification of the hemagglutinin and the neuraminidase genes. *Proc. Natl. Acad. Sci. USA* **1976**, *73*, 2142–2146. [CrossRef] [PubMed]

30. Rogers, G.N.; Herrler, G.; Paulson, J.C.; Klenk, H.D. Influenza C virus uses 9-O-acetyl-N-acetylneuraminic acid as a high affinity receptor determinant for attachment to cells. *J. Biol. Chem.* **1986**, *261*, 5947–5951. [CrossRef]
31. Hause, B.M.; Collin, E.A.; Liu, R.; Huang, B.; Sheng, Z.; Lu, W.; Wang, D.; Nelson, E.A.; Li, F. Characterization of a novel influenza virus in cattle and swine: Proposal for a new genus in the orthomyxoviridae family. *MBio* **2014**, *5*, e00031-14. [CrossRef] [PubMed]
32. *Types of Influenza Viruses*; CDC: Atlanta, GA, USA, 2019.
33. Du, R.; Cui, Q.; Rong, L. Competitive cooperation of hemagglutinin and neuraminidase during influenza A virus entry. *Viruses* **2019**, *11*, 458. [CrossRef]
34. Gamblin, S.J.; Skehel, J.J. Influenza hemagglutinin and neuraminidase membrane glycoproteins. *J. Biol. Chem.* **2010**, *285*, 28403–28409. [CrossRef]
35. Yoon, S.-W.; Webby, R.J.; Webster, R.G. Evolution and ecology of influenza A viruses. In *Influenza Pathogenesis and Control*; Compans, R.W., Oldstone, M.B.A., Eds.; Springer International Publishing: Midtown Manhattan, NY, USA, 2014.
36. Fouchier, R.A.M.; Munster, V.; Wallensten, A.; Bestebroer, T.M.; Herfst, S.; Smith, D.; Rimmelzwaan, G.F.; Olsen, B.; Osterhaus, A.D.M.E. Characterization of a novel influenza a virus hemagglutinin subtype (H16) obtained from black-headed gulls. *J. Virol.* **2005**, *79*, 2814–2822. [CrossRef]
37. Tong, S.; Zhu, X.; Li, Y.; Shi, M.; Zhang, J.; Bourgeois, M.; Yang, H.; Chen, X.; Recuenco, S.; Gomez, J.; et al. New world bats harbor diverse influenza A viruses. *PLoS Pathog.* **2013**, *9*, e1003657. [CrossRef]
38. Tong, S.; Li, Y.; Rivailler, P.; Conrardy, C.; Castillo, D.A.A.; Chen, L.-M.; Recuenco, S.; Ellison, J.A.; Davis, C.T.; York, I.A.; et al. A distinct lineage of influenza A virus from bats. *Proc. Natl. Acad. Sci. USA* **2012**, *109*, 4269–4274. [CrossRef]
39. Rota, P.A.; Wallis, T.R.; Harmon, M.W.; Rota, J.S.; Kendal, A.P.; Nerome, K. Cocirculation of two distinct evolutionary lineages of influenza type B virus since 1983. *Virology* **1990**, *175*, 59–68. [CrossRef]
40. Webster, R.G.; Bean, W.J.; Gorman, O.T.; Chambers, T.M.; Kawaoka, Y. Evolution and ecology of influenza A viruses. *Microbiol. Rev.* **1992**, *56*, 152–179. [CrossRef]
41. Hurt, A.C.; Vijaykrishna, D.; Butler, J.; Baas, C.; Maurer-Stroh, S.; Silva-De-La-Fuente, M.C.; Medina-Vogel, G.; Olsen, B.; Kelso, A.; Barr, I.G.; et al. Detection of evolutionarily distinct avian influenza A viruses in antarctica. *MBio* **2014**, *5*, e01098-14. [CrossRef]
42. Caini, S.; Kusznierz, G.; Garate, V.V.; Wangchuk, S.; Thapa, B.; de Paula Júnior, F.J.; de Ferreira Almeida, W.A.; Njouom, R.; Fasce, R.A.; Bustos, P.; et al. The epidemiological signature of influenza B virus and its B/Victoria and B/Yamagata lineages in the 21st century. *PLoS ONE* **2019**, *14*, e0222381. [CrossRef] [PubMed]
43. Webster, R.G.; Shortridge, K.F.; Kawaoka, Y. Influenza: Interspecies transmission and emergence of new pandemics. *FEMS Immunol. Med. Microbiol.* **1997**, *18*, 275–279. [CrossRef] [PubMed]
44. Hampson, A.W. Influenza virus antigens and 'antigenic drift'. *Perspect. Med. Virol.* **2002**, *7*, 49–85. [CrossRef]
45. Garman, E.; Laver, G. The structure, function, and inhibition of influenza virus neuraminidase. In *Viral Membrane Proteins: Structure, Function, and Drug Design*; Fischer, W.B., Ed.; Springer: Boston, MA, USA, 2005.
46. Rossman, J.S.; Lamb, R.A. Viral membrane scission. *Annu. Rev. Cell Dev. Biol.* **2013**, *29*, 551–569. [CrossRef] [PubMed]
47. Badham, M.D.; Rossman, J.S. Filamentous influenza viruses. *Curr. Clin. Microbiol. Rep.* **2016**, *3*, 155–161. [CrossRef] [PubMed]
48. Racaniello, V. Structure of Influenza Virus. Available online: http://www.virology.ws/2009/04/30/structure-of-influenza-virus/ (accessed on 10 September 2020).
49. Mcgeoch, D.; Fellner, P.; Newton, C. Influenza virus genome consists of eight distinct RNA species. *Proc. Natl. Acad. Sci. USA* **1976**, *73*, 3045–3049. [CrossRef] [PubMed]
50. Lamb, R.A.; Choppin, P.W.; Chanock, R.M.; Lai, C.J. Mapping of the two overlapping genes for polypeptides NS1 and NS2 on RNA segment 8 of influenza virus genome. *Proc. Natl. Acad. Sci. USA* **1980**, *77*, 1857–1861. [CrossRef] [PubMed]
51. Briedis, D.J.; Lamb, R.A. Influenza B virus genome: Sequences and structural organization of RNA segment 8 and the mRNAs coding for the NS1 and NS2 proteins. *J. Virol.* **1982**, *42*, 186–193. [CrossRef]
52. Colacino, J.M.; Staschke, K.A.; Laver, W.G. Approaches and strategies for the treatment of influenza virus infections. *Anti Viral Chem. Chemother.* **1999**, *10*, 155–185. [CrossRef] [PubMed]
53. Arranz, R.; Coloma, R.; Chichón, F.J.; Conesa, J.J.; Carrascosa, J.L.; Valpuesta, J.M.; Ortín, J.; Martín-Benito, J. The structure of native influenza virion ribonucleoproteins. *Science* **2012**, *338*, 1634–1637. [CrossRef]
54. Moeller, A.; Kirchdoerfer, R.N.; Potter, C.S.; Carragher, B.; Wilson, I.A. Organization of the influenza virus replication machinery. *Science* **2012**, *338*, 1631–1634. [CrossRef]
55. Pflug, A.; Guilligay, D.; Reich, S.; Cusack, S. Structure of influenza A polymerase bound to the viral RNA promoter. *Nature* **2014**, *516*, 355–360. [CrossRef]
56. Bouvier, N.M.; Palese, P. The biology of influenza viruses. *Vaccine* **2008**, *26*, D49–D53. [CrossRef] [PubMed]
57. Furukawa, T.; Muraki, Y.; Noda, T.; Takashita, E.; Sho, R.; Sugawara, K.; Matsuzaki, Y.; Shimotai, Y.; Hongo, S. Role of the CM2 protein in the influenza C virus replication cycle. *J. Virol.* **2011**, *85*, 1322–1329. [CrossRef]
58. Denney, L.; Ho, L.-P. The role of respiratory epithelium in host defence against influenza virus infection. *Biomed. J.* **2018**, *41*, 218–233. [CrossRef] [PubMed]
59. van Riel, D.; Den Bakker, M.A.; Leijten, L.M.E.; Chutinimitkul, S.; Munster, V.J.; de Wit, E.; Rimmelzwaan, G.F.; Fouchier, R.A.M.; Osterhaus, A.D.M.E.; Kuiken, T. Seasonal and pandemic human influenza viruses attach better to human upper respiratory tract epithelium than avian influenza viruses. *Am. J. Pathol.* **2010**, *176*, 1614–1618. [CrossRef]
60. Hutchinson, E.C. Influenza virus. *Trends Microbiol.* **2018**, *26*, 809–810. [CrossRef]

61. Weis, W.; Brown, J.H.; Cusack, S.; Paulson, J.C.; Skehel, J.J.; Wiley, D.C. Structure of the influenza virus haemagglutinin complexed with its receptor, sialic acid. *Nature* **1988**, *333*, 426–431. [CrossRef] [PubMed]
62. Nobusawa, E.; Aoyama, T.; Kato, H.; Suzuki, Y.; Tateno, Y.; Nakajima, K. Comparison of complete amino acid sequences and receptor-binding properties among 13 serotypes of hemagglutinins of influenza a viruses. *Virology* **1991**, *182*, 475–485. [CrossRef]
63. Matrosovich, M.; Tuzikov, A.; Bovin, N.; Gambaryan, A.; Klimov, A.; Castrucci, M.R.; Donatelli, I.; Kawaoka, Y. Early alterations of the receptor-binding properties of H1, H2, and H3 avian influenza virus hemagglutinins after their introduction into mammals. *J. Virol.* **2000**, *74*, 8502. [CrossRef] [PubMed]
64. Rogers, G.N.; Paulson, J.C. Receptor determinants of human and animal influenza virus isolates: Differences in receptor specificity of the H3 hemagglutinin based on species of origin. *Virology* **1983**, *127*, 361–373. [CrossRef]
65. Matrosovich, M.N.; Matrosovich, T.Y.; Gray, T.; Roberts, N.A.; Klenk, H.-D. Human and avian influenza viruses target different cell types in cultures of human airway epithelium. *Proc. Natl. Acad. Sci. USA* **2004**, *101*, 4620–4624. [CrossRef] [PubMed]
66. Couceiro, J.N.; Paulson, J.C.; Baum, L.G. Influenza virus strains selectively recognize sialyloligosaccharides on human respiratory epithelium; the role of the host cell in selection of hemagglutinin receptor specificity. *Virus Res.* **1993**, *29*, 155–165. [CrossRef]
67. Matlin, K.S.; Reggio, H.; Helenius, A.; Simons, K. Infectious entry pathway of influenza virus in a canine kidney cell line. *J. Cell Biol.* **1981**, *91*, 601–613. [CrossRef]
68. Sieczkarski, S.B.; Whittaker, G.R. Influenza virus can enter and infect cells in the absence of clathrin-mediated endocytosis. *J. Virol.* **2002**, *76*, 10455–10464. [CrossRef]
69. Rust, M.J.; Lakadamyali, M.; Zhang, F.; Zhuang, X. Assembly of endocytic machinery around individual influenza viruses during viral entry. *Nat. Struct. Mol. Biol.* **2004**, *11*, 567–573. [CrossRef]
70. White, J.; Helenius, A.; Gething, M.-J. Haemagglutinin of influenza virus expressed from a cloned gene promotes membrane fusion. *Nature* **1982**, *300*, 658–659. [CrossRef]
71. Burmeister, W.P.; Ruigrok, R.W.; Cusack, S. The 2.2 A resolution crystal structure of influenza B neuraminidase and its complex with sialic acid. *EMBO J.* **1992**, *11*, 49–56. [CrossRef]
72. Bullough, P.A.; Hughson, F.M.; Skehel, J.J.; Wiley, D.C. Structure of influenza haemagglutinin at the pH of membrane fusion. *Nature* **1994**, *371*, 37–43. [CrossRef] [PubMed]
73. Stegmann, T. Membrane fusion mechanisms: The influenza hemagglutinin paradigm and its implications for intracellular fusion. *Traffic* **2000**, *1*, 598–604. [CrossRef] [PubMed]
74. Sieczkarski, S.B.; Whittaker, G.R. Viral entry. *Curr. Top. Microbiol. Immunol.* **2005**, *285*. [CrossRef]
75. Lakadamyali, M.; Rust, M.J.; Babcock, H.P.; Zhuang, X. Visualizing infection of individual influenza viruses. *Proc. Natl. Acad. Sci. USA* **2003**, *100*, 9280–9285. [CrossRef]
76. Pinto, L.H.; Lamb, R.A. The M2 proton channels of influenza A and B viruses. *J. Biol. Chem.* **2006**, *281*, 8997–9000. [CrossRef] [PubMed]
77. Martin, K.; Helenius, A. Transport of incoming influenza virus nucleocapsids into the nucleus. *J. Virol.* **1991**, *65*, 232–244. [CrossRef]
78. Bui, M.; Whittaker, G.; Helenius, A. Effect of M1 protein and low pH on nuclear transport of influenza virus ribonucleoproteins. *J. Virol.* **1996**, *70*, 8391–8401. [CrossRef] [PubMed]
79. Steinhauer, D.A.; Wharton, S.A.; Skehel, J.J.; Wiley, D.C.; Hay, A.J. Amantadine selection of a mutant influenza virus containing an acid-stable hemagglutinin glycoprotein: Evidence for virus-specific regulation of the pH of glycoprotein transport vesicles. *Proc. Natl. Acad. Sci. USA* **1991**, *88*, 11525–11529. [CrossRef] [PubMed]
80. Takeuchi, K.; Lamb, R.A. Influenza virus M2 protein ion channel activity stabilizes the native form of fowl plague virus hemagglutinin during intracellular transport. *J. Virol.* **1994**, *68*, 911–919. [CrossRef] [PubMed]
81. Kemler, I.; Whittaker, G.; Helenius, A. Nuclear import of microinjected influenza virus ribonucleoproteins. *Virology* **1994**, *202*, 1028–1033. [CrossRef] [PubMed]
82. O'neill, R.E.; Jaskunas, R.; Blobel, G.; Palese, P.; Moroianu, J. Nuclear import of influenza virus rna can be mediated by viral nucleoprotein and transport factors required for protein import. *J. Biol. Chem.* **1995**, *270*, 22701–22704. [CrossRef]
83. Cros, J.F.; Palese, P. Trafficking of viral genomic RNA into and out of the nucleus: Influenza, Thogoto and Borna disease viruses. *Virus Res.* **2003**, *95*, 3–12. [CrossRef]
84. Fodor, E.; Seong, B.L.; Brownlee, G.G. Photochemical cross-linking of influenza a polymerase to its virion RNA promoter defines a polymerase binding site at residues 9 to 12 of the promoter. *J. Gen. Virol.* **1993**, *74*, 1327–1333. [CrossRef]
85. Matsuoka, Y.; Matsumae, H.; Katoh, M.; Eisfeld, A.J.; Neumann, G.; Hase, T.; Ghosh, S.; Shoemaker, J.E.; Lopes, T.J.S.; Watanabe, T.; et al. A comprehensive map of the influenza A virus replication cycle. *BMC Syst. Biol.* **2013**, *7*, 1–18. [CrossRef]
86. Plotch, S.J.; Bouloy, M.; Ulmanen, I.; Krug, R.M. A unique cap(m7GpppXm)-dependent influenza virion endonuclease cleaves capped RNAs to generate the primers that initiate viral RNA transcription. *Cell* **1981**, *23*, 847–858. [CrossRef]
87. Krug, R.M. Priming of influenza viral RNA transcription by capped heterologous RNAs. *Curr. Top Microbiol. Immunol.* **1981**, *93*, 125–149.
88. Robertson, J.S.; Schubert, M.; Lazzarini, R.A. Polyadenylation sites for influenza virus mRNA. *J. Virol.* **1981**, *38*, 157–163. [CrossRef]
89. Li, X.; Palese, P. Characterization of the polyadenylation signal of influenza virus RNA. *J. Virol.* **1994**, *68*, 1245–1249. [CrossRef]

90. Jorba, N.; Coloma, R.; Ortín, J. Genetic trans-complementation establishes a new model for influenza virus rna transcription and replication. *PLoS Pathog.* **2009**, *5*, e1000462. [CrossRef] [PubMed]
91. Fodor, E. The RNA polymerase of influenza A virus: Mechanisms of viral transcription and replication. *Acta Virol.* **2013**, *57*, 113–122. [CrossRef]
92. Newcomb, L.L.; Kuo, R.-L.; Ye, Q.; Jiang, Y.; Tao, Y.J.; Krug, R.M. Interaction of the influenza A virus nucleocapsid protein with the viral rna polymerase potentiates unprimed viral rna replication. *J. Virol.* **2009**, *83*, 29. [CrossRef]
93. York, A.; Hengrung, N.; Vreede, F.T.; Huiskonen, J.T.; Fodor, E. Isolation and characterization of the positive-sense replicative intermediate of a negative-strand RNA virus. *Proc. Natl. Acad. Sci. USA* **2013**, *110*, E4238–E4245. [CrossRef] [PubMed]
94. Amorim, M.J.; Bruce, E.A.; Read, E.K.C.; Foeglein, A.; Mahen, R.; Stuart, A.D.; Digard, P. A Rab11- and microtubule-dependent mechanism for cytoplasmic transport of influenza A virus viral RNA. *J. Virol.* **2011**, *85*, 4143–4156. [CrossRef] [PubMed]
95. Eisfeld, A.J.; Kawakami, E.; Watanabe, T.; Neumann, G.; Kawaoka, Y. RAB11A is essential for transport of the influenza virus genome to the plasma membrane. *J. Virol.* **2011**, *85*, 6117–6126. [CrossRef] [PubMed]
96. Momose, F.; Sekimoto, T.; Ohkura, T.; Jo, S.; Kawaguchi, A.; Nagata, K.; Morikawa, Y. Apical transport of influenza A virus ribonucleoprotein requires Rab11-positive recycling endosome. *PLoS ONE* **2011**, *6*, e21123. [CrossRef] [PubMed]
97. Enami, M.; Sharma, G.; Benham, C.; Palese, P. An influenza virus containing nine different RNA segments. *Virology* **1991**, *185*, 291–298. [CrossRef]
98. Fujii, Y.; Goto, H.; Watanabe, T.; Yoshida, T.; Kawaoka, Y. Selective incorporation of influenza virus RNA segments into virions. *Proc. Natl. Acad. Sci. USA* **2003**, *100*, 2002–2007. [CrossRef]
99. Lingwood, D.; Simons, K. Lipid rafts as a membrane-organizing principle. *Science* **2010**, *327*, 46–50. [CrossRef]
100. Gerl, M.J.; Sampaio, J.L.; Urban, S.; Kalvodova, L.; Verbavatz, J.-M.; Binnington, B.; Lindemann, D.; Lingwood, C.A.; Shevchenko, A.; Schroeder, C.; et al. Quantitative analysis of the lipidomes of the influenza virus envelope and MDCK cell apical membrane. *J. Cell Biol.* **2012**, *196*, 213–221. [CrossRef] [PubMed]
101. Ali, A.; Avalos, R.T.; Ponimaskin, E.; Nayak, D.P. Influenza virus assembly: Effect of influenza virus glycoproteins on the membrane association of M1 protein. *J. Virol.* **2000**, *74*, 8709. [CrossRef] [PubMed]
102. Burnet, F.M.; Mccrea, J.F.; Stone, J.D. Modification of human red cells by virus action; the receptor gradient for virus action in human red cells. *Br. J. Exp. Pathol.* **1946**, *27*, 228–236. [PubMed]
103. Webster, R.G.; Laver, W.G. Preparation and properties of antibody directed specifically against the neuraminidase of influenza virus. *J. Immunol.* **1967**, *99*, 49–55.
104. Lamb, R.A.; Zebedee, S.L.; Richardson, C.D. Influenza virus M2 protein is an integral membrane protein expressed on the infected-cell surface. *Cell* **1985**, *40*, 627–633. [CrossRef]
105. von Heijne, G.; Gavel, Y. Topogenic signals in integral membrane proteins. *Eur. J. Biochem.* **1988**, *174*, 671–678. [CrossRef] [PubMed]
106. Pinto, L.H.; Holsinger, L.J.; Lamb, R.A. Influenza virus M2 protein has ion channel activity. *Cell* **1992**, *69*, 517–528. [CrossRef]
107. Chizhmakov, I.V.; Geraghty, F.M.; Ogden, D.C.; Hayhurst, A.; Antoniou, M.; Hay, A.J. Selective proton permeability and pH regulation of the influenza virus M2 channel expressed in mouse erythroleukaemia cells. *J. Physiol.* **1996**, *494*, 329–336. [CrossRef]
108. Wang, C.; Lamb, R.A.; Pinto, L.H. Direct measurement of the influenza A virus M2 protein ion channel activity in mammalian cells. *Virology* **1994**, *205*, 133–140. [CrossRef] [PubMed]
109. Kurtz, S.; Luo, G.; Hahnenberger, K.M.; Brooks, C.; Gecha, O.; Ingalls, K.; Numata, K.; Krystal, M. Growth impairment resulting from expression of influenza virus M2 protein in Saccharomyces cerevisiae: Identification of a novel inhibitor of influenza virus. *Antimicrob. Agents Chemother.* **1995**, *39*, 2204. [CrossRef] [PubMed]
110. Tu, Q.; Pinto, L.H.; Luo, G.; Shaughnessy, M.A.; Mullaney, D.; Kurtz, S.; Krystal, M.; Lamb, R.A. Characterization of inhibition of M2 ion channel activity by BL-1743, an inhibitor of influenza A virus. *J. Virol.* **1996**, *70*, 4246. [CrossRef] [PubMed]
111. Helenius, A. Unpacking the incoming influenza virus. *Cell* **1992**, *69*, 577–578. [CrossRef]
112. Ciampor, F.; Bayley, P.M.; Nermut, M.V.; Hirst, E.M.A.; Sugrue, R.J.; Hay, A.J. Evidence that the amantadine-induced, M2-mediated conversion of influenza A virus hemagglutinin to the low pH conformation occurs in an acidic trans golgi compartment. *Virology* **1992**, *188*, 14–24. [CrossRef]
113. Sakaguchi, T.; Leser, G.P.; Lamb, R.A. The ion channel activity of the influenza virus M2 protein affects transport through the Golgi apparatus. *J. Cell Biol.* **1996**, *133*, 733–747. [CrossRef]
114. Moorthy, N.S.H.N.; Poongavanam, V.; Pratheepa, V. Viral M2 ion channel protein: A promising target for anti-influenza drug discovery. *Mini Rev. Med. Chem.* **2014**, *14*, 819–830.
115. Deamer, D.W. Visualizing proton conductance in the gramicidin channel. *Biophys. J.* **1996**, *71*, 5. [CrossRef]
116. Pinto, L.H.; Dieckmann, G.R.; Gandhi, C.S.; Papworth, C.G.; Braman, J.; Shaughnessy, M.A.; Lear, J.D.; Lamb, R.A.; Degrado, W.F. A functionally defined model for the M2 proton channel of influenza A virus suggests a mechanism for its ion selectivity. *Proc. Natl. Acad. Sci. USA* **1997**, *94*, 11301–11306. [CrossRef] [PubMed]
117. Tang, Y.; Zaitseva, F.; Lamb, R.A.; Pinto, L.H. The gate of the influenza virus M2 proton channel is formed by a single tryptophan residue. *J. Biol. Chem.* **2002**, *277*, 39880–39886. [CrossRef]
118. Sansom, M.S.; Kerr, I.D.; Smith, G.R.; Son, H.S. The influenza A virus M2 channel: A molecular modeling and simulation study. *Virology* **1997**, *233*, 163–173. [CrossRef] [PubMed]

119. Zhong, Q.; Husslein, T.; Moore, P.B.; Newns, D.M.; Pattnaik, P.; Klein, M.L. The M2 channel of influenza A virus: A molecular dynamics study. *FEBS Lett.* **1998**, *434*, 265–271. [CrossRef]
120. Schnell, J.R.; Chou, J.J. Structure and mechanism of the M2 proton channel of influenza A virus. *Nature* **2008**, *451*, 591–595. [CrossRef] [PubMed]
121. Stouffer, A.L.; Acharya, R.; Salom, D.; Levine, A.S.; Di Costanzo, L.; Soto, C.S.; Tereshko, V.; Nanda, V.; Stayrook, S.; Degrado, W.F. Structural basis for the function and inhibition of an influenza virus proton channel. *Nature* **2008**, *451*, 596–599. [CrossRef]
122. Cady, S.D.; Schmidt-Rohr, K.; Wang, J.; Soto, C.S.; Degrado, W.F.; Hong, M. Structure of the amantadine binding site of influenza M2 proton channels in lipid bilayers. *Nature* **2010**, *463*, 689–692. [CrossRef]
123. Sharma, M.; Yi, M.; Dong, H.; Qin, H.; Peterson, E.; Busath, D.D.; Zhou, H.-X.; Cross, T.A. Insight into the mechanism of the influenza A proton channel from a structure in a lipid bilayer. *Science* **2010**, *330*, 509–512. [CrossRef]
124. Park, E.K.; Castrucci, M.R.; Portner, A.; Kawaoka, Y. The M2 ectodomain is important for its incorporation into influenza A virions. *J. Virol.* **1998**, *72*, 2449–2455. [CrossRef]
125. Pinto, L.H.; Lamb, R.A. Controlling influenza virus replication by inhibiting its proton channel. *Mol. Biosyst.* **2007**, *3*, 18–23. [CrossRef]
126. Acharya, R.; Carnevale, V.; Fiorin, G.; Levine, B.G.; Polishchuk, A.L.; Balannik, V.; Samish, I.; Lamb, R.A.; Pinto, L.H.; Degrado, W.F.; et al. Structure and mechanism of proton transport through the transmembrane tetrameric M2 protein bundle of the influenza A virus. *Proc. Natl. Acad. Sci. USA* **2010**, *107*, 15075–15080. [CrossRef]
127. Thomaston, J.L.; Woldeyes, R.A.; Nakane, T.; Yamashita, A.; Tanaka, T.; Koiwai, K.; Brewster, A.S.; Barad, B.A.; Chen, Y.; Lemmin, T.; et al. XFEL structures of the influenza M2 proton channel: Room temperature water networks and insights into proton conduction. *Proc. Natl. Acad. Sci. USA* **2017**, *114*, 13357–13362. [CrossRef]
128. Pielak, R.M.; Chou, J.J. Flu channel drug resistance: A tale of two sites. *Protein Cell* **2010**, *1*, 246–258. [CrossRef]
129. Holsinger, L.J.; Lamb, R.A. Influenza virus M2 integral membrane protein is a homotetramer stabilized by formation of disulfide bonds. *Virology* **1991**, *183*, 32–43. [CrossRef]
130. Sugrue, R.J.; Hay, A.J. Structural characteristics of the M2 protein of influenza A viruses: Evidence that it forms a tetrameric channel. *Virology* **1991**, *180*, 617–624. [CrossRef]
131. Okada, A.; Miura, T.; Takeuchi, H. Protonation of histidine and histidine-tryptophan interaction in the activation of the M2 ion channel from influenza A virus. *Biochemistry* **2001**, *40*, 6053–6060. [CrossRef]
132. Betakova, T.; Ciampor, F.; Hay, A.J. Influence of residue 44 on the activity of the M2 proton channel of influenza A virus. *J. Gen. Virol.* **2005**, *86*, 181–184. [CrossRef] [PubMed]
133. Pielak, R.M.; Chou, J.J. Influenza M2 proton channels. *Biochim. Biophys. Acta* **2011**, *1808*, 522–529. [CrossRef] [PubMed]
134. Ito, T.; Gorman, O.T.; Kawaoka, Y.; Bean, W.J.; Webster, R.G. Evolutionary analysis of the influenza A virus M gene with comparison of the M1 and M2 proteins. *J. Virol.* **1991**, *65*, 5491–5498. [CrossRef] [PubMed]
135. Deng, L.; Cho, K.J.; Fiers, W.; Saelens, X. M2e-based universal influenza A vaccines. *Vaccines* **2015**, *3*, 105–136. [CrossRef]
136. Wang, C.; Lamb, R.A.; Pinto, L.H. Activation of the M2 ion channel of influenza virus: A role for the transmembrane domain histidine residuE. *Biophys. J.* **1995**, *69*, 1363–1371. [CrossRef]
137. Venkataraman, P.; Lamb, R.A.; Pinto, L.H. Chemical rescue of histidine selectivity filter mutants of the M2 ion channel of influenza A virus. *J. Biol. Chem.* **2005**, *280*, 21463–21472. [CrossRef]
138. Kass, I.; Arkin, I.T. How pH opens a H^+ channel: The gating mechanism of influenza A M2. *Structure* **2005**, *13*, 1789–1798. [CrossRef]
139. Shimbo, K.; Brassard, D.L.; Lamb, R.A.; Pinto, L.H. Ion selectivity and activation of the M2 ion channel of influenza virus. *Biophys. J.* **1996**, *70*, 1335–1346. [CrossRef]
140. Yi, M.; Cross, T.A.; Zhou, H.-X. Conformational heterogeneity of the M2 proton channel and a structural model for channel activation. *Proc. Natl. Acad. Sci. USA* **2009**, *106*, 13311–13316. [CrossRef] [PubMed]
141. Khurana, E.; Dal Peraro, M.; Devane, R.; Vemparala, S.; Degrado, W.F.; Klein, M.L. Molecular dynamics calculations suggest a conduction mechanism for the M2 proton channel from influenza A virus. *Proc. Natl. Acad. Sci. USA* **2009**, *106*, 1069–1074. [CrossRef] [PubMed]
142. Mould, J.A.; Li, H.-C.; Dudlak, C.S.; Lear, J.D.; Pekosz, A.; Lamb, R.A.; Pinto, L.H. Mechanism for proton conduction of the M2 ion channel of influenza A virus. *J. Biol. Chem.* **2000**, *275*, 8592–8599. [CrossRef] [PubMed]
143. Smondyrev, A.M.; Voth, G.A. Molecular dynamics simulation of proton transport through the influenza A virus M2 channel. *Biophys. J.* **2002**, *83*, 1987–1996. [CrossRef]
144. Hu, F.; Luo, W.; Hong, M. Mechanisms of proton conduction and gating in influenza M2 proton channels from solid-state NMR. *Science* **2010**, *330*, 505–508. [CrossRef]
145. Cady, S.D.; Luo, W.; Hu, F.; Hong, M. Structure and function of the influenza A M2 proton channel. *Biochemistry* **2009**, *48*, 7356–7364. [CrossRef] [PubMed]
146. Hong, M.; Degrado, W.F. Structural basis for proton conduction and inhibition by the influenza M2 protein. *Protein Sci.* **2012**, *21*, 1620–1633. [CrossRef] [PubMed]
147. Hu, J.; Fu, R.; Nishimura, K.; Zhang, L.; Zhou, H.-X.; Busath, D.D.; Vijayvergiya, V.; Cross, T.A. Histidines, heart of the hydrogen ion channel from influenza A virus: Toward an understanding of conductance and proton selectivity. *Proc. Natl. Acad. Sci. USA* **2006**, *103*, 6865–6870. [CrossRef]

148. Liang, R.; Swanson, J.M.J.; Madsen, J.J.; Hong, M.; Degrado, W.F.; Voth, G.A. Acid activation mechanism of the influenza A M2 proton channel. *Proc. Natl. Acad. Sci. USA* **2016**, *113*, E6955–E6964. [CrossRef]
149. Hu, F.; Schmidt-Rohr, K.; Hong, M. NMR detection of pH-dependent histidine-water proton exchange reveals the conduction mechanism of a transmembrane proton channel. *J. Am. Chem. Soc.* **2012**, *134*, 3703–3713. [CrossRef]
150. Hay, A.J.; Wolstenholme, A.J.; Skehel, J.J.; Smith, M.H. The molecular basis of the specific anti-influenza action of amantadine. *EMBO J.* **1985**, *4*, 3021–3024. [CrossRef]
151. Balannik, V.; Carnevale, V.; Fiorin, G.; Levine, B.G.; Lamb, R.A.; Klein, M.L.; Degrado, W.F.; Pinto, L.H. Functional studies and modeling of pore-lining residue mutants of the influenza A virus M2 ion channel. *Biochemistry* **2010**, *49*, 696–708. [CrossRef] [PubMed]
152. Wright, A.K.; Batsomboon, P.; Dai, J.; Hung, I.; Zhou, H.-X.; Dudley, G.B.; Cross, T.A. Differential binding of rimantadine enantiomers to influenza A M2 proton channel. *J. Am. Chem. Soc.* **2016**, *138*, 1506–1509. [CrossRef] [PubMed]
153. Hirst, G.K. Adsorption of influenza hemagglutinins and virus by red blood cells. *J. Exp. Med.* **1942**, *76*, 195–209. [CrossRef] [PubMed]
154. Griffin, J.A.; Basak, S.; Compans, R.W. Effects of hexose starvation and the role of sialic acid in influenza virus release. *Virology* **1983**, *25*, 324–334. [CrossRef]
155. Kolocouris, A.; Spearpoint, P.; Martin, S.R.; Hay, A.J.; López-Querol, M.; Sureda, F.X.; Padalko, E.; Neyts, J.; de Clercq, E. Comparisons of the influenza virus A M2 channel binding affinities, anti-influenza virus potencies and NMDA antagonistic activities of 2-alkyl-2-aminoadamantanes and analogues. *Bioorg. Med. Chem. Lett.* **2008**, *18*, 6156–6160. [CrossRef] [PubMed]
156. Wang, J.; Cady, S.D.; Balannik, V.; Pinto, L.H.; Degrado, W.F.; Hong, M. Discovery of spiro-piperidine inhibitors and their modulation of the dynamics of the M2 proton channel from influenza A virus. *J. Am. Chem. Soc.* **2009**, *131*, 8066–8076. [CrossRef]
157. Jing, X.; Ma, C.; Ohigashi, Y.; Oliveira, F.A.; Jardetzky, T.S.; Pinto, L.H.; Lamb, R.A. Functional studies indicate amantadine binds to the pore of the influenza A virus M2 proton-selective ion channel. *Proc. Natl. Acad. Sci. USA* **2008**, *105*, 10967–10972. [CrossRef]
158. Luo, W.; Hong, M. Conformational changes of an ion channel detected through water-protein interactions using solid-state NMR spectroscopy. *J. Am. Chem. Soc.* **2010**, *132*, 2378–2384. [CrossRef]
159. Laursen, N.S.; Wilson, I.A. Broadly neutralizing antibodies against influenza viruses. *Antivir. Res.* **2013**, *98*, 476–483. [CrossRef]
160. Zebedee, S.L.; Lamb, R.A. Influenza A virus M2 protein: Monoclonal antibody restriction of virus growth and detection of M2 in virions. *J. Virol.* **1988**, *62*, 2762–2772. [CrossRef]
161. Padilla-Quirarte, H.O.; Lopez-Guerrero, D.V.; Gutierrez-Xicotencatl, L.; Esquivel-Guadarrama, F. Protective antibodies against influenza proteins. *Front. Immunol.* **2019**, *10*. [CrossRef]
162. Manzoor, R.; Eguchi, N.; Yoshida, R.; Ozaki, H.; Kondoh, T.; Okuya, K.; Miyamoto, H.; Takada, A. A novel mechanism underlying antiviral activity of an influenza virus M2-specific antibody. *J. Virol.* **2020**, *95*. [CrossRef]
163. Okuya, K.; Eguchi, N.; Manzoor, R.; Yoshida, R.; Saito, S.; Suzuki, T.; Sasaki, M.; Saito, T.; Kida, Y.; Mori-Kajihara, A.; et al. Comparative analyses of the antiviral activities of IgG and IgA antibodies to influenza A virus M2 protein. *Viruses* **2020**, *12*, 780. [CrossRef] [PubMed]
164. Kolpe, A.; Arista-Romero, M.; Schepens, B.; Pujals, S.; Saelens, X.; Albertazzi, L. Super-resolution microscopy reveals significant impact of M2e-specific monoclonal antibodies on influenza A virus filament formation at the host cell surface. *Sci. Rep.* **2019**, *9*. [CrossRef] [PubMed]
165. Skalickova, S.; Heger, Z.; Krejcova, L.; Pekarik, V.; Bastl, K.; Janda, J.; Kostolansky, F.; Vareckova, E.; Zitka, O.; Adam, V.; et al. Perspective of use of antiviral peptides against influenza virus. *Viruses* **2015**, *7*, 5428–5442. [CrossRef] [PubMed]
166. Jung, Y.; Kong, B.; Moon, S.; Yu, S.H.; Chung, J.; Ban, C.; Chung, W.J.; Kim, S.G.; Kweon, D.H. Envelope-deforming antiviral peptide derived from influenza virus M2 protein. *Biochem. Biophys. Res. Commun.* **2019**, *517*, 507–512. [CrossRef]
167. Webster, R.G.; Laver, W.G.; Kilbourne, E.D. Reactions of antibodies with surface antigens of influenza virus. *J. Gen. Virol.* **1968**, *3*, 315–326. [CrossRef]
168. Palese, P.; Tobita, K.; Ueda, M.; Compans, R.W. Characterization of temperature sensitive influenza virus mutants defective in neuraminidase. *Virology* **1974**, *61*, 397–410. [CrossRef]
169. Burnet, F.M.; Stone, J.D. The receptor-destroying enzyme of V. cholerae. *Aust. J. Exp. Biol. Med. Sci.* **1947**, *25*, 227–233. [CrossRef]
170. Colman, P.M.; Tulip, W.R.; Varghese, J.N.; Tulloch, P.A.; Baker, A.T.; Laver, W.G.; Air, G.M.; Webster, R.G. Three-dimensional structures of influenza virus neuraminidase-antibody complexes. *Philos. Trans. R. Soc. Lond. B. Biol. Sci.* **1989**, *323*, 511–518.
171. Varghese, J.N.; Laver, W.G.; Colman, P.M. Structure of the influenza virus glycoprotein antigen neuraminidase at 2.9 Å resolution. *Nature* **1983**, *303*, 35–40. [CrossRef] [PubMed]
172. Russell, R.J.; Gamblin, S.J.; Skehel, J.J. Influenza glycoproteins: Hemagglutinin and neuraminidase. *Textb. Influenza* **2013**. [CrossRef]
173. Vavricka, C.J.; Liu, Y.; Kiyota, H.; Sriwilaijaroen, N.; Qi, J.; Tanaka, K.; Wu, Y.; Li, Q.; Li, Y.; Yan, J.; et al. Influenza neuraminidase operates via a nucleophilic mechanism and can be targeted by covalent inhibitors. *Nat. Commun.* **2013**, *4*, 1491. [CrossRef] [PubMed]
174. Russell, R.J.; Haire, L.F.; Stevens, D.J.; Collins, P.J.; Lin, Y.P.; Blackburn, G.M.; Hay, A.J.; Gamblin, S.J.; Skehel, J.J. The structure of H5N1 avian influenza neuraminidase suggests new opportunities for drug design. *Nature* **2006**, *443*, 45–49. [CrossRef]
175. Zhu, X.; Xu, X.; Wilson, I.A. Structure determination of the 1918 H1N1 neuraminidase from a crystal with lattice-translocation defects. *Acta Crystallogr. D Biol. Crystallogr.* **2008**, *D64*, 843–850. [CrossRef]

176. Wang, M.; Qi, J.; Liu, Y.; Vavricka, C.J.; Wu, Y.; Li, Q.; Gao, G.F. Influenza A virus N5 neuraminidase has an extended 150-cavity. *J. Virol.* **2011**, *85*, 8431–8435. [CrossRef]
177. Baker, A.T.; Varghese, J.N.; Laver, W.G.; Air, G.M.; Colman, P.M. Three-dimensional structure of neuraminidase of subtype N9 from an avian influenza virus. *Proteins Struct. Funct. Bioinform.* **1987**, *2*, 111–117. [CrossRef]
178. Cheng, C.K.; Tsai, C.H.; Shie, J.J.; Fang, J.M. From neuraminidase inhibitors to conjugates: A step towards better anti-influenza drugs? *Future Med. Chem.* **2014**, *6*, 757–774. [CrossRef] [PubMed]
179. Colman, P.M.; Varghese, J.N.; Laver, W.G. Structure of the catalytic and antigenic sites in influenza virus neuraminidase. *Nature* **1983**, *303*, 41–44. [CrossRef] [PubMed]
180. Bossart-Whitaker, P.; Carson, M.; Babu, Y.S.; Smith, C.D.; Laver, W.G.; Air, G.M. Three-dimensional structure of influenza a N9 neuraminidase and its complex with the inhibitor 2-deoxy 2,3-dehydro-N-acetyl neuraminic acid. *J. Mol. Biol.* **1993**, *232*, 1069–1083. [CrossRef] [PubMed]
181. Varghese, J.N.; Colman, P.M. Three-dimensional structure of the neuraminidase of influenza virus A/Tokyo/3/67 at 2·2 Å resolution. *J. Mol. Biol.* **1991**, *221*, 473–486. [CrossRef]
182. McAuley, J.L.; Gilbertson, B.P.; Trifkovic, S.; Brown, L.E.; McKimm-Breschkin, J.L. Influenza virus neuraminidase structure and functions. *Front. Microbiol.* **2019**, *10*, 39. [CrossRef] [PubMed]
183. Vavricka, C.J.; Li, Q.; Wu, Y.; Qi, J.; Wang, M.; Liu, Y.; Gao, F.; Liu, J.; Feng, E.; He, J.; et al. Structural and functional analysis of laninamivir and its octanoate prodrug reveals group specific mechanisms for influenza NA inhibition. *PLoS Pathog.* **2011**, *7*, e1002249. [CrossRef]
184. Krammer, F.; Fouchier, R.A.M.; Eichelberger, M.C.; Webby, R.J.; Shaw-Saliba, K.; Wan, H.; Wilson, P.C.; Compans, R.W.; Skountzou, I.; Monto, A.S. NAction! how can neuraminidase-based immunity contribute to better influenza virus vaccines? *MBio* **2018**, *9*. [CrossRef]
185. Colman, P.M.; Hoyne, P.A.; Lawrence, M.C. Sequence and structure alignment of paramyxovirus hemagglutinin-neuraminidase with influenza virus neuraminidase. *J. Virol.* **1993**, *67*, 2972–2980. [CrossRef]
186. Kim, C.U.; Chen, X.; Mendel, D.B. Neuraminidase inhibitors as anti-influenza virus agents. *Anti Viral Chem. Chemother.* **1999**, *10*, 141–154. [CrossRef]
187. Gong, J.; Xu, W.; Zhang, J. Structure and functions of influenza virus neuraminidase. *Curr. Med. Chem.* **2007**, *14*, 113–122. [CrossRef]
188. Stoll, V.; Stewart, K.D.; Maring, C.J.; Muchmore, S.; Giranda, V.; Gu, Y.-G.Y.; Wang, G.; Chen, Y.; Sun, M.; Zhao, C.; et al. Influenza neuraminidase inhibitors: Structure-based design of a novel inhibitor series. *Biochemistry* **2003**, *42*, 718–727. [CrossRef]
189. von Itzstein, M.; Wu, W.-Y.; Kok, G.B.; Pegg, M.S.; Dyason, J.C.; Jin, B.; van Phan, T.; Smythe, M.L.; White, H.F.; Oliver, S.W.; et al. Rational design of potent sialidase-based inhibitors of influenza virus replication. *Nature* **1993**, *363*, 418–423. [CrossRef] [PubMed]
190. Ge, H.; Wang, Y.-F.; Xu, J.; Gu, Q.; Liu, H.-B.; Xiao, P.-G.; Zhou, J.; Liu, Y.; Yang, Z.; Su, H. Anti-influenza agents from Traditional Chinese Medicine. *Nat. Prod. Rep.* **2010**, *27*, 1758. [CrossRef]
191. Meyer, E. Internal water molecules and H-bonding in biological macromolecules: A review of structural features with functional implications. *Protein Sci.* **1992**, *1*, 1543–1562. [CrossRef] [PubMed]
192. Chong, A.K.J.; Pegg, M.S.; Taylor, N.R.; von Itzstein, M. Evidence for a sialosyl cation transition-state complex in the reaction of sialidase from influenza virus. *Eur. J. Biochem.* **1992**, *207*, 335–343. [CrossRef]
193. Taylor, N.R.; von Itzstein, M. Molecular modeling studies on ligand binding to sialidase from influenza virus and the mechanism of catalysis. *J. Med. Chem.* **1994**, *37*, 616–624. [CrossRef]
194. Meindl, P.; Bodo, G.; Palese, P.; Schulman, J.; Tuppy, H. Inhibition of neuraminidase activity by derivatives of 2-deoxy-2,3-dehydro-N-acetylneuraminic acid. *Virology* **1974**, *58*, 457–463. [CrossRef]
195. Goodford, P. Multivariate characterization of molecules for QSAR analysis. *J. Chemom.* **1996**, *10*, 107–117. [CrossRef]
196. Holzer, C.T.; von Itzstein, M.; Jin, B.; Pegg, M.S.; Stewart, W.P.; Wu, W.-Y. Inhibition of sialidases from viral, bacterial and mammalian sources by analogues of 2-deoxy-2,3-didehydro-N-acetylneuraminic acid modified at the C-4 position. *Glycoconj. J.* **1993**, *10*, 40–44. [CrossRef]
197. von Itzstein, M.; Dyason, J.C.; Oliver, S.W.; White, H.F.; Wu, W.-Y.; Kok, G.B.; Pegg, M.S. A study of the active site of influenza virus sialidase: An approach to the rational design of novel anti-influenza drugs. *J. Med. Chem.* **1996**, *39*, 388–391. [CrossRef]
198. Phillips, D.C. The three-dimensional structure of an enzyme molecule. *Sci. Am.* **1966**, *215*, 78–90. [CrossRef] [PubMed]
199. Kim, C.U.; Lew, W.; Williams, M.A.; Liu, H.; Zhang, L.; Swaminathan, S.; Bischofberger, N.; Chen, M.S.; Mendel, D.B.; Tai, C.Y.; et al. Influenza neuraminidase inhibitors possessing a novel hydrophobic interaction in the enzyme active site: Design, synthesis, and structural analysis of carbocyclic sialic acid analogues with potent anti-influenza activity. *J. Am. Chem. Soc.* **1997**, *119*, 681–690. [CrossRef] [PubMed]
200. Li, W.; Escarpe, P.A.; Eisenberg, E.J.; Cundy, K.C.; Sweet, C.; Jakeman, K.J.; Merson, J.; Lew, W.; Williams, M.; Zhang, L.; et al. Identification of GS 4104 as an orally bioavailable prodrug of the influenza virus neuraminidase inhibitor GS 4071. *Antimicrob. Agents Chemother.* **1998**, *42*, 647. [CrossRef]
201. Kim, C.U.; Lew, W.; Williams, M.A.; Wu, H.; Zhang, L.; Chen, X.; Escarpe, P.A.; Mendel, D.B.; Laver, W.G.; Stevens, R.C. Structure—Activity relationship studies of novel carbocyclic influenza neuraminidase inhibitors. *J. Med. Chem.* **1998**, *41*, 2451–2460. [CrossRef]

202. Babu, Y.S.; Chand, P.; Bantia, S.; Kotian, P.; Dehghani, A.; El-Kattan, Y.; Lin, T.-H.; Hutchison, T.L.; Elliott, A.J.; Parker, C.D.; et al. BCX-1812 (RWJ-270201): Discovery of a novel, highly potent, orally active, and selective influenza neuraminidase inhibitor through structure-based drug design. *J. Med. Chem.* **2000**, *43*, 3482–3486. [CrossRef]
203. Bantia, S.; Arnold, C.S.; Parker, C.D.; Upshaw, R.; Chand, P. Anti-influenza virus activity of peramivir in mice with single intramuscular injection. *Antivir. Res.* **2006**, *69*, 39–45. [CrossRef]
204. Mclaughlin, M.M.; Skoglund, E.W.; Ison, M.G. Peramivir: An intravenous neuraminidase inhibitor. *Expert Opin. Pharmacother.* **2015**, *16*, 1889–1900. [CrossRef]
205. Scott, L.J. Peramivir: A review in uncomplicated influenza. *Drugs* **2018**, *78*, 1363–1370. [CrossRef] [PubMed]
206. Yamashita, M. Laninamivir and its prodrug, CS-8958: Long-acting neuraminidase inhibitors for the treatment of influenza. *Anti-viral Chem. Chemother.* **2010**, *21*, 71–84. [CrossRef] [PubMed]
207. Ikematsu, H.; Kawai, N. Laninamivir octanoate: A new long-acting neuraminidase inhibitor for the treatment of influenza. *Expert Rev. Anti Infect. Ther.* **2011**, *9*, 851–857. [CrossRef] [PubMed]
208. Ishizuka, H.; Toyama, K.; Yoshiba, S.; Okabe, H.; Furuie, H. Intrapulmonary distribution and pharmacokinetics of laninamivir, a neuraminidase inhibitor, after a single inhaled administration of its prodrug, laninamivir octanoate, in healthy volunteers. *Antimicrob. Agents Chemother.* **2012**, *56*, 3873. [CrossRef] [PubMed]
209. Zhao, Z.X.; Cheng, L.P.; Li, M.; Pang, W.; Wu, F.H. Discovery of novel acylhydrazone neuraminidase inhibitors. *Eur. J. Med. Chem.* **2019**, *173*, 305–313. [CrossRef] [PubMed]
210. Yu, R.; Cheng, L.P.; Li, M.; Pang, W. Discovery of novel neuraminidase inhibitors by structure-based virtual screening, structural optimization, and bioassay. *ACS Med. Chem. Lett.* **2019**, *10*, 1667–1673. [CrossRef]
211. Li, M.; Cheng, L.P.; Pang, W.; Zhong, Z.J.; Guo, L.L. Design, synthesis, and biological evaluation of novel acylhydrazone derivatives as potent neuraminidase inhibitors. *ACS Med. Chem. Lett.* **2020**, *11*, 1745–1750. [CrossRef] [PubMed]
212. Jia, R.; Zhang, J.; Ai, W.; Ding, X.; Desta, S.; Sun, L.; Sun, Z.; Ma, X.; Li, Z.; Wang, D.; et al. Design, synthesis and biological evaluation of "Multi-Site"-binding influenza virus neuraminidase inhibitors. *Eur. J. Med. Chem.* **2019**, *178*, 64–80. [CrossRef]
213. Ju, H.; Zhang, J.; Sun, Z.; Huang, Z.; Qi, W.; Huang, B.; Zhan, P.; Liu, X. Discovery of C-1 modified oseltamivir derivatives as potent influenza neuraminidase inhibitors. *Eur. J. Med. Chem.* **2018**, *146*, 220–231. [CrossRef] [PubMed]
214. Xie, Y.; Xu, D.; Huang, B.; Ma, X.; Qi, W.; Shi, F.; Liu, X.; Zhang, Y.; Xu, W. Discovery of N-substituted oseltamivir derivatives as potent and selective inhibitors of H5N1 influenza neuraminidase. *J. Med. Chem.* **2014**, *57*, 8445–8458. [CrossRef]

Chapter 3

COMPUTATIONAL METHODS

3. COMPUTATIONAL METHODS

3.1 INTRODUCTION

Recent years have seen wonderful growth in the use of computers to calculate chemical properties, such as molecular geometry, discrete spectra, mechanisms behind reactivity, and electronics to name a few [1]. As a result, computational techniques such as molecular dynamics (MD) since become more beneficial in drug discovery and development [2]. A method of solving chemical problems, MD was discovered in the late 1970s [3,4]. It employs tools such as molecular mechanics (MM), quantum mechanics (QM), statistical mechanics, semi-empirical methods, and hybrid techniques [5]. By combining features from a number of approximations, hybrid techniques can deliver cost-effective solutions with good accuracy [6]. This chapter provides an outline of computational methods used in this study.

3.2 MOLECULAR MECHANICS

Conventional physics approximations are used to simulate molecular systems in molecular mechanics [7–9]. These techniques rely on mathematical models that define atoms and bonds as particles that are connected by springs. MM defines a molecule as a group of massed particles interacting by means of harmonic forces, similar to Hooke's ball and spring model [10]. In MM, the bond length and angle of each molecule are assumed to have ideal values at equilibrium [11,12]. According to equation **3.1**, the sum potential energy of a molecular system is therefore directly related to the deviation of a molecule from its ideal geometry caused by the bonding and non-bonding interactions [13]**.**

$$v = \sum_{bonds} V_{stretch} + \sum_{angles} V_{bend} + \sum_{dihedrals} V_{torsion} + \sum_{non-bonded\ pairs} V_{non-bonded} \qquad \textbf{(3.1)}$$

Interactions between bonded systems include stretching, torsion and angle bending, while non-bonded interactions (Equation **(3.2)**) cover van der Waal's and electrostatic forces, dependent upon distance r.

$$V_{non-bonded}(r) = V_{Van\ der\ Waals}(r) + V_{Coulombic}(r) \qquad \textbf{(3.2)}$$

Due to the large mass difference between the nucleus and electrons, the Born-Oppenheimer approximation reveals that motions of nuclei and electrons can be separated. Since the mass of a nucleus is larger than that of electrons, the movement of each nucleus causes an instantaneous motion of its electrons. An atom's energy can thus be calculated solely based on its nuclear coordinates without taking into consideration its electrons. A set of parameterized functions (FFs) [14,15] of the type outlined in equation **(3.3)** is then used to calculate the potential energy of a system.

$$v = \sum_{i}^{bonds} \frac{k_{l,i}}{2}(l_i - l_{o,i})^2 + \sum_{i}^{angles} \frac{k_{\alpha,i}}{2}(\alpha_i - \alpha_{o,i})^2 + \sum_{i}^{torsions} \left\{\sum_{k}^{M} \frac{V_{i,k}}{2}\left[1 + \cos(n_{ik}.\theta_{ik} - \theta_{ik})\right]\right\} + \sum_{i,j}^{pairs} \varepsilon_{ij}\left[\left(\frac{r_{o,ij}}{r_{ij}}\right)^{12} - 2\left(\frac{r_{o,ij}}{r_{ij}}\right)^{6}\right] + \sum_{i,j}^{pairs} \frac{q_i q_j}{4\pi\varepsilon_o\varepsilon_r r_{ij}} \quad \textbf{(3.3)}$$

As a function of bonding relations such as stretching, bending and twisting, the first three terms of the equation are models of harmonic potentials to show the variations in potential energy of atoms. The first term represents the deviation of bond lengths where k_l defines the force constant, l_i and $l_{0,i}$ denote the normal and optimal bond length amongst two atoms, respectively. In the second term, k_α is the force potential. It measures the deviation of bond *angles* $\alpha_{0,1}$ from its equilibrium value α_1. In the third term, for each dihedral angle, the torsional rotations are determined by a cosine series of M terms due to their inherent periodicity. A parameter n_{ik} is used to define the *k*th term of the series, while the phase angle is given by $\theta_{0,ik}$ and the energy barrier is defined by V_{ik} [5].

The last two terms in the FF correspond to the nonbonded van der Waal's interaction and Coulomb's interaction, respectively. The van der Waal's contributions to the energy between atoms *i* and *j* have been treated with a 12-6 Lennard-Jones (L-J) potential [16], with ε_{ij} being L-J well depth; r_{ij} refers to the distance between the two atoms *i* and *j* and $r_{0,ij}$ refers to the interatomic distance at the L-J energy minima. Last but not least is the Coulombic potential, which describes electrostatic interactions. In this case, q_i and q_j represent the partial charges of interacting atoms, ε_o and ε_r denote the inductive capacity of free space and the relative dielectric constant, respectively [17].

The unique advantage of MM methods is that they are fast, allowing them to compute molecules made up of thousands of atoms. In computational chemistry, MM tools are extensively explored for studying conformational analysis and energy minimization [5]. The standard parameterization of MM FF energy calculations are not suitable for modeling chemical reactions, even though they are fast and inexpensive. The reason for this is that FFs do not take into account the electronic structure. As the years have gone by, many general FFs have been developed and those that are specific to particular functional groups and compounds have also been developed. These comprise of CHARMM [18], GROMOS [19], OPLS [20–22], and AMBER [23] among the widely used FFs for the simulation of biomolecules. In this thesis, ligands were parameterized using General AMBER Force Field (GAFF), and water was modelled using 3-point transferable intermolecular potential (TIP3P) due to its computational efficiency [24].

3.3 QUANTUM MECHANICS

The Born Oppenheimer approximation in MM models separates the motion of the electrons in an atom from that of its nuclei, but in quantum mechanics molecules are treated as nuclei and electrons as their electrons [11,25]. QM's fundamental principles are Heisenberg theories or non-relativistic time-dependent Schrödinger equations. Equation **3.4** summarizes those principles that are discussed in this thesis [2,10].

$$\hat{\mathrm{H}}\psi = \mathrm{E}\psi \tag{3.4}$$

Schrödinger wave equation is given by equation **3.4**, where $\hat{H}$ denotes the Hamiltonian operator [26], E describes the energy of state, and the wavefunction Ψ mathematically denotes the state of the system. Schrödinger's wave equation describes the relationship between space and time by using the function Ψ. QM can be used to model energy and associated properties of some molecule, however, in practice it is only possible to model electron dynamics for a single electron species [5,26].

3.3.1 Electronic structure methods

Electronic structure methods employ quantum mechanics laws, based on the Schr*ö*dinger wave equation [1,10,13]. Among these are *ab-initio* methods, semi-empirical and the density functional methods. Using theoretical approaches founded on physical constants and the Schr*ö*dinger wave equation, *ab-initio* methods use a wavefunction to calculate the electronic structure [25]. It is not practical to solve the Schr*ö*dinger wave equation for multi-electron systems directly. Therefore, numerous approximations are employed in *ab initio* methods. By extension, these approximations determine a system's cost and reliability. Semi-empirical methods use simplified Hamiltonians and parameters derived from experimental data [10]. Semi-empirical methods are faster than *ab-initio* techniques and do remarkably well for the systems they are parameterized for. Semi-empirical methods have the disadvantage of being less accurate than ab-initio methods [25,26]. In contrast to *ab-initio* methods, density functional methods use electron density rather than wavefunctions to discover electronic structure. The speed of density functional methods is dependent on the approximation used for *ab-initio* methods. Here, as a preface to the discussion of the chosen methods, several concepts of interest are briefly outlined.

3.3.1.1 The Hamiltonian operator

The Schr*ö*dinger wave equation contains Hamiltonian operator terms that combine electron and nuclear kinetic and potential energy [25,26].

$$H = T_e + T_n + V_{en} + V_{ee} + V_{nn} \tag{3.5}$$

Here T_e and T_n are the operators for electrons and nuclei kinetic energy respectively; V_{en} denotes the electron-nuclei Coulombic attraction; V_{ee} defines the electron-electron Coulombic repulsion; and V_{nn} represents the nucleus-nucleus repulsion. For N electrons (i,j) and M nuclei (A,B) the Hamiltonian is denoted by:

$$H = -\sum_{i=1}^{N}\frac{1}{2}\nabla_i^2 - \sum_{A=1}^{M}\frac{1}{2M_A}\nabla_i^2 - \sum_{i=1}^{N}\sum_{A=1}^{M}\frac{Z_A}{r_{iA}} + \sum_{i=1}^{N}\sum_{j>1}^{N}\frac{1}{r_{ij}} + \sum_{A=1}^{M}\sum_{B>1}^{M}\frac{Z_A Z_B}{R_{AB}} \tag{3.6}$$

In this case, R_{AB} and r_{ij} are the distance vectors between the nuclei and electrons respectively, Z_A represents the atomic number of nucleus A and M_A defines the mass ratio of nucleus A and an electron [13,25,26].

3.3.1.2 Born-Oppenheimer approximation

Due to the weight of nuclei being much greater than that of electrons, their relative speeds are much slower than those of electrons surrounding them. Assuming that nuclei have a fixed position, it is possible to solve the Schrödinger wave equation solely for electrons at a given nuclear position [27]. With the Born-Oppenheimer approximation, nuclei and electron movements are separated, yielding an electronic Hamiltonian that is dependent only on nuclei positions [25,28].

$$H_{el} = -\sum_{i=1}^{N}\frac{1}{2}\nabla_i^2 - \sum_{i-1}^{N}\sum_{A=1}^{M}\frac{Z_A}{r_{iA}} + \sum_{i-1}^{N}\sum_{J>I}^{N}\frac{1}{r_{iJ}} \quad \textbf{(3.7)}$$

3.4 HYBRID QUANTUM MECHANICS/MOLECULAR MECHANICS (QM/MM)

In addition to the objective of gathering accurate electronic and dynamic structural information of large biological systems, like enzymes, simulations are meant to do so in a rapid, cost-effective manner. MM approaches with a large computation capacity are preferred [13]. QM gives electronic structure information of these systems, but it is computationally expensive and especially suited to small molecular systems. MM however does not offer this information, and on that basis, QM is preferred. Hybrid QM/MM approaches have been extensively used in large biological systems in order to combine the speed and accuracy of MM and QM methods [29]. QM analyses the tiny reactive and electronically significant part of the system and Force Field defines the smaller nonreactive part of the system [11]. In a MD simulation, the whole system is simulated. The energy of the hybrid QM/MM system is expressed as follows:

$$E_{tot} = E_{QM} + E_{MM} + E_{\frac{QM}{MM}} \quad \textbf{(3.8)}$$

an inner system plus link atom energy is EQM, EMM is the energy treated with a Force Field and $E_{\frac{QM}{MM}}$ defines the energy of the MD area coupling between inner QM and outer FF [26]. QM/MM's MD area consists of both bonded and non-bonded terms, so it is of the utmost importance. The coupling energy is expressed as follows:

$$E_{\frac{QM}{MM}} = E^{b}_{\frac{QM}{MM}} + E^{van\ der\ Waals}_{\frac{QM}{MM}} + E^{Coulombic}_{\frac{QM}{MM}} \quad \textbf{(3.9)}$$

To treat the electrostatic coupling amongst QM charge density and FF point charge field, mechanical, electrostatic, or electronic strategies are used. The mechanical embedding scheme can be evaluated at FF level and does not polarize the reactive region. As QM simulation is performed in the presence of a Force Field point charge field [29], electrostatic embedding

improves this by adding one electron terms to the Hamiltonian incorporating the Force Field point charge. Adding electronic embedding to electrostatic coupling increases simulation cost dramatically [30]. Hamiltonian with electrostatic coupling electronic embedding is as follows:

$$\hat{H}_{\frac{QM}{MM}}^{Coulombic} = -\sum_{l}^{N_{Coulombic}} \sum_{B}^{N_{MM}} \frac{q_B}{|r_l - R_B|} + \sum_{A}^{N_{QM}} \sum_{B}^{N_{MM}} \frac{q_B Z_A}{|R_A - R_B|} \quad \textbf{(3.10)}$$

where I, B and A indices cover the number of electrons *($N_{Coulombic}$),* the number of QM nuclei *(N_{QM}),* and the Force Field point charges *(N_{MM}).* The first term denotes the interaction of the QM electrons and FF point charges, and the second represents the interaction of the QM nuclei A of charge Z_A with FF point charges q_B. For hybrid QM/MM techniques, good descriptions of the QM zone are key, and the interaction between QM and FF parts needs to be calibrated. [10,30]. MD simulations produce dynamic and structural results for the two parts. An overview of MD simulation techniques can be found below.

3.5 MOLECULAR DYNAMICS

Predictive molecular dynamics is a technique of molecular dynamics wherein present conditions of the system are used to forecast future conditions [32]. The potential energy of the system is employed to calculate the forces acting on each atom in order to compute a profile of the subsequent states using molecular mechanics [8]. Using Newton's second law of motion (Equation **3.11**), forces derived from molecular mechanical computations are translated into accelerations of atoms in accordance with classical physics:

$$\overrightarrow{F_l}(t) = \frac{d^2\overrightarrow{r_l}(t)}{dt^2} . m_i = -\frac{dE_{tot}(t)}{d\overrightarrow{r_l}} \quad \textbf{(3.11)}$$

where $\overrightarrow{r_l}$ and E_{tot} are the i^{th} atom position and the total energy. Because force is directly proportional to acceleration, MD simulations calculate future positions of atoms by incorporating acceleration with their current positions along with their velocities. The motion profile of all atoms is generated by repeating this process in minute time steps [5,13,33]. Numerous structural and dynamic attributes of proteins may be determined from the MD trajectory data output. These post-dynamics methods and calculations were used in this thesis to describe the protein features.

3.5.1 Root Mean Square Deviation (RMSD)

Calculating Root Mean Square Deviation allows measurement of the atoms or atom groups displacement [34]. For a set of N atoms, the time averaged RMSD is calculated as follows:

$$RMSD = \sqrt{\frac{\sum_{i=1}^{N} di^2}{N}} \quad \textbf{(3.12)}$$

where *di* is the distance from atom *i* to the arithmetic mean location of the N corresponding atoms [13,35].

3.5.2 Root mean square fluctuations (RMSF)

Root Mean Square Fluctuation is a calculation that approximates the fluctuation of an atom or group of atoms based on [34]:

$$sRMSF_i = \frac{(RSMSF_i - RMSF)}{\sigma(RMSF)} \quad \textbf{(3.13)}$$

where $RMSF_i$ denotes the RMSF of the i^{th} amino acid residue, which is deducted from the average RMSF. The standardized RMSF (sRMSF*i*) is computed by dividing standard deviation of the RMSF [σ(RMSF)] by RMSF [13,35].

3.5.3 Radius of gyration (RoG)

The equilibrium conformation of a protein in each trajectory in MD simulation is called RoG. The RoG describes the RMSD of atom or atom groups from the mutual centre of gravity of a given protein structure [36]. The RoG is calculated using the following equation:

$$r^2g = \frac{\sum_{i=0}^{n} W_i(r_i - r^-)^2}{\sum_{i=1}^{n} W_i} \quad \textbf{(3.14)}$$

where r_i denotes the location of the i^{th} atom whereas r represents the central mass atom of *i*. RoG values are divided by the number of frames in each trajectory to determine the mean.

3.5.4 Binding Energy Calculations

A Molecular Mechanics/Generalized Born Surface Area (MM/GBSA) approach was employed to approximate the binding free energy profiles [37–40]. Binding free energy calculations provide a worthful understanding into the interactions of the protein-ligand complex. The following equations provide a detailed explanation of binding free energy calculations:

$$\Delta G_{bind} = G_{complex} - G_{receptor} - G_{ligand} \quad \textbf{(3.15)}$$

$$\Delta G_{bind} = E_{gas} + G_{sol} - T\Delta S \quad \textbf{(3.16)}$$

$$E_{gas} = E_{int} + E_{vdW} + E_{ele} \quad \textbf{(3.17)}$$

$$G_{sol} = G_{GB} + G_{SA} \quad \textbf{(3.18)}$$

$$G_{SA} = \gamma SASA \quad \textbf{(3.19)}$$

where $G_{complex}$ represent the total binding free energy of the protein-ligand complex, $G_{receptor}$ denotes the total binding free energies of the protein while ΔG_{ligand} represent the total binding free energies of the ligand [40]. E_{gas} signifies gas-phase energy and denotes evaluated directly from the Amber ff99SB force field terms. G_{sol} is solvation-free energy that could be

disintegrated into polar and nonpolar contribution conditions. TΔS defines the temperature and entropy contribution to the free energy. E_{int} denotes the internal energy, E_{ele} represent the intramolecular electrostatic energies and E_{vdW} is the van der Waals energies. The solvation-free energy, G_{sol}, is the energy needed to channel a solute from vacuum into a solvent. The electrostatic contribution to the solvation binding free energy is G_{GB}, while the non-electrical contribution is G_{SA}. G_{GB} was calculated by the Poisson-Boltzmann (PB) equation whereas G_{SA} was estimated using the solvent accessible surface area (SASA) equation.

3.5.5 Principal components analysis (PCA)

PCA was used visualize and analyze atomic dynamic movements of MD simulations' trajectories [41]. Each trajectory of MD simulation was calculated for the covariance matrix between residues i and j [42]. In-house scripts were used to calculate the first two principal components (PC1 and PC2) and generate the covariance matrix. The first two principal components equate to the first two Eigenvectors of the covariance matrix. The equations **3.20** and **3.21** below provide a technique for determining the flexibility of a system.

$$cov\ (X,Y) = \frac{1}{n-1}\left(\sum_{i}^{n}(X_i - \bar{X})\ (Y_i - \bar{Y})\right) \quad \textbf{(3.20)}$$

$$cov\ (X,Y) = \frac{1}{n-1}\left(\sum_{i}^{n} X_i Y_i - n\bar{X}\ \bar{Y}\right) \quad \textbf{(3.21)}$$

The covariance function is represented as, $cov\ (X, Y)$. It is defined by the size of the data set (n), the mean of X and Y values ($\bar{X}\ \bar{Y}$), and the sum product of data values X and Y ($\sum_i^n X_i Y_i$). Additionally, correlation is another way to identify and compare proteins during a trajectory.

$$r_{XY} = \frac{cov\ (X,Y)}{\sqrt{Var(X)Var(Y)}} \quad \textbf{(3.22)}$$

A correlation coefficient (equation **3.22**) indicates the strength of linear association between two variables which are quantified as being independent of one another. A correlation coefficient (r_{XY}), on the other hand, is not ruled by any measures or units imposed by the system. This is accomplished by relating the covariance ($Cov\ (X, Y)$) and variance of X and Y ($Var(X)Var(Y)$) [43,44].

3.6 REFERENCES

1. Van Eldik, R.; Puchta, R. *Computational Chemistry*; 2019; Vol. 73; ISBN 9780128157299.

2. Cavasotto, C.N.; Aucar, M.G.; Adler, N.S. Computational chemistry in drug lead discovery and design. *Int. J. Quantum Chem.* **2019**, *119*, 25678,

doi:10.1002/qua.25678.

3. McCammon, J.A.; Gelin, B.R.; Karplus, M. Dynamics of folded proteins. *Nature* **1977**, *267*, 585–590, doi:10.1038/267585a0.

4. Khan, S.H.; Prakash, A.; Pandey, P.; Lynn, A.M.; Islam, A.; Hassan, M.I.; Ahmad, F. Protein folding: Molecular dynamics simulations and in vitro studies for probing mechanism of urea- and guanidinium chloride-induced unfolding of horse cytochrome-c. *Int. J. Biol. Macromol.* **2019**, *122*, 695–704, doi:10.1016/J.IJBIOMAC.2018.10.186.

5. De Vivo, M.; Masetti, M.; Bottegoni, G.; Cavalli, A. Role of Molecular Dynamics and Related Methods in Drug Discovery. *J. Med. Chem.* 2016, *59*, 4035–4061.

6. Durrant, J.D.; McCammon, J.A. Molecular dynamics simulations and drug discovery. *BMC Biol.* **2011**, *9*, 71, doi:10.1186/1741-7007-9-71.

7. Hartmann, M. Molecular mechanics. *Acta Polym.* **1984**, *35*, 528–528, doi:10.1002/actp.1984.010350714.

8. Sansom, C.E.; Smith, C.A. Computer applications in the biomolecular sciences. Part 1: molecular modelling. *Biochem. Educ.* **1998**, *26*, 103–110, doi:10.1016/S0307-4412(97)00155-6.

9. Hofer, T.S.; de Visser, S.P. Editorial: Quantum Mechanical/Molecular Mechanical Approaches for the Investigation of Chemical Systems – Recent Developments and Advanced Applications. *Front. Chem.* **2018**, *6*, 357, doi:10.3389/FCHEM.2018.00357/BIBTEX.

10. Lewars, E.G. *Computational Chemistry - Introduction to the Theory and Applications of Molecular and Quantum Mechanics*; 2003; ISBN 9048138612.

11. Mallipeddi, P.; Kumar, G.; White, S.; Webb, T. Recent advances in computer-aided drug design as applied to anti-influenza drug discovery. *Curr. Top. Med. Chem.* **2014**, *14*, 1875–1889, doi:10.2174/1568026614666140929153812.

12. Yu, D.; Wang, L.; Wang, Y. Recent Advances in Application of Computer-Aided Drug Design in Anti-Influenza A Virus Drug Discovery. *Int. J. Mol. Sci.* **2022**, *23*, doi:10.3390/IJMS23094738.

13. Bultinck, P.; Winter, H.; Langenaeker, W.; Tollenaere, J. *Computational Medicinal Chemistry for Drug Discovery*; 2004; ISBN 0-8247-4774-7.

14. Rappé, A.K.; Casewit, C.J.; Colwell, K.S.; Goddard, W.A.; Skiff, W.M. UFF, a Full Periodic Table Force Field for Molecular Mechanics and Molecular Dynamics Simulations. *J. Am. Chem. Soc.* **1992**, *114*, 10024–10035, doi:10.1021/ja00051a040.

15. Lin, F.Y.; MacKerell, A.D. Force fields for small molecules. *Methods Mol. Biol.* **2019**, *2022*, 21, doi:10.1007/978-1-4939-9608-7_2.

16. Jones, J.E. On the determination of molecular fields. -II. From the equation of state of a gas. *Proc. R. Soc. London. Ser. A, Contain. Pap. a Math. Phys. Character* **1924**, *106*, 463–477, doi:10.1098/rspa.1924.0082.

17. Bayly, C.I.; Merz, K.M.; Ferguson, D.M.; Cornell, W.D.; Fox, T.; Caldwell, J.W.; Kollman, P.A.; Cieplak, P.; Gould, I.R.; Spellmeyer, D.C. A Second Generation Force Field for the Simulation of Proteins, Nucleic Acids, and Organic Molecules. *J. Am. Chem. Soc.* **1995**, *117*, 5179–5197, doi:10.1021/ja00124a002.

18. Brooks, B.R.; Bruccoleri, R.E.; Olafson, B.D.; States, D.J.; Swaminathan, S.; Karplus, M. CHARMM: A program for macromolecular energy, minimization, and dynamics calculations. *J. Comput. Chem.* **1983**, *4*, 187–217, doi:10.1002/jcc.540040211.

19. Christen, M.; Hünenberger, P.H.; Bakowies, D.; Baron, R.; Bürgi, R.; Geerke, D.P.; Heinz, T.N.; Kastenholz, M.A.; Kräutler, V.; Oostenbrink, C.; et al. The GROMOS software for biomolecular simulation: GROMOS05. *J. Comput. Chem.* **2005**, *26*, 1719–1751, doi:10.1002/jcc.20303.

20. Shivakumar, D.; Williams, J.; Wu, Y.; Damm, W.; Shelley, J.; Sherman, W. Prediction of absolute solvation free energies using molecular dynamics free energy perturbation and the opls force field. *J. Chem. Theory Comput.* **2010**, *6*, 1509–1519, doi:10.1021/ct900587b.

21. Jorgensen, W.L.; Tirado-Rives, J. The OPLS Potential Functions for Proteins. Energy Minimizations for Crystals of Cyclic Peptides and Crambin. *J. Am. Chem. Soc.* **1988**, *110*, 1657–1666, doi:10.1021/ja00214a001.

22. Nikhar, R.; Szalewicz, K. Reliable crystal structure predictions from first principles. *Nat. Commun. 2022 131* **2022**, *13*, 1–9, doi:10.1038/s41467-022-30692-y.

23. Case, D.A.; Cheatham, T.E.; Darden, T.; Gohlke, H.; Luo, R.; Merz, K.M.; Onufriev, A.; Simmerling, C.; Wang, B.; Woods, R.J. The Amber biomolecular simulation programs. *J. Comput. Chem.* **2005**, *26*, 1668–1688, doi:10.1002/jcc.20290.

24. Izadi, S.; Onufriev, A. V. Accuracy limit of rigid 3-point water models. *J. Chem. Phys.* **2016**, *145*, 74501, doi:10.1063/1.4960175.

25. Singh, T. Ab-initio studies of a pentacyclo-undecane cage lactam. *Chem. Durban Inst. Technol.* **2003**, doi:https://doi.org/10.51415/10321/237.

26. Hehre, W.J. *A guide to molecular mechanics and quantum chemical calculations.*; 2003; ISBN 1-890661-18-X.

27. Jayatilleke, P.R.N.; Nair, A.C.; Zauhar, R.; Welsh, W.J. Computational studies on HIV-1 protease inhibitors: influence of calculated inhibitor-enzyme binding affinities on the statistical quality of 3D-QSAR CoMFA models. *J. Med. Chem.* **2000**, *43*, 4446–4451, doi:10.1021/JM9905357.

28. Foresman, J.B.; Frish, E. *Exploring chemistry with electronic structure methods*; 1996; ISBN 978-0963676931.

29. Lin, H.; Truhlar, D.G. QM/MM: What have we learned, where are we, and where do we go from here? *Theor. Chem. Acc.* **2007**, *117*, 185–199, doi:10.1007/s00214-006-0143-z.

30. Frank, J. Introduction to computational chemistry. *Editor. Off. October.* **1999**.

31. Dykstra, C..; Frenking, G.; Kim, K..; Scuseria, G.. *Theory and Applications of Computational Chemistry: The First Forty Years*; Elsevier, 2005; ISBN 0-444-51719-7.

32. Lamberti, V. E., Fosdick, L. D., Jessup, E. R., Schauble, C.J. A hands-on introduction to molecular dynamics. *J. Chem. Educ.* **2002**, *79*, 1489, doi:10.1021/ed079p1489.

33. Leach, A.R. *Molecular modelling: principles and applications*; 2001; ISBN 9780582382107.

34. Buthelezi, N.M.; Mhlongo, N.N.; Amoako, D.G.; Somboro, A.M.; Sosibo, S.C.; Shunmugam, L.; Machaba, K.E.; Kumalo, H.M. Exploring the impact of H5N1 neuraminidase (H274Y) mutation on Peramivir: a bio-computational study from a molecular perspective. *J. Biomol. Struct. Dyn.* **2020**, *38*, 4344–4352, doi:10.1080/07391102.2019.1677501.

35. Glaab, E. Computational systems biology approaches for Parkinson's disease. *Cell Tissue Res.* **2018**, *373*, 91, doi:10.1007/S00441-017-2734-5.

36. Lobanov, M.Y.; Bogatyreva, N.S.; Galzitskaya, O. V. Radius of gyration as an indicator of protein structure compactness. *Mol. Biol.* **2008**, *42*, 623–628, doi:10.1134/S0026893308040195.

37. Kollman, P.A.; Massova, I.; Reyes, C.; Kuhn, B.; Huo, S.; Chong, L.; Lee, M.; Lee, T.; Duan, Y.; Wang, W.; et al. Calculating structures and free energies of complex molecules: combining molecular mechanics and continuum models. *Acc. Chem. Res.* **2000**, *33*, 889–897, doi:10.1021/ar000033j.

38. Massova, I.; Kollman, P.A. Combined molecular mechanical and continuum solvent approach (MM-PBSA/GBSA) to predict ligand binding. *Perspect. Drug Discov. Des.* **2000**, *18*, 113–135, doi:10.1023/A:1008763014207.

39. Hou, T.; Wang, J.; Li, Y.; Wang, W. Assessing the performance of the MM/PBSA and MM/GBSA methods. 1. The accuracy of binding free energy calculations based on molecular dynamics simulations. *J. Chem. Inf. Model.* **2011**, *51*, 69–82, doi:10.1021/ci100275a.

40. Xu, L.; Sun, H.; Li, Y.; Wang, J.; Hou, T. Assessing the performance of MM/PBSA and MM/GBSA methods. 3. The impact of force fields and ligand charge models. *J. Phys. Chem. B* **2013**, *117*, 8408–8421, doi:10.1021/jp404160y.

41. Altis, A.; Nguyen, P.H.; Hegger, R.; Stock, G. Dihedral angle principal component analysis of molecular dynamics simulations. *J. Chem. Phys.* **2007**, *126*, 244111, doi:10.1063/1.2746330.

42. Cocco, S.; Monasson, R.; Weigt, M. From Principal Component to Direct Coupling Analysis of Coevolution in Proteins: Low-Eigenvalue Modes are Needed for Structure Prediction. *PLoS Comput. Biol.* **2013**, *9*, 1003176, doi:10.1371/JOURNAL.PCBI.1003176.

43. Jolliffe, I.T. *Principal Component Analysis*; Springer, New York: New York, 2002; Vol. 803; ISBN 0-387-95442-2.

44. Shlens, J. A Tutorial on Principal Component Analysis. *Univ. California, San Diego* **2005**, 1–13.

Chapter 4

RESEARCH ARTICLE

molecules

MDPI

Article

Impact of the R292K Mutation on Influenza A (H7N9) Virus Resistance towards Peramivir: A Molecular Dynamics Perspective

Sphamandla E. Mtambo, Samuel C. Ugbaja and Hezekiel M. Kumalo *

Drug Research and Innovation Unit, Discipline of Medical Biochemistry, School of Laboratory Medicine and Medical Science, University of KwaZulu-Natal, Durban 4000, South Africa; sphamtambo@gmail.com (S.E.M.); ugbajasamchii@yahoo.com (S.C.U.)

* Correspondence: kumaloh@ukzn.ac.za; Tel.: +27-031-260-4940

Abstract: In March 2013, a novel avian influenza A (H7N9) virus emerged in China. By March 2021, it had infected more than 1500 people, raising concerns regarding its epidemic potential. Similar to the highly pathogenic H5N1 virus, the H7N9 virus causes severe pneumonia and acute respiratory distress syndrome in most patients. Moreover, genetic analysis showed that this avian H7N9 virus carries human adaptation markers in the hemagglutinin and polymerase basic 2 (PB2) genes associated with cross-species transmissibility. Clinical studies showed that a single mutation, neuraminidase (NA) R292K (N2 numbering), induces resistance to peramivir in the highly pathogenic H7N9 influenza A viruses. Therefore, to evaluate the risk for human public health and understand the possible source of drug resistance, we assessed the impact of the NA-R292K mutation on avian H7N9 virus resistance towards peramivir using various molecular dynamics approaches. We observed that the single point mutation led to a distorted peramivir orientation in the enzyme active site which, in turn, perturbed the inhibitor's binding. The R292K mutation induced a decrease in the interaction among neighboring amino acid residues when compared to its wild-type counterpart, as shown by the high degree of fluctuations in the radius of gyration. MM/GBSA calculations revealed that the mutation caused a decrease in the drug binding affinity by 17.28 kcal/mol when compared to the that for the wild-type enzyme. The mutation caused a distortion of hydrogen bond-mediated interactions with peramivir and increased the accessibility of water molecules around the K292 mutated residue.

Keywords: influenza A; H7N9; neuraminidase; peramivir; principal components analysis

Citation: Mtambo, S.E.; Ugbaja, S.C.; Kumalo, H.M. Impact of the R292K Mutation on Influenza A (H7N9) Virus Resistance towards Peramivir: A Molecular Dynamics Perspective. *Molecules* **2022**, *27*, 1645. https://doi.org/10.3390/molecules27051645

Academic Editor: Anna Maria Almerico

Received: 2 November 2021
Accepted: 9 December 2021
Published: 2 March 2022

1. Introduction

The seasonal upsurge of infections and pandemics from influenza viruses continues to cause death and morbidity. This also poses great economic stress and decreases productivity, especially in countries with temperate and tropical weather conditions [1,2]. The influenza virus is classified as *Orthomyxoviridae*, with classes A and B responsible for pandemic upsurges in humans [3,4]. The influenza virus contains three membrane proteins, i.e., matrix protein (M2), hemagglutinin (HA), and neuraminidase (NA) [5]. Hitherto, there are 9 NA and 16 HA of influenza A virus (IAV) subtypes, found especially in birds (aquatic), which have been responsible for major pandemic upsurges in humans [2]. Furthermore, there are other potentially pandemic IAV subtypes such as H5N1, H7N9, and H9N,2 which are transmitted to humans through aerosols [6]. IAV transmitted via aerosols are responsible for respiratory flu-like disorders especially among children, older persons, and persons with weakened immune system [7].

The emergence of the H7N9 subtype and its subsequent infection to humans were reported in March 2013 in China [7]. It was further reported within four months of its discovery, that about 130 persons were infected [8]. In January 2017, the World Health Organization recorded about 106 H7N9 human infections in China [8]. The World Health Organization had earlier postulated that there are about 250,000–500,000 global annual

deaths due to influenza viruses; however, a recent study estimated higher figures of 290,000–650,000 global annual deaths from influenza, approximated to one billion people annually [9,10]. In 2019, it was reported that about 99,000–200,000 deaths resulted from respiratory tract influenza-related illnesses in populations less than 65 years old [10].

Recently, antiviral medications and vaccinations have been effectively employed in the fight against the influenza virus [11]. There are two major classes of anti-IAV drugs approved for the treatment of IAV diseases, i.e., neuraminidase (NA) inhibitors and adamantanes [1]. The ready availability of anti-IAV drugs gives them an edge over vaccines, which require a longer time to be developed [12]. Following the emergence of mutations and subsequent resistance of IAV to adamantane drugs, NA drugs such as laninamivir, zanamivir, oseltamivir, and peramivir have been widely employed for the treatment of IAV infections. Scientists are worried about the growing resistance of IAVs, nevertheless, NA appear to be the only type of IAV inhibitors currently in circulation [1]. Neuraminidases remain the preferred drugs for treating IAV, therefore resistance to the drug constitutes a setback in the fight against influenza pandemics [13]. The influenza A virus is known to produce diverse antigens through two processes. First, antigenic shifting due to the reassortment of the genetic compartments of two different IAVs in the same person, which results in a new strain of the virus; secondly, antigenic drifting in neuraminidase and hemagglutinin, which results in novel antigenic species. This is significantly facilitated by the imperfect nature of the viral polymerase [9]. Presently, the resistance to NA inhibitors is not very common, but might surface due to frequent use and administration of these drugs to the vulnerable groups [13]. Therefore, increased observation and additional studies on the mode of mutation/transmission are imperative.

The Food and Drug Administration lately approved an alternative intravenous NA drug called peramivir in addition to zanamivir and oseltamivir (Figure 1). Peramivir is a cyclopentane molecule that exhibited high selectivity and potency for influenza virus NA. In a recent study by Hseir et al. [14] the efficacy of intravenous peramivir over oseltamivir was investigated in the emergency department, and the results showed that influenza patients administered a single dose of peramivir showed a quick recovery [14]. In a laboratory study by Aoki et al., an in vitro influenza virus resistant to peramivir was also investigated [1]. It was observed that resistance to peramivir is due to changes in the gene for hemagglutinin, related to dual resistance to zanamivir and oseltamivir [1].

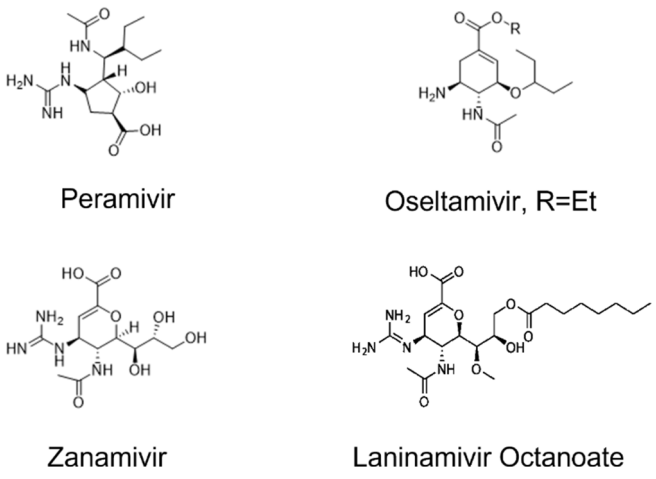

Figure 1. Structure of neuraminidase inhibitors.

Neuraminidase inhibitors function by inactivating the viral NA enzyme [15]. NA is inactivated by blocking its ability to cleave sialic acid residues, thereby preventing the unleashing of the virus and stopping the infection of the host cells [15]. Neuraminidase inhibitors prevent the cleaving of sialic acid by the enzyme, and thereby virus spreading [16]. Several avian influenza subtypes (e.g., H5N1, H7N7, and H9N2) have caused human

infections before. Their transmission has been controlled, possibly because avian viruses binding to the sialic acid receptors located in the human upper airways is inefficient [17]. NA inhibitors are sialic acid analogues that block the enzymatic active site and prevent its sialidase activity [18,19]. A single nucleotide change in the NA gene can generate resistance to NA inhibitors, as shown by the arginine-to-lysine amino acid mutation (R292K in N2 numbering, and R294K in N9 numbering) in the enzymatic active site. This R292K neuraminidase mutation has been reported in patients infected with H7N9 influenza A viruses and treated with NA inhibitors [20,21].

H7N9 normally circulates amongst avian virus populations with some variants known to occasionally infect humans [21,22]. Novel H7N9 viruses cause a severe respiratory disease in humans and have infected 1565 humans; about 39% of the people confirmed to be infected with Asian H7N9 virus have died since its emergence in 2013 [23]. Because of the lack of immunity against H7 subtype influenza viruses in the human population, the H7N9 virus is of concern as a potential cause of a pandemic [7]. The novel R292K variant virus has mammalian adaptation mutations in the receptor-binding site of the hemagglutinin gene and the polymerase basic 2 (PB2) gene (E627K) of the virus and can spread from poultry to man more easily [24].

Because of H7N9 resistance to the M2-ion channel blockers such as amantadine and rimantadine, neuraminidase inhibitors have been widely used for the antiviral treatment of patients with H7N9 [25,26]. Influenza virus H7N9 isolates (A/Anhui/1/2013, A/Shanghai/1/2013, and A/Shanghai/2/2013) were found to carry the NA-R292K mutation. This R292K mutation was determined to confer resistance to the inhibitory action of peramivir, which significantly impairs NA catalytic activity and virus replication in vitro and in vivo [26].

R292 is one of three key conserved arginine residues in the active site that surrounds the carboxylate group of sialic acid [27]. Neuraminidase inhibitors such as oseltamivir, peramivir, and zanamivir often interact with sialic acid at the enzyme's active sites. This three-arginine cluster is a major factor for distorting the sialic acid pyranose ring from a chair to a boat conformation, a critical step for the hydrolytic cleavage of terminal sialic acid from adjacent membrane glycoproteins by influenza virus NA [4]. Peramivir contains a C4-guanidino group and a bulky hydrophobic pentyl ether side chain, like zanamivir and oseltamivir, respectively. These features lead to multiple interactions (higher binding affinity) with the NA catalytic site [28,29]. Features of the R292K mutant (Figure 2) and its contribution to peramivir resistance have not been deeply examined.

This present study was aimed at investigating the impact of the R292K mutation on H7N9 resistance towards peramivir at the interatomic level, as this promises to further elucidate other experimental studies previously conducted [27]. To achieve this, we employed the computational instruments of advanced molecular dynamic simulations [30]. We further investigated the intermolecular interactions between enzyme and ligand. The binding free energies of the peramivir-free neuraminidase and of the peramivir–wild-type neuraminidase and peramivir–R292K neuraminidase complexes were analyzed to unravel the molecular dynamics affecting the binding of peramivir. Understanding the molecular basis of resistance caused by such deleterious mutations is critical for the development of more effective anti-influenza virus compounds.

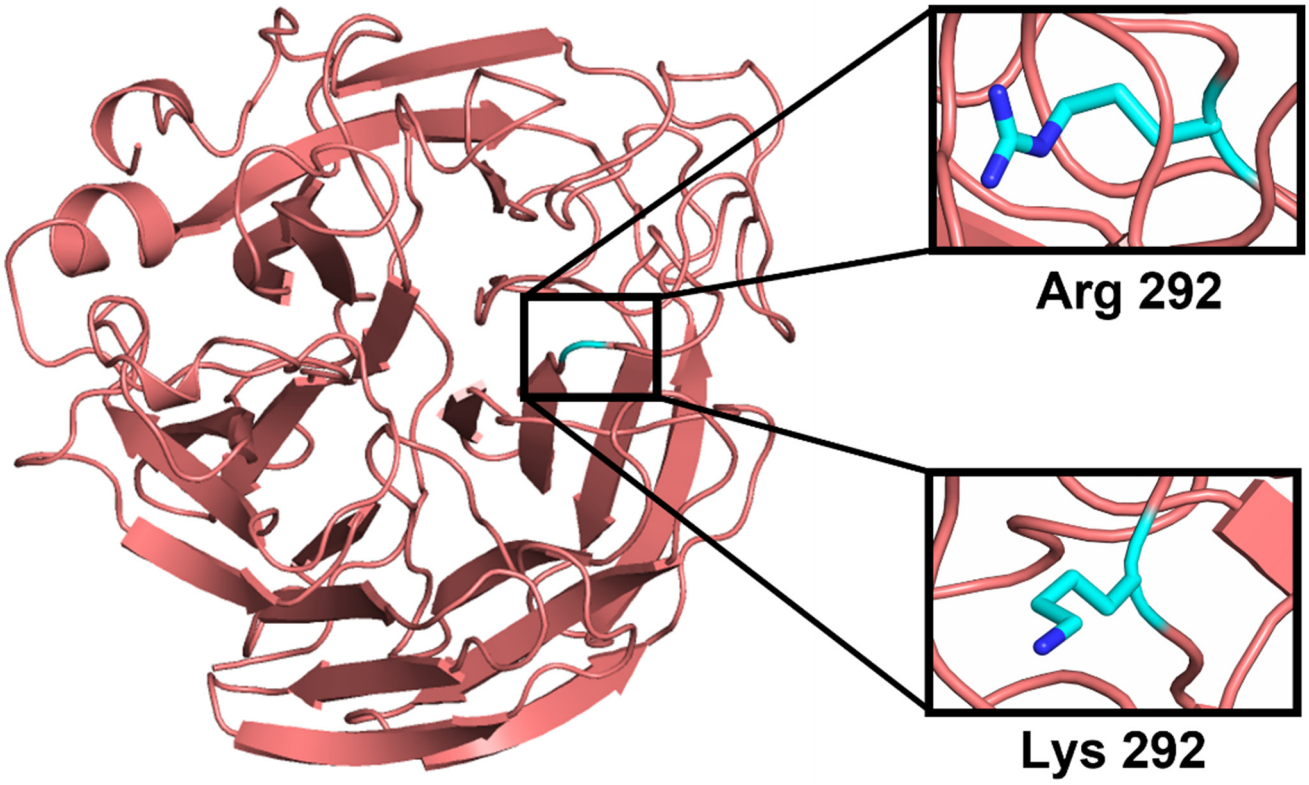

Figure 2. Representation of the R292K point mutation displaying the atomic Arginine and Lysine at residue number 292.

2. Results and Discussion

2.1. Root-Mean-Square Deviations (RMSD)

The RMSD of backbone C-α atoms was calculated to analyze the conformational stability of peramivir-free neuraminidase and peramivir-bound (wild-type and R292K) neuraminidase complexes and to observe the alignment of all the protein frames with that of the reference frame backbone. This type of analysis can yield information on the RMSD evolution of a protein and offer insights into its structural conformation throughout the simulation [31]. Figure 3 shows the RMSD values computed for peramivir-free neuraminidase and peramivir-bound wild-type and R292K neuraminidase complexes as a function of time. RMSD remained stable over most of the 200 ns simulation, thus providing a suitable basis for further analyses. The peramivir-free simulation showed relatively higher mean RMSD values, followed by peramivir–R292K variant complex and lastly by the peramivir-wild-type neuraminidase complex. A higher average RMSD for peramivir-free neuraminidase indicated higher flexibility of the molecule due to the absence of peramivir, resulting in an increased freedom for protein movement [31]. The higher average RMSD for the peramivir–R292K variant complex, when compared to that of the peramivir–wild-type neuraminidase complex demonstrated the flexibility of peramivir interaction with the protein and consequent interference with the active site structural framework, causing protein instability.

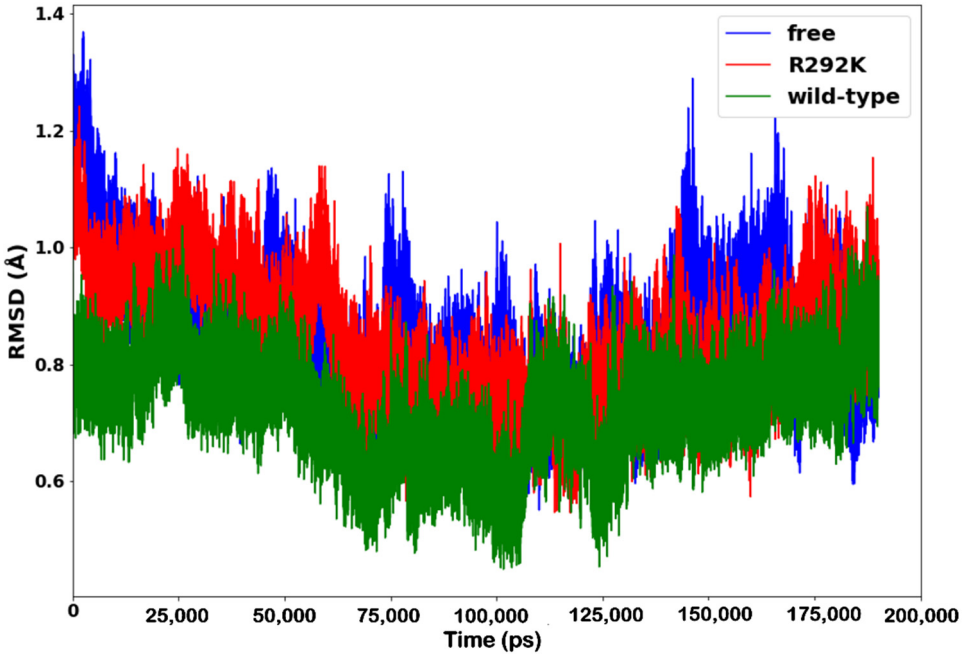

Figure 3. RMSD plot of C-α atoms of peramivir-free neuraminidase and peramivir–wild-type and peramivir–R292K neuraminidase complexes over simulation time (ps).

2.2. Root-Mean-Square Fluctuation (RMSF) and B Factors

Figure 4 shows the per-residue C-α root-mean-square fluctuations (RMSF) and the atomic temperature factor (B-factor) of the simulations of peramivir-free neuraminidase and peramivir-bound (wild-type and R292K) neuraminidase complexes, calculated to gain an insight into the conformational flexibility of the overall residues in peramivir-free neuraminidase and peramivir-bound neuraminidase (wild-type and R292K) complexes. Fluctuations can indirectly lead to significant conformational changes in the active site and affect the dynamics of the protein, ultimately resulting in reduced functionality [32–34].

The average RMSF for all the amino acid residues was found to be 0.63 Å for the peramivir complex wild-type virus, 0.71 Å for the complex with the R292K variant, and 0.76 Å for the peramivir-free H7N9. A higher average RMSF for the peramivir-free virus indicated conformational instability because of the absence of peramivir (Figure 4). The R292K mutation was also found to impact the dynamics of some amino acid regions, i.e., 160–170, 190–200, 210–230, 260–270, and 350–370, when compared to the wild-type molecule, with the R292K variant having more fluctuations. Amino acid residues in the region 280–320 which contains the mutation site at position 292 showed higher fluctuation in the variant compared with the wild-type molecule. These fluctuations are suggested to be due to differences between the interactions of Arg or Lys side-chain atoms with surrounding molecules, and these differences may lead to a conformational disproportion between the wild-type and the R292K protein.

The atomic temperature factor (B-factor) measures the dynamic disorder caused by the temperature-dependent vibration of an atom, as well as the static disorder resulting from subtle structural differences in different unit cells throughout the crystal. It is very important to inspect the B-factors during a structural analysis. The identified flexible regions with a high average B-factor were found in peramivir-free neuraminidase (19.2 $Å^2$), followed by the peramivir complex with the R292K variant (18.8 $Å^2$) and lastly with wild-type neuraminidase (14.0 $Å^2$). These results are in overall agreement with the RMSF-based flexibility analysis, suggesting that the absence of peramivir affects the overall conformational dynamics of the enzyme and that the R292K variant has significant conformational instability in the active site which results in reduced functionality.

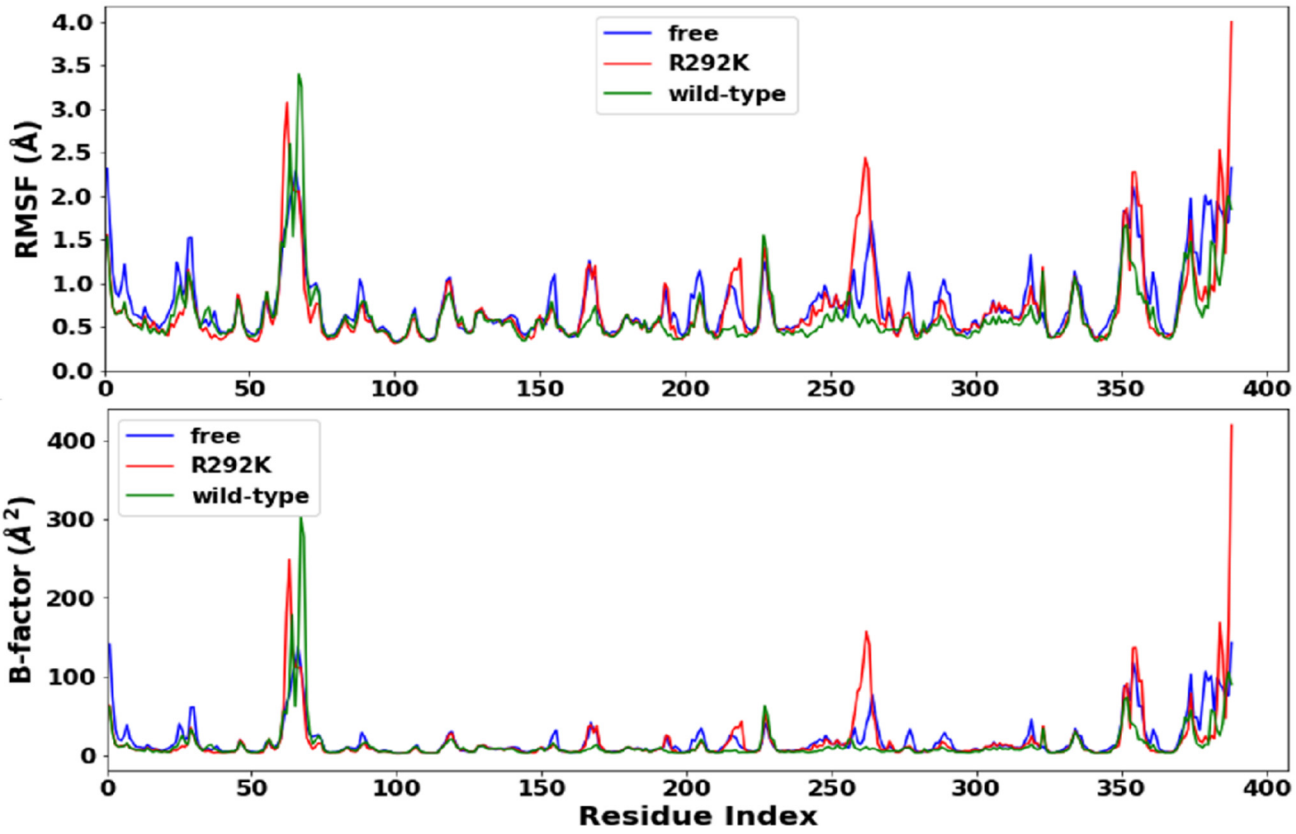

Figure 4. RMSF (**top**) and B-factors (**bottom**) plots of C-α atoms of peramivir-free neuraminidase, peramivir–wild-type, and peramivir–R292K neuraminidase complexes over simulation time (ps).

2.3. Radius of Gyration (RoG)

The radius of gyration yields quantitative measures such as folding, compactness, and shape of the protein in a biological system along with the MD simulation [35]. The assessment of protein collapse dynamics for the peramivir-free neuraminidase and the peramivir–(wild-type and R292K) neuraminidase complexes was performed as a function of time, as shown in Figure 5. The radius of gyration of the wild-type complex was significantly higher in comparison to that of the R292K complex and of peramivir-free neuraminidase throughout the simulation period. This indicates that the wild-type complex exhibits an overall more stable conformation than both the R292K complex and the peramivir-free enzyme. However, when comparing the stability of peramivir-free neuraminidase and the R292K complex, it was observed that the R292K complex was less compact than the peramivir-free enzyme. This indicates that the mutation of Arg292 to Lys292 decreased the compactness, negatively affecting the folding of the protein relative to the wild-type molecule. As the mutant structure became less compact, the interaction among neighboring amino acids decreased, which led to an unstable moment of inertia of the group of atoms from their center of mass. Such evidence implies that the mutant exhibits high conformational flexibility which decreases the receptor–ligand stability. The fluctuation of the radius of gyration is in agreement with the RMSF and the B-factor determined in the flexibility studies.

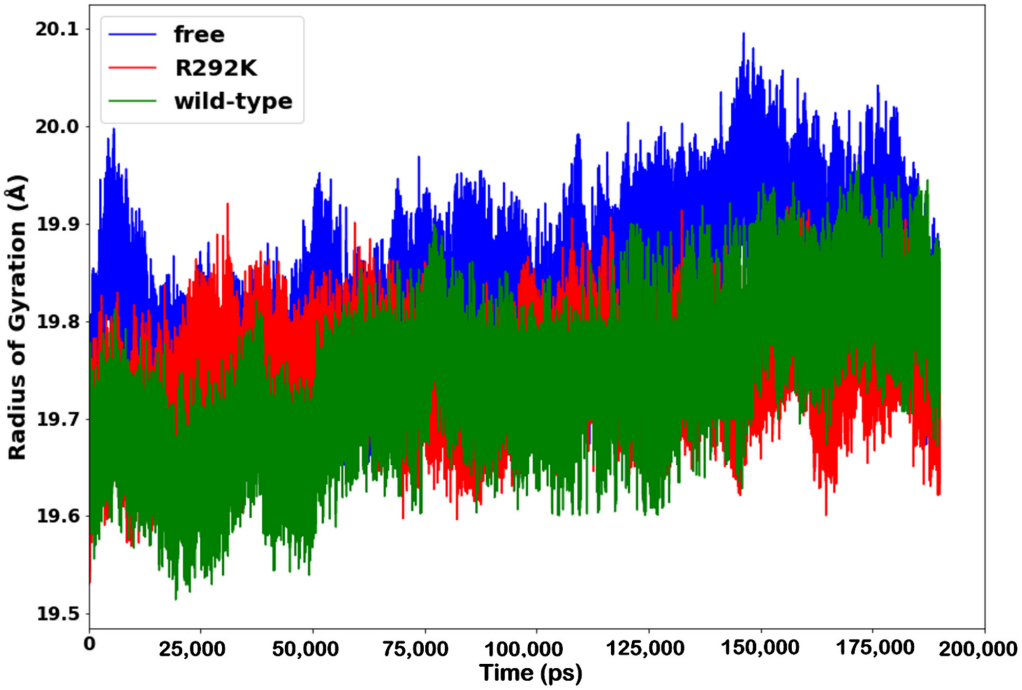

Figure 5. Radius of gyration plot of C-α atoms of the peramivir-free enzyme and peramivir–wild-type, and peramivir–R292K neuraminidase complexes over the simulation time (ps).

2.4. MM/GBSA Binding Free Energy Calculation

All molecular mechanics and solvation energy components were calculated using the MM/GBSA approach over a 200 ns MD trajectory, as listed in Table 1.

Table 1. MM/GBSA binding free energies profile of peramivir bound to H7N9 wild-type neuraminidase and R292K mutant neuraminidase.

Complexes	ΔG_{bind}	ΔE_{ele}	ΔE_{vdw}	ΔE_{gas}	ΔG_{sol}
Wild-type	-38.95 ± 5.66	-104.55 ± 15.85	-38.28 ± 2.33	-130.93 ± 13.66	105.12 ± 14.5
R292K	-21.67 ± 2.10	-81.29 ± 8.85	-28.43 ± 3.49	-112.02 ± 10.9	92.57 ± 7.22

ΔG_{bind}—binding free energy; ΔE_{ele}—electrostatic interaction; ΔE_{vdW}—van der Waals forces; ΔG_{gas}—gas–phase interaction; ΔG_{sol}—solvation energy.

The calculated binding free energy (ΔG_{bind}) for the wild-type neuraminidase complex was -38.95 ± 5.66 kcal/mol, while that of the R292K mutant was -21.67 ± 2.10 kcal/mol. Such a large reduction in binding affinity (-17.28 kcal/mol) due to thermodynamic instability of the protein–ligand complex could impair drug binding and thus reduce the effectiveness of peramivir against the mutant. These calculations agree with experimental data that indicated that the R292K mutation leads to a 563-fold increased relative resistance towards peramivir [26]. Peramivir comprises a C4-guanidino group and a bulky hydrophobic pentyl ether side chain. These features lead to higher binding affinity with the NA binding site [27]. Thus, the R292K mutation in the binding site might reduce peramivir binding affinity.

The calculated van der Waals contributions (ΔE_{vdW}) to the binding free energy in the wild-type neuraminidase complex (-38.28 ± 2.33 kcal/mol) were lower than those in the R292K mutant neuraminidase complex (-28.43 ± 3.49 kcal/mol). On the other hand, the calculated electrostatic contributions (ΔE_{ele}) to the binding free energy for the R292K mutant neuraminidase complex (-81.29 ± 8.85 kcal/mol) were higher compared to those for the wild-type neuraminidase complex (-104.55 ± 15.85 kcal/mol). The free energy components presented in Table 1 suggest that ΔE_{vdW} and ΔE_{ele} are the major energy contributors to peramivir binding. This is due to the amino acid residues present in the

binding site of the wild-type molecule, exhibiting strong hydrophobic interactions and thus stabilizing the conformation of the protein–ligand complex.

The calculated solvation energy (ΔG_{sol}) of the wild-type neuraminidase complex (105.12 ± 14.5 kcal/mol) was higher than that of the R292K mutant neuraminidase complex (92.57 ± 7.22 kcal/mol). The significant difference in the ΔG_{sol} (12.55 kcal/mol) resulting in weak intermolecular interactions between the neuraminidase complex and water molecules also confirmed that the R292K mutation has the potential to significantly affect the efficacy of peramivir against H7N9 avian influenza virus. Due to limitations associated with approximations in the binding free energy calculations, the binding free energy values represent a trend for the wild-type and the mutant binding free energies.

2.5. Hydrogen Bond Formation

One of the most important analyses is that of the number of hydrogen bonds between residues to evaluate the stability of a protein. A high number of intermolecular hydrogen bonds in a protein might help to maintain its rigidity, while a low number of hydrogen bonds with a solvent makes the protein more flexible. The introduction of a single mutation in a protein is expected to cause changes in hydrogen bonds around the site of mutation. Therefore, we examined hydrogen bond formation during the simulation for peramivir-free neuraminidase and the peramivir–(wild-type and R292K) neuraminidase complexes.

To further examine the effect of the R292K mutation on peramivir binding, we monitored hydrogen bond distances (Å) and hydrogen bond occupancy (%) between amino acid residues interacting with peramivir in the active site of the wild-type and R292K mutant neuraminidase complexes. A summary of the average hydrogen bond distances and occupancy attained during simulation is presented in Table 2. Hydrogen bonds were recorded throughout the 200 ns trajectory. Hydrogen bonds of the mutant complex exhibited an increase in average distance when compared to the wild-type complex. The wild-type complex showed a higher occupancy of hydrogen bonds when compared to the mutant complex throughout the simulation. This indicated a strong attraction interaction between active site residue atoms and peramivir. It also showed that the mutation affects the hydrogen bond network of the complex. The long-distance hydrogen bond network causes a loss of hydrogen bond interactions between the active site residues and peramivir, which in turn leads to structural instability and eventually affects peramivir binding.

Table 2. Average hydrogen bond distances and percentage occupancy between amino acid residues interacting with peramivir calculated over the simulation time.

H-bond	Average Distance (Å)		Percentage Occupancy (%)	
	Wild-Type	Mutant	Wild-Type	Mutant
Glu120 (OE_2) ... (O_3) Peramivir	2.84	-	7.1	-
Asp152 (OD_2) ... (N_3) Peramivir	2.68	2.83	92.3	87.3
Asp152 (OD_2) ... (N_4) Peramivir	2.89	2.93	72.4	67.2
Glu278 (OE_1) ... (O_1) Peramivir	2.90	-	12.6	-
Glu279 (OE_2) ... (O_2) Peramivir	2.79	2.94	68.7	60.8
Glu279 (OE_2) ... (N_1) Peramivir	2.64	2.84	75.0	67.7
Tyr406 (OH) ... (N_3) Peramivir	2.81	2.95	89.5	80.2

LigPlot software was used to analyze the interaction between peramivir bound to wild-type and R292K mutant neuraminidase (Figure 6) [36]. Certain amino acid residues elicited strong hydrogen interactions with peramivir, which accounted for the enzyme stability and high affinity towards peramivir. As illustrated in Figure 6A, among all interactions between peramivir and wild-type NA, certain amino acid residues consistently established interactions with peramivir throughout the simulation. Notable amongst these residues are Glu 120 and Glu 278, which consistently maintained a hydrogen bond interaction with peramivir at 10 ns, 100 ns, and 200 ns. These hydrogen bond interactions, in addition to the

many hydrophobic interactions with other active site residues, could jointly contribute to the favorable binding free energies that we calculated. The binding of peramivir to R292K mutant NA was also characterized by consistent hydrogen bond interactions with some specific residues throughout the simulation, but Glu 120 and Glu 278 were not involved in these hydrogen bond interactions (Figure 6B). This suggests that the R292K mutation induced a loss of hydrogen bond interactions between peramivir and Glu 120 as well as Glu 278, thus resulting in a reduction of the binding affinity of peramivir to the active site. This could imply that interactions of these amino acids with peramivir could be significant for the high-affinity binding and stability of the peramivir–NA complex.

The analysis of hydrogen bond formation between amino acid residues indicated that the wild-type complex displayed a relatively higher hydrogen bond participation with other amino acids and comparatively less flexibility over the simulation time when compared to the R292K complex and peramivir-free neuraminidase (Figure 7). Based on the observed RMSF values and number of hydrogen bonds, it was confirmed that the mutation led to a more flexible conformation due to the formation of a smaller number of hydrogen bonds. The lower number of hydrogen bond interactions between amino acid residues in the R292K variant led to a distinct reduction in the peramivir binding affinity due to conformational distortion and, as such, to a decrease in receptor–ligand interaction.

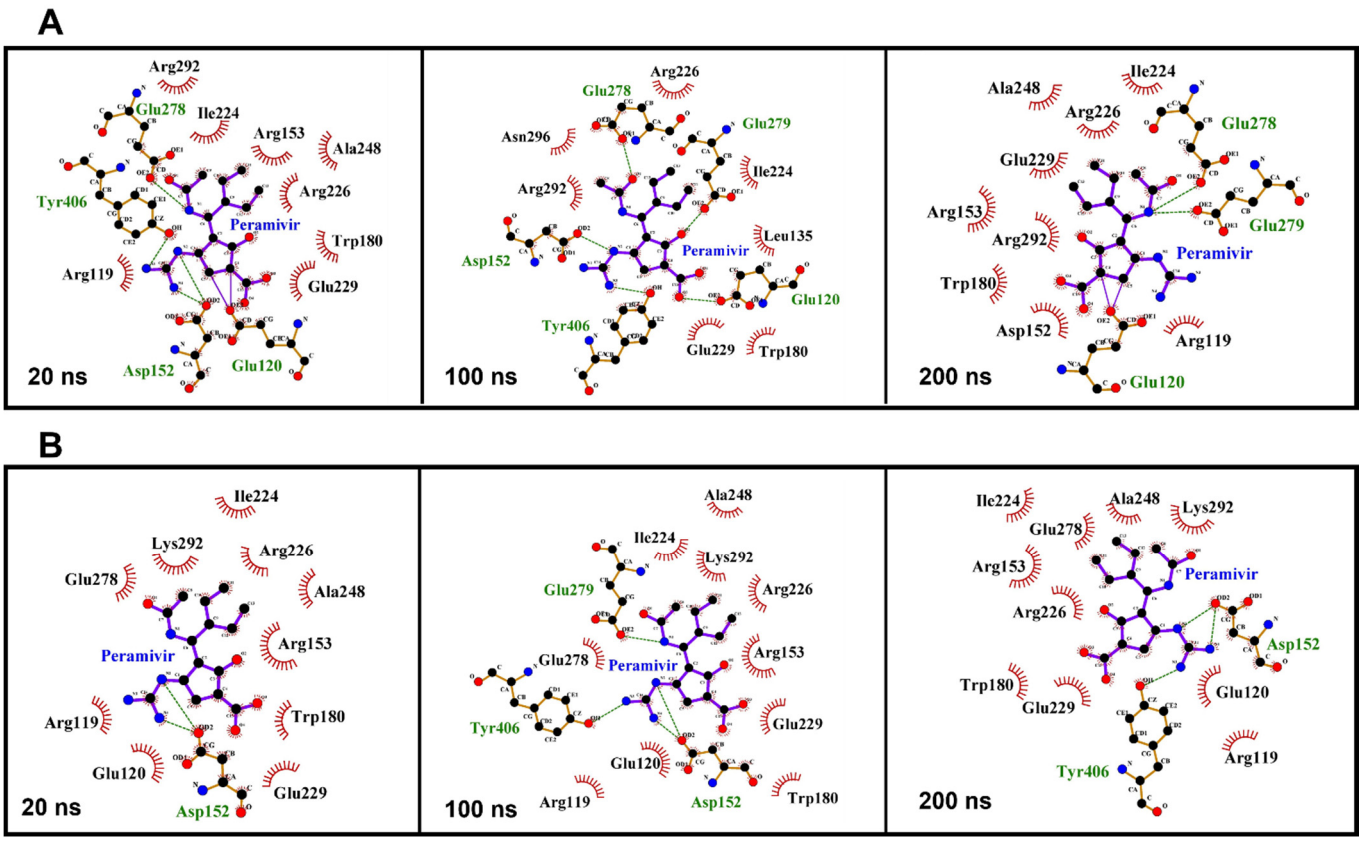

Figure 6. Amino acid residue interactions with peramivir in the active site of the wild-type (**A**) and R292K mutant (**B**) at 20 ns, 100 ns, and 200 ns simulation time.

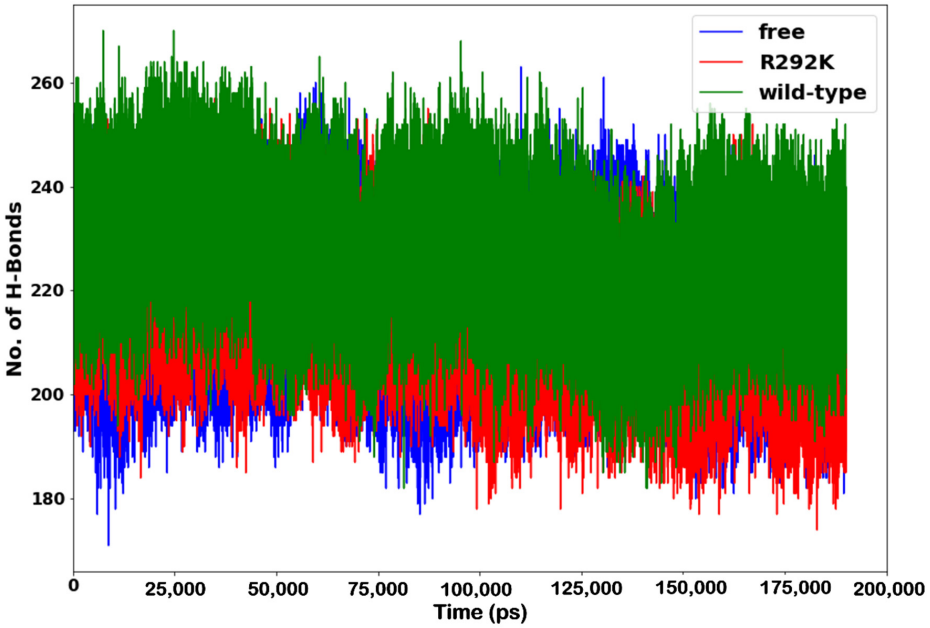

Figure 7. Number of H-bond formation in peramivir-free neuraminidase and the peramivir–wild-type and peramivir–R292K neuraminidase complexes over the simulation time (ps).

2.6. Solvent-Accessible Surface Area (SASA)

The interactions of a protein with various solvents and ligands depend primarily on its surface properties. Thus, understanding the changes in solvent-accessible surface area (SASA) due to structural deviations can be important. SASA is the total amount of surface area available for interacting with other ligands, proteins, or solvents and is used to characterize the compactness of protein structures. The plot of solvent-accessible surface area (SASA) of peramivir-free neuraminidase and peramivir-bound (wild-type and R292K) neuraminidase complexes against time at 300 K is shown in Figure 8. Major fluctuations were observed throughout the simulation time. It was evident that SASA for the peramivir-free neuraminidase was higher compared to those of the R292K variant and the wild-type complexes. Also, when comparing SASA between the wild-type and R292K variant complexes, the latter had higher SASA. The higher values of SASA for the peramivir–R292K complex indicated that the variant structure is thermodynamically unstable. This is due to the Arg292 mutation causing the protein structure to become less compact and thus exposing more protein to water molecules. Therefore, the SASA induced by the R292K mutation markedly influences the structure as well as the activity of neuraminidase.

2.7. Principal Components Analysis (PCA)

The assessment of the functionally relevant global aggregate motion of a protein is a very demanding task. However, PCA helps in reducing the complexity of classifying collective motions of a protein, since it segregates global aggregate motions from local fast motions. These essential movements in a protein are directly interconnected to protein stability and therefore associated with protein function. The 2D projection of the trajectory plot elucidates the overall collective motion of a protein in the essential subspace of the system. The flexibility of peramivir-free neuraminidase, peramivir-bound wild-type, and peramivir-bound R292K neuraminidase complexes was assessed using the PCA method, showing a significant difference between the systems and indicating a difference in protein motion (Figure 9). In the PCA plot, we observed that the wild-type complex occupies a lower subspace in comparison to peramivir-free neuraminidase and the R292K complex. The highly compact and stable structure of the wild-type complex makes the residue side-chain atoms fluctuate in a smaller subspace when compared to the variant complex and

peramivir-free neuraminidase. Such evidence suggests that the mutant structure has a high degree of flexibility which disturbs the binding interaction with peramivir.

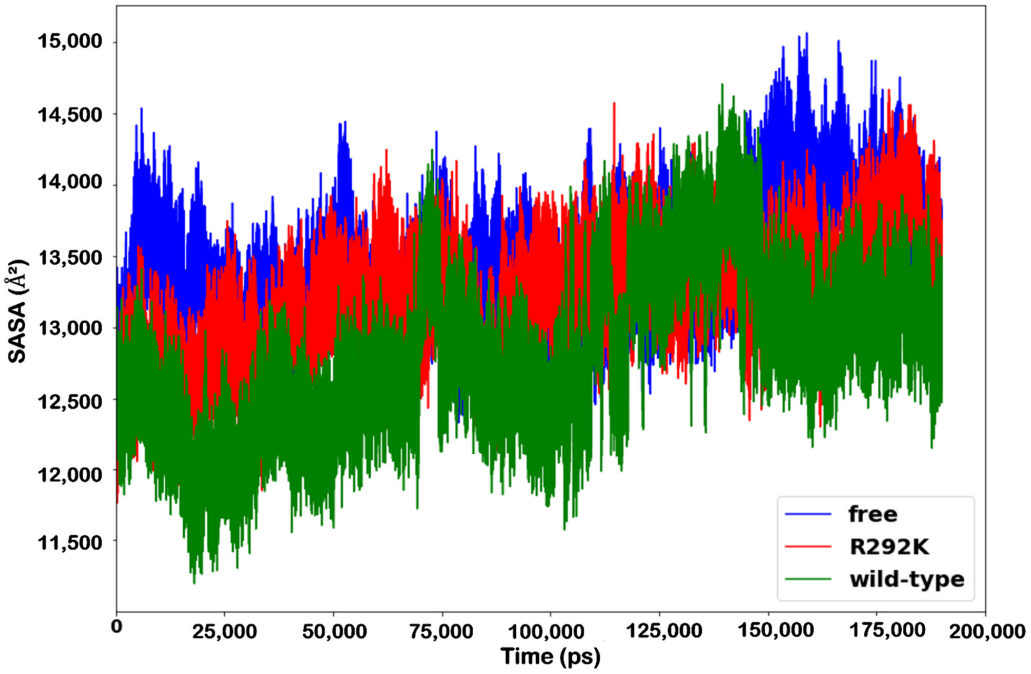

Figure 8. SASA (Å^2) plot of peramivir-free neuraminidase and the peramivir-wild-type and peramivir-R292K neuraminidase complexes over the simulation time (ps).

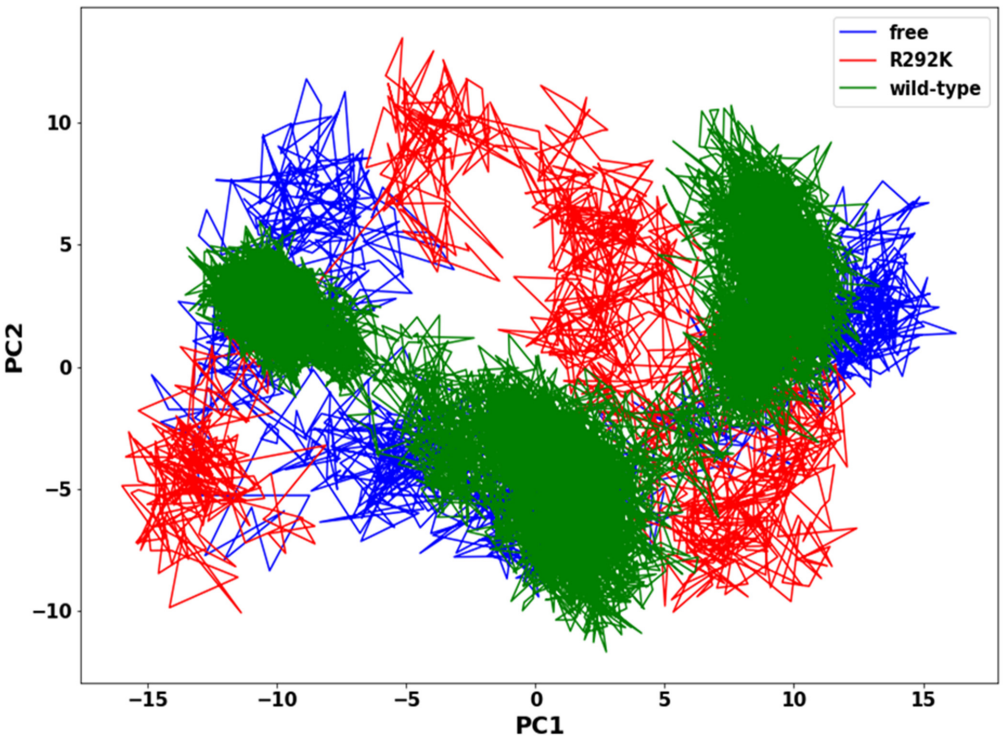

Figure 9. PCA scatter plot projection of C-α atoms motion of the first two principal components, PC1 and PC2, for peramivir-free neuraminidase and peramivir–wild-type and peramivir–R292K neuraminidase complexes conformations.

3. Materials and Methods

3.1. System Preperation

The X-ray crystal structure of the Anhui N9–peramivir (PDB code: 4MWV) complex was retrieved from the Protein Data Bank (http://www.rcsb.org, accessed on 6 September 2021). The crystal structure of neuraminidase established by X-ray showed that it exists as a homo-tetramer. However, only one chain (chain A) was used for simulations in this study to reduce the computational cost. The Arginine to Lysine point mutation 292 (R292K) was introduced using PyMol (Version 2.5) [37]. Ligand and receptor were modified and visualized by PyMol and Avogadro software (Version 1.2) [38], respectively.

3.2. Molecular Dynamic Simulations

Molecular dynamic simulations of peramivir-free neuraminidase and peramivir–neuraminidase complexes (wild-type and R292K) were performed using Amber 14 software package [39–41]. Gaussian 09 at the HF/6–31G* level was utilized to optimize the geometry for the ligand. The antechamber module was used for the generation of atomic partial charges for the ligand using Restrained Electrostatic Potential (RESP) and the General Amber Force Field (GAFF) procedures [42]. The ff99SB force field in the Amber 14 suite was used to define the parameters of the protein system [43]. Missing hydrogen and heavy atoms were added using the LEAP module of AMBER 14. The system was neutralized by the addition of sodium ions. The entire system was solvated within a box of TIP3P [44] water molecules such that any solute atoms were within 10 Å of any box edge during the MD simulations. The periodic boundary conditions were adopted, and the long-range electrostatic interactions were treated with the Particle mesh Ewald (PME) method [45] with a direct space and van der Waals cut-off of 12 Å. Initial energy minimization of 2000 steps was carried out with a restraint potential of 500 kcal/mol Å applied to the solute, for 1000 steps using the steepest descent method followed by conjugate gradient minimization of 1000 steps. An additional full minimization of 1000 steps was carried out by unrestrained conjugate gradient. Gradual heating of the systems from 0 to 300 K with a 5 kcal/mol Å harmonic restraint potential and a Langevin thermostat of collision frequency of 1/ps using a canonical ensemble (NVT) molecular dynamics simulation were then carried out [46]. The systems were equilibrated at 300 K in an NPT ensemble for 500 ps without restraint. A Berendsen barostat was used to maintain the pressure of the systems at 1 bar. All hydrogen bonds were constrained using the SHAKE algorithm [47], and a time scale of 2 fs for all MD runs using the SPFP precision model [48] was applied. A 200 ns production run was performed without any restrain on the systems in an NPT ensemble at a temperature of 300 K with a target coupling constant of 2 ps and pressure at 1 bar. The coordinates were saved every 1ps time interval, and the trajectories were analyzed every 1 ps. The PTRAJ and CPPTRAJ modules [49] of Amber14 suite were utilized for post-dynamic analyses, such as root-mean-square deviation (RMSD) and root-mean-square fluctuations (RMSF), radius of gyration (RoG), solvent-accessible surface area (SASA), B-factor, hydrogen bond occupancy over time, and principal component analysis (PCA). All molecular visualization and plots were carried out using the PyMol system and Matplotlib data analysis tools, respectively [50].

3.3. Thermodynamic Calculations

The binding free energy profiles of the peramivir-bound neuraminidase (wild-type and R292K) complexes were computed using the Molecular Mechanics/Generalized Born Surface Area (MM/GBSA) approach [51–54]. The free energies of binding were calculated considering 1000 snapshots from the 200 ns trajectory. Binding free energy calculation is an endpoint energy calculation that offers a valuable insight into the formation of the protein–ligand complex. The following set of equations procide a detailed explanation of the calculation of binding free energy:

$$\Delta G_{bind} = G_{complex} - G_{receptor} - G_{ligand} \quad (1)$$

$$\Delta G_{bind} = E_{gas} + G_{sol} - T\Delta S \quad (2)$$

$$E_{gas} = E_{int} + E_{vdW} + E_{ele} \quad (3)$$

$$G_{sol} = G_{GB} + G_{SA} \quad (4)$$

$$G_{SA} = \gamma SASA \quad (5)$$

where $G_{complex}$ is the total free energy of the protein–ligand complex, $G_{receptor}$ and ΔG_{ligand} are total free energies of the isolated protein and ligand in the solvent, respectively [54]. E_{gas} signifies the gas-phase energy and is evaluated directly from the Amber ff99SB force field terms. G_{sol} denotes the solvation-free energy that can be decomposed into polar and nonpolar contribution states. TΔS refers to the entropic contribution to the free energy in a vacuum where T and S denote the temperature and entropy, respectively. E_{int} signifies the internal energy, E_{ele} is the intramolecular electrostatic energy, and E_{vdW} is the van der Waals energy. The solvation-free energy G_{sol} is the energy required to transfer a solute from the vacuum into a solvent. G_{GB} and G_{SA} are the electrostatic and non-electrostatic contributions to the solvation free energy, respectively. G_{GB} was computed using the Poisson–Boltzmann (PB) equation, and G_{SA} was estimated from the solvent-accessible surface area (SASA) equation estimated by using a water probe radius of 1.4 Å. T and S are the temperature and the total solute entropy, respectively; γ is a coefficient related to the surface tension of the solvent [55,56]. A constant γ = 0.0072 kcal/mol/Å2 was used with Amber PB polar solvation energies. The external and internal dielectric constants were set at 80 and 1, respectively.

3.4. Principal Components Analysis (PCA)

Before processing the MD trajectories for PCA, the 200 ns MD trajectories of peramivir-free neuraminidase and peramivir-bound neuraminidase (wild-type and R292K) complexes were stripped of solvent and ions using the PTRAJ module [50] of AMBER 14. The covariance matrix (C-α atoms) between residues i and j were calculated for each of the 200 ns MD simulation trajectories. PCA was performed on C-α atoms over 10 snapshots taken from trajectories at a time interval of 20 ps, overall translation and rotation trajectories were removed, and only C-α was kept for the analysis. To obtain collective motion coordinates that represented the overall dynamics of each trajectory, PCA was performed, in which the covariance matrix was diagonalized to yield a set of eigenvectors and eigenvalues. Using in-house scripts, the first two principal components (PC1 and PC2) were calculated, and covariance matrices were generated. The first two principal components correspond to the first two Eigenvectors of the covariance matrix. PCA scatter plots were then constructed using Matplotlib [57,58].

4. Conclusions

In this study, the impact of the single point mutation R292K on pathogenic H7N9 in influenza neuraminidase on peramivir binding to the enzyme was investigated using various computational approaches. These approaches, including MD simulations, principal component analysis, root-mean-square deviation, radius of gyration, and solvent-accessible surface area, aided us to understand the impact of the R292K mutation on resistance to peramivir. Our findings showed that the R292K mutation in H7N9 neuraminidase decreased the binding with peramivir, as shown by the high flexibility of peramivir RMSD and RMSF in the mutant pocket; a large radius of gyration of the mutant complex decreased the interaction among neighboring amino acid residues such that it reduced receptor–ligand clutching and increased the accessibility for water molecules around the K292 mutated residue and the carboxylate group of peramivir, thus disturbing the drug binding process.

The results of this work suggest that the bulky hydrophobic pentyl ether side chain of peramivir weakly binds to K292; thus, zanamivir and laninamivir with their hydrophilic bulky groups promise to be potent neuraminidase inhibitors. This study verified that the R292K mutation decreases peramivir binding affinity by 17.28 kcal/mol, distorts the ligand

optimum orientation in the neuraminidase active site, affects the overall peramivir conformational shape, and distorts the hydrogen bond interaction network between enzyme and ligand. The findings of this study can be useful for the investigation of other mutations that can affect the effect of peramivir on H7N9 influenza A virus.

Author Contributions: Conceptualization, S.E.M. and H.M.K.; methodology, All; software, S.E.M. and H.M.K.; validation, S.C.U. and H.M.K.; formal analysis, S.E.M. and S.C.U.; investigation, S.E.M.; resources, H.M.K.; data curation, All; writing—original draft preparation, S.E.M.; writing—review and editing, All; visualization, All; supervision, H.M.K.; project administration, H.M.K.; funding acquisition, H.M.K. All authors have read and agreed to the published version of the manuscript.

Funding: This research received no external funding.

Institutional Review Board Statement: Not applicable.

Informed Consent Statement: Not applicable.

Data Availability Statement: The data presented in this study are available on request from the corresponding author.

Acknowledgments: The authors acknowledge the UKZN School of Health Sciences and the Center for High Performance Computing (CHPC, http://www.chpc.ac.za, accessed on 18 October 2021) for computational resources.

Conflicts of Interest: The authors declare no conflict of interest.

Sample Availability: Not available.

References

1. Aoki, F.Y. Antiviral Drugs for Influenza and Other Respiratory Virus Infections. *Mand. Douglas Bennett's Princ. Pract. Infect. Dis.* **2014**, *1*, 531–545. [CrossRef]
2. Alame, M.M.; Massaad, E.; Zaraket, H. Peramivir: A novel intravenous neuraminidase inhibitor for treatment of acute influenza infections. *Front. Microbiol.* **2016**, *7*, 1–14. [CrossRef]
3. Wolff, T.; Veit, M. Influenza B, C and D Viruses (Orthomyxoviridae). *Encycl. Virol.* **2021**, 561–574. [CrossRef]
4. Mtambo, S.E.; Amoako, D.G.; Somboro, A.M.; Agoni, C.; Lawal, M.M.; Gumede, N.S.; Khan, R.B.; Kumalo, H.M. Influenza Viruses: Harnessing the Crucial Role of the M2 Ion-Channel and Neuraminidase toward Inhibitor Design. *Molecules* **2021**, *26*, 880. [CrossRef] [PubMed]
5. Petrich, A.; Dunsing, V.; Bobone, S.; Chiantia, S. Influenza A M2 recruits M1 to the plasma membrane: A fluorescence fluctuation microscopy study. *bioRxiv* **2021**, *2*, 1–39. [CrossRef]
6. Lam, T.T.Y.; Zhou, B.; Wang, J.; Chai, Y.; Shen, Y.; Chen, X.; Ma, C.; Hong, W.; Chen, Y.; Zhang, Y.; et al. Dissemination, divergence and establishment of H7N9 influenza viruses in China. *Nature* **2015**, *522*, 102–105. [CrossRef] [PubMed]
7. Zhou, J.; Wang, D.; Gao, R.; Zhao, B.; Song, J.; Qi, X.; Zhang, Y.; Shi, Y.; Yang, L.; Zhu, W.; et al. Biological features of novel avian influenza A (H7N9) virus. *Nature* **2013**, *499*, 500–503. [CrossRef] [PubMed]
8. Zhou, L.; Ren, R.; Yang, L.; Bao, C.; Wu, J.; Wang, D.; Li, C.; Xiang, N.; Wang, Y.; Li, D.; et al. Sudden increase in human infection with avian influenza A(H7N9) virus in China, September-December 2016. *West. Pac. Surveill. Response J. WPSAR* **2017**, *8*, 6–14. [CrossRef] [PubMed]
9. Lampejo, T. Influenza and antiviral resistance: An overview. *Eur. J. Clin. Microbiol. Infect. Dis.* **2020**, *39*, 1201–1208. [CrossRef] [PubMed]
10. Paget, J.; Spreeuwenberg, P.; Charu, V.; Taylor, R.J.; Iuliano, A.D.; Bresee, J.; Simonsen, L.; Viboud, C. Global mortality associated with seasonal influenza epidemics: New burden estimates and predictors from the GLaMOR Project. *J. Glob. Health* **2019**, *9*, 1–12. [CrossRef] [PubMed]
11. Chan, Y.; Ng, S.W.; Mehta, M.; Anand, K.; Kumar Singh, S.; Gupta, G.; Chellappan, D.K.; Dua, K. Advanced drug delivery systems can assist in managing influenza virus infection: A hypothesis. *Med. Hypotheses* **2020**, *144*, 110298. [CrossRef]
12. Wong, S.S.; Webby, R.J. Traditional and new influenza vaccines. *Clin. Microbiol. Rev.* **2013**, *26*, 476–492. [CrossRef] [PubMed]
13. Lee, N.; Hurt, A.C. Neuraminidase inhibitor resistance in influenza: A clinical perspective. *Curr. Opin. Infect. Dis.* **2018**, *31*, 520–526. [CrossRef] [PubMed]
14. Hsieh, Y.H.; Dugas, A.F.; LoVecchio, F.; McBryde, B.; Ricketts, E.P.; Saliba-Shaw, K.; Rothman, R.E. Intravenous peramivir vs oral oseltamivir in high-risk emergency department patients with influenza: Results from a pilot randomized controlled study. *Influenza Other Respir. Viruses* **2021**, *15*, 121–131. [CrossRef] [PubMed]
15. Mahal, A.; Duan, M.; Zinad, D.S.; Mohapatra, R.K.; Obaidullah, A.J.; Wei, X.; Pradhan, M.K.; Das, D.; Kandi, V.; Zinad, H.S.; et al. Recent progress in chemical approaches for the development of novel neuraminidase inhibitors. *RSC Adv.* **2021**, *11*, 1804–1840. [CrossRef]

16. Dai, M.; Du, W.; Martínez-Romero, C.; Leenders, T.; Wennekes, T.; Rimmelzwaan, G.F.; van Kuppeveld, F.J.M.; Fouchier, R.A.M.; Garcia-Sastre, A.; de Vries, E.; et al. Analysis of the evolution of pandemic influenza a(H1N1) virus neuraminidase reveals entanglement of different phenotypic characteristics. *mBio* **2021**, *12*, e00287-21. [CrossRef] [PubMed]
17. Sha, J.; Dong, W.; Liu, S.; Chen, X.; Zhao, N.; Luo, M.; Dong, Y.; Zhang, Z. Differences in the epidemiology of childhood infections with avian influenza a H7N9 and H5N1 viruses. *PLoS ONE* **2016**, *11*, 1–15. [CrossRef] [PubMed]
18. Nobusawa, E.; Aoyama, T.; Kato, H.; Suzuki, Y.; Tateno, Y.; Nakajima, K. Comparison of complete amino acid sequences and receptor-binding properties among 13 serotypes of hemagglutinins of influenza A viruses. *Virology* **1991**, *182*, 475–485. [CrossRef]
19. Matrosovich, M.; Tuzikov, A.; Bovin, N.; Gambaryan, A.; Klimov, A.; Castrucci, M.R.; Donatelli, I.; Kawaoka, Y. Early Alterations of the Receptor-Binding Properties of H1, H2, and H3 Avian Influenza Virus Hemagglutinins after Their Introduction into Mammals. *J. Virol.* **2000**, *74*, 8502–8512. [CrossRef]
20. Wu, Y.; Bi, Y.; Vavricka, C.J.; Sun, X.; Zhang, Y.; Gao, F.; Zhao, M. Characterization of two distinct neuraminidases from avian-origin human-infecting H7N9 influenza viruses. *Cell Res.* **2013**, *23*, 1347–1355. [CrossRef]
21. Gao, H.-N.; Lu, H.-Z.; Cao, B.; Du, B.; Shang, H.; Gan, J.-H.; Lu, S.-H.; Yang, Y.-D.; Fang, Q.; Shen, Y.-Z.; et al. Clinical Findings in 111 Cases of Influenza A (H7N9) Virus Infection. *N. Engl. J. Med.* **2013**, *368*, 2277–2285. [CrossRef] [PubMed]
22. Quan, C.; Shi, W.; Yang, Y.; Yang, Y.; Liu, X.; Xu, W.; Li, H.; Li, J.; Wang, Q.; Tong, Z.; et al. New Threats from H7N9 Influenza Virus: Spread and Evolution of High- and Low-Pathogenicity Variants with High Genomic Diversity in Wave Five. *J. Virol.* **2018**, *92*, e00301-18. [CrossRef] [PubMed]
23. Wolrd Health Organisation (WHO). Analysis of Recent Scientific Information on Avian Influenza A(H7N9) Virus. Available online: https://www.who.int/influenza/human_animal_interface/avian_influenza/riskassessment_AH7N9_201702/en/ (accessed on 1 October 2021).
24. Steel, J.; Lowen, A.C.; Mubareka, S.; Palese, P. Transmission of Influenza Virus in a Mammalian Host Is Increased by PB2 Amino Acids 627K or 627E/701N. *PLoS Pathog.* **2009**, *5*, e1000252. [CrossRef] [PubMed]
25. Hu, Y.; Lu, S.; Song, Z.; Wang, W.; Hao, P.; Li, J.; Zhang, X.; Yen, H.; Shi, B.; Li, T.; et al. Association between adverse clinical outcome in human disease caused by novel infl uenza A H7N9 virus and sustained. *Lancet* **2013**, *381*, 2273–2279. [CrossRef]
26. Hai, R.; Schmolke, M.; Leyva-Grado, V.H.; Thangavel, R.R.; Margine, I.; Jaffe, E.L.; Krammer, F.; Solórzano, A.; García-Sastre, A.; Palese, P.; et al. Influenza A(H7N9) virus gains neuraminidase inhibitor resistance without loss of in vivo virulence or transmissibility. *Nat. Commun.* **2013**, *4*, 2854. [CrossRef]
27. Karnchanapandh, K.; Hanpaibool, C.; Mahalapbutr, P.; Rungrotmongkol, T. Source of oseltamivir resistance due to single E276D, R292K, and double E276D/R292K mutations in H10N4 influenza neuraminidase. *J. Mol. Liq.* **2021**, *326*, 115294. [CrossRef]
28. McLaughlin, M.M.; Skoglund, E.W.; Ison, M.G. Peramivir: An intravenous neuraminidase inhibitor. *Expert Opin. Pharmacother.* **2015**, *16*, 1889–1900. [CrossRef]
29. Scott, L.J. Peramivir: A Review in Uncomplicated Influenza. *Drugs* **2018**, *78*, 1363–1370. [CrossRef]
30. Kadupitiya, J.C.S.; Sun, F.; Fox, G.; Jadhao, V. Machine learning surrogates for molecular dynamics simulations of soft materials. *J. Comput. Sci.* **2020**, *42*, 101107. [CrossRef]
31. Meli, R.; Biggin, P.C. Spyrmsd: Symmetry-corrected RMSD calculations in Python. *J. Cheminformatics* **2020**, *12*, 1–7. [CrossRef]
32. Chandra, A.; Goyal, N.; Qamar, I.; Singh, N. Identification of hot spot residues on serine-arginine protein kinase-1 by molecular dynamics simulation studies. *J. Biomol. Struct. Dyn.* **2021**, *39*, 1579–1587. [CrossRef] [PubMed]
33. Lee, J.; Worrall, L.J.; Vuckovic, M.; Rosell, F.I.; Gentile, F.; Ton, A.T.; Caveney, N.A.; Ban, F.; Cherkasov, A.; Paetzel, M.; et al. Crystallographic structure of wild-type SARS-CoV-2 main protease acyl-enzyme intermediate with physiological C-terminal autoprocessing site. *Nat. Commun.* **2020**, *11*. [CrossRef] [PubMed]
34. Sinha, S.; Wang, S.M. Classification of VUS and unclassified variants in BRCA1 BRCT repeats by molecular dynamics simulation. *Comput. Struct. Biotechnol. J.* **2020**, *18*, 723–736. [CrossRef] [PubMed]
35. Kesharwani, A.; Chaurasia, D.K.; Katara, P. Repurposing of FDA approved drugs and their validation against potential drug targets for Salmonella enterica through molecular dynamics simulation. *J. Biomol. Struct. Dyn.* **2021**. [CrossRef] [PubMed]
36. Wallace, A.; Laskowski, R.; Thornton, J. LIGPLOT: A program to generate schematic diagrams of protein-ligand interactions. *Protein Eng.* **1995**, *8*, 127–134. [CrossRef] [PubMed]
37. Azizah, R.N. A molecular docking study of dehydroevodiamine as an inhibitor of epstein-barr virus protease. *IOP Conf. Ser. Mater. Sci. Eng.* **2020**, *833*, 012006. [CrossRef]
38. Hanwell, M.D.; Curtis, D.E.; Lonie, D.C.; Vandermeersch, T.; Zurek, E.; Hutchison, G.R. Avogadro: An advanced semantic chemical editor, visualization, and analysis platform. *J. Cheminformatics* **2012**, *4*, 17. [CrossRef] [PubMed]
39. Götz, A.W.; Williamson, M.J.; Xu, D.; Poole, D.; Le Grand, S.; Walker, R.C. Routine Microsecond Molecular Dynamics Simulations with AMBER on GPUs. 1. Generalized Born. *J. Chem. Theory Comput.* **2012**, *8*, 1542–1555. [CrossRef]
40. Salomon-Ferrer, R.; Götz, A.W.; Poole, D.; Le Grand, S.; Walker, R.C. Routine Microsecond Molecular Dynamics Simulations with AMBER on GPUs. 2. Explicit Solvent Particle Mesh Ewald. *J. Chem. Theory Comput.* **2013**, *9*, 3878–3888. [CrossRef]
41. Salomon-Ferrer, R.; Case, D.A.; Walker, R.C. An overview of the Amber biomolecular simulation package. *WIREs Comput. Mol. Sci.* **2013**, *3*, 198–210. [CrossRef]
42. Sprenger, K.G.; Jaeger, V.W.; Pfaendtner, J. The General AMBER Force Field (GAFF) Can Accurately Predict Thermodynamic and Transport Properties of Many Ionic Liquids. *J. Phys. Chem. B* **2015**, *119*, 5882–5895. [CrossRef] [PubMed]

43. Wang, L.-P.; McKiernan, K.A.; Gomes, J.; Beauchamp, K.A.; Head-Gordon, T.; Rice, J.E.; Swope, W.C.; Martínez, T.J.; Pande, V.S. Building a More Predictive Protein Force Field: A Systematic and Reproducible Route to AMBER-FB15. *J. Phys. Chem. B* **2017**, *121*, 4023–4039. [CrossRef] [PubMed]
44. Jorgensen, W.L.; Chandrasekhar, J.; Madura, J.D.; Impey, R.W.; Klein, M.L. Comparison of simple potential functions for simulating liquid water. *J. Chem. Phys.* **1983**, *79*, 926–935. [CrossRef]
45. Kholmurodov, K.; Smith, W.; Yasuoka, K.; Darden, T.; Ebisuzaki, T. A smooth-particle mesh Ewald method for DL_POLY molecular dynamics simulation package on the Fujitsu VPP700. *J. Comput. Chem.* **2000**, *21*, 1187–1191. [CrossRef]
46. Ejalonibu, M.A.; Elrashedy, A.A.; Lawal, M.M.; Kumalo, H.M.; Mhlongo, N.N. Probing the dual inhibitory mechanisms of novel thiophenecarboxamide derivatives against Mycobacterium tuberculosis PyrG and PanK: An insight from biomolecular modeling study. *J. Biomol. Struct. Dyn.* **2020**, 1–13. [CrossRef]
47. Gonnet, P. P-SHAKE: A quadratically convergent SHAKE in O(n2). *J. Comput. Phys.* **2007**, *220*, 740–750. [CrossRef]
48. Peramo, A. Solvated and generalised Born calculations differences using GPU CUDA and multi-CPU simulations of an antifreeze protein with AMBER. *Mol. Simul.* **2016**, *42*, 1263–1273. [CrossRef]
49. Roe, D.R.; Cheatham, T.E. 3rd PTRAJ and CPPTRAJ: Software for Processing and Analysis of Molecular Dynamics Trajectory Data. *J. Chem. Theory Comput.* **2013**, *9*, 3084–3095. [CrossRef]
50. Elfiky, A.A.; Ibrahim, I.M.; Ibrahim, I.M. Zika virus envelope—heat shock protein A5 (GRP78) binding site prediction. *J. Biomol. Struct. Dyn.* **2020**, *39*, 1–13. [CrossRef]
51. Kollman, P.A.; Massova, I.; Reyes, C.; Kuhn, B.; Huo, S.; Chong, L.; Lee, M.; Lee, T.; Duan, Y.; Wang, W.; et al. Calculating structures and free energies of complex molecules: Combining molecular mechanics and continuum models. *Acc. Chem. Res.* **2000**, *33*, 889–897. [CrossRef] [PubMed]
52. Massova, I.; Kollman, P.A. Combined molecular mechanical and continuum solvent approach (MM-PBSA/GBSA) to predict ligand binding. *Perspect. Drug Discov. Des.* **2000**, *18*, 113–135. [CrossRef]
53. Hou, T.; Wang, J.; Li, Y.; Wang, W. Assessing the performance of the MM/PBSA and MM/GBSA methods. 1. The accuracy of binding free energy calculations based on molecular dynamics simulations. *J. Chem. Inf. Model.* **2011**, *51*, 69–82. [CrossRef] [PubMed]
54. Xu, L.; Sun, H.; Li, Y.; Wang, J.; Hou, T. Assessing the performance of MM/PBSA and MM/GBSA methods. 3. The impact of force fields and ligand charge models. *J. Phys. Chem. B* **2013**, *117*, 8408–8421. [CrossRef]
55. Xu, Z.; Peng, C.; Shi, Y.; Zhu, Z.; Mu, K.; Wang, X.; Zhu, W. Nelfinavir was predicted to be a potential inhibitor of 2019-nCov main protease by an integrative approach combining homology modelling, molecular docking and binding free energy calculation. *bioRxiv* **2020**, *1201*. [CrossRef]
56. Wang, W.B.; Liang, Y.; Jin, Y.Q.; Zhang, J.; Su, J.G.; Li, Q.M. E484K mutation in SARS-CoV-2 RBD enhances binding affinity with hACE2 but reduces interactions with neutralizing antibodies and nanobodies: Binding free energy calculation studies. *bioRxiv* **2021**, 1–18. [CrossRef]
57. Mohammad, A.; Al-Mulla, F.; Wei, D.Q.; Abubaker, J. Remdesivir md simulations suggest a more favourable binding to sars-cov-2 rna dependent rna polymerase mutant p323l than wild-type. *Biomolecules* **2021**, *11*, 919. [CrossRef] [PubMed]
58. Wu, S.L.; Wang, L.F.; Sun, H.B.; Wang, W.; Yu, Y.X. Probing molecular mechanism of inhibitor bindings to bromodomain-containing protein 4 based on molecular dynamics simulations and principal component analysis. *SAR QSAR Environ. Res.* **2020**, *31*, 547–570. [CrossRef] [PubMed]

Chapter 5

RESEARCH ARTICLE

molecules

MDPI

Article

Intermolecular Mechanism and Dynamic Investigation of Avian Influenza H7N9 Virus' Susceptibility to E119V-Substituted Peramivir–Neuraminidase Complex

Sphamandla E. Mtambo [1], Samuel C. Ugbaja [1,*], Aganze G. Mushebenge [1], Bahijjahtu H. Abubakar [2], Mthobisi L. Ntuli [3] and Hezekiel M. Kumalo [1,*]

[1] Drug Research and Innovation Unit, Discipline of Medical Biochemistry, School of Laboratory Medicine and Medical Science, University of KwaZulu-Natal, Durban 4000, South Africa; sphamtambo@gmail.com (S.E.M.); aganzedar@gmail.com (A.G.M.)
[2] Renewable Energy Programme, Federal Ministry of Environment, 444 Aguiyi Ironsi Way, Maitama, Abuja 904101, Nigeria; bahijjah@yahoo.com
[3] Department of Mathematics, Faculty of Applied Science, Durban University of Technology, Durban 4001, South Africa; mthobisin2@dut.ac.za
* Correspondence: ugbajasamchii@yahoo.com (S.C.U.); kumaloh@ukzn.ac.za (H.M.K.)

Abstract: The H7N9 virus attaches itself to the human cell receptor protein containing the polysaccharide that terminates with sialic acid. The mutation of neuraminidase at residue E119 has been explored experimentally. However, there is no adequate information on the substitution with E119V in peramivir at the intermolecular level. Therefore, a good knowledge of the interatomic interactions is a prerequisite in understanding its transmission mode and subsequent effective inhibitions of the sialic acid receptor cleavage by neuraminidase. Herein, we investigated the mechanism and dynamism on the susceptibility of the E119V mutation on the peramivir–neuraminidase complex relative to the wildtype complex at the intermolecular level. This study aims to investigate the impact of the 119V substitution on the neuraminidase–peramivir complex and unveil the residues responsible for the complex conformations. We employed molecular dynamic (MD) simulations and extensive post-MD analyses in the study. These extensive computational investigations were carried out on the wildtype and the E119V mutant complex of the protein for holistic insights in unveiling the effects of this mutation on the binding affinity and the conformational terrain of peramivir–neuraminidase E119V mutation. The calculated total binding energy (ΔG_{bind}) for the peramivir wildtype is -49.09 ± 0.13 kcal/mol, while the E119V mutant is -58.55 ± 0.15 kcal/mol. The increase in binding energy (9.46 kcal/mol) is consistent with other post-MD analyses results, confirming that E119V substitution confers a higher degree of stability on the protein complex. This study promises to proffer contributory insight and additional knowledge that would enhance future drug designs and help in the fight targeted at controlling the avian influenza H7N9 virus. Therefore, we suggest that experimentalists collaborate with computational chemists for all investigations of this topic, as we have done in our previous studies.

Keywords: peramivir; neuraminidase; H7N9; influenza; virus; hemagglutinin; mutation; E119V

Citation: Mtambo, S.E.; Ugbaja, S.C.; Mushebenge, A.G.; Abubakar, B.H.; Ntuli, M.L.; Kumalo, H.M. Intermolecular Mechanism and Dynamic Investigation of Avian Influenza H7N9 Virus' Susceptibility to E119V-Substituted Peramivir–Neuraminidase Complex. *Molecules* **2022**, *27*, 1640. https://doi.org/10.3390/molecules27051640

Academic Editor: Michael John Plater

Received: 20 December 2021
Accepted: 14 January 2022
Published: 2 March 2022

1. Introduction

The influenza virus has been considered one of the most common respiratory diseases. The avian influenza virus has three popular types: A, B and C viruses. The presence of hemagglutinin (HA) and neuraminidase (NA) proteins in A and B types makes them treatment targets for drug inhibition [1,2]. These viruses spread from human to human through droplets and aerosol contents of the coughs and sneezes of an infected human. They enter the body's cells through the upper respiratory tract in a process called endocytosis [3]. The common symptoms of influenza virus infection include headache, sore throat, fever,

cough, muscle aches, catarrh and general weakness. The infection can lead to diseases in other parts of the body, such as the heart, lungs, and central nervous system [4]. Influenza A and B viruses are made up of single genomic strands of ribonucleic acid (RNA), which is needed for the viral polymerase to replicate within the cell of the infected person. In addition, they comprise viral glycoproteins, such as hemagglutinin and neuraminidase, which regulate the entrance and exit of the virus to and from the cell. Other components include matrix protein M1, membrane protein M2, nuclear export protein (NEP), non-structural protein (NS1) and viral nucleoprotein (NP) [5,6].

According to the World Health Organization, the first human case of avian influenza A H7N9 was reported in China on the 31st of March, 2013. Good knowledge of its mode of transmission is a prerequisite for effective management of the situation. The H7N9 virus attaches itself to the human cell receptor protein containing the polysaccharide which terminates with sialic acid. The upper respiratory tract predominantly consists of α-2,6-link receptors where the H7N9 virus attaches [7,8]. The HA has trimeric subunits; each has one domain that goes through the viral envelop domain while the other attaches through the sialic acid receptor on the human cell. For the H7N9 to effectively enter the host cell, the hemagglutinin HA must be cleaved; this cleaving is facilitated by an enzyme released from the epithelial lining of the human respiratory tract. This cleaving of the HA produces a hydrophobically hidden fusion peptide in the HA trimeric complex [6]. The host cell takes up the virus through endocytosis, and the endocytic vesicles combine with the lysosomes and result in its internal acidification (lowers its pH). This lowering of pH causes backwards shifting in the receptor binding conformation, thereby activating the forward shifting of the fusion peptide to enter the vesicular membrane. This fusion process discharges the contents of the virus into the cytoplasm, making the H7N9 virus fit for the replication cycle [9].

Neuraminidase's significant role in releasing the H7N9 virus that has already entered the human host cell through endocytosis makes them the most common human avian H7N9 virus therapeutic target known to date. Neuraminidase splits sialic acid, thereby allowing the trapped virus to exit the cell. The neuraminidase inhibition target aims to halt the splitting of sialic acid and subsequent prevention of the exit of the virus from the human cell. This prevention of the H7N9 virus from exiting the cell deprives it of accessing the required resources for replication, thereby directly stopping its activities [10,11]. Neuraminidase inhibitor (NAI) binds to NA, preventing the virus from leaving the cell [12]. The NAI can only inhibit influenza type A and B and not C because type C does not possess the neuraminidase protein [13]. Therefore, the World Health Organization approved NAIs as the most effective drugs for treating influenza viral infections since 2010. The approved neuraminidase drugs (Figure 1) include oseltamivir, zanamivir and laninamivir [14,15]. Donald et al. (2010) carried out combinatory research on peramivir and oseltamivir. The conducted experimental research studied the chemotherapeutic effects of the combined treatment on mice infected with the influenza virus. The treatment was carried out with peramivir and oseltamivir for three days. The result showed that such combination yielded an improved outcome, better than treatment with suboptimal doses of peramivir and oseltamivir, in the treatment of influenza virus in mice [16].

The later approval of an intravenous highly selective potent peramivir (Figure 1) by the Food and Drug Administration has positively contributed to the fight against the influenza H7N9 virus. Hseir et al. (2021) investigated the efficacy of peramivir over oseltamivir in an emergency unit. They found that patients administered with a single dose of peramivir exhibited a quicker and better recovery than those administered with oseltamivir. The structure of peramivir consists of carboxylic and guanidino moieties in addition to the lipophilic side chain of the cyclopentane backbone. These structural moieties enable peramivir to establish a stronger bond with the N9 of the neuraminidase enzyme with a low dissociation rate. Zhang et al. investigated the pharmacokinetic properties of peramivir in selected healthy Chinese volunteers. Three hundred to four hundred milligram doses of peramivir were intravenously administered to them. When blood samples were collected at intervals after administering the doses, it was discovered that peramivir exhibited linear

pharmacokinetics with an observed increase in maximum concentration. In another study by Sato et al., aimed at determining and predicting the peramivir concentration–time curve of the H7N9 virus, a reduced susceptibility to neuraminidase inhibitors was observed. Ten milligram per kilogram of peramivir was intravenously administered to paediatric patients; peramivir resulted in reduced maximal concentration of about 0.1 percent within 24 h of the drug administration. The study suggested re-administering peramivir in cases of delayed improvement in patients with normal susceptibility to influenza A and B, and that better viral inhibition and lower frequency of adverse effects may be expected with divided administration [17–23]. This further informed our aim to investigate the interatomic and intermolecular interactions of peramivir to ascertain the reasons for this observation [24]. Generally, in both A and B influenza virus types, neuraminidase proteins have characteristic conserved active site residues. The conserved catalytic residues in direct contact with sialic acid are Arg118 (R118), Asp 151 (D151), Arg152 (R152), Arg224 (R224), Glu276 (E276), Arg292 (R292), Arg371 (R371) and Tyr406 (Y406). In addition, other enzymes are supporting binding domain framework residues, which include Glu119 (E119), Arg156 (R156), Trp178 (W178), Ser179 (S179), Asp198 (D198), Ile222 (I222), Glu227 (R227), His274 (H274), Glu227 (R227), Asn294 (N294) and Glu425 (R425) [25–27].

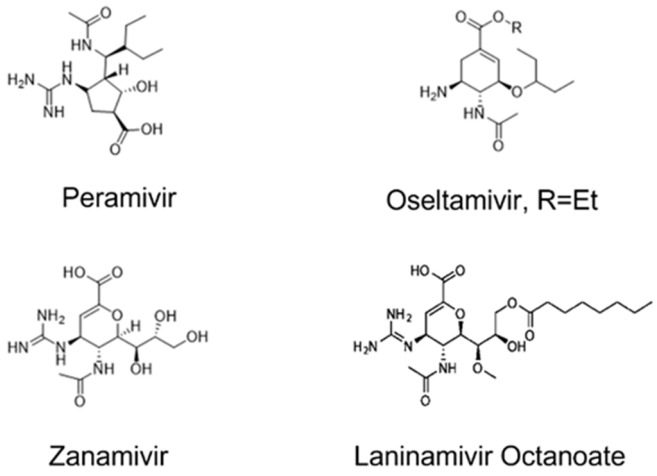

Figure 1. 2D structures of neuraminidase inhibitors.

Transcription of DNA leads to messenger RNA, and subsequent translation of messenger RNA leads to protein formation. Therefore, mutation is an alteration in gene structure as a result of a variant form, which could be transmitted to the next generations [28]. This results from a change in either one of the base units of the DNA or when a more significant portion of the genes/chromosomes are rearranged or deleted [28]. The mutation of any central region of the conserved active domain of the amino acid affects the responsiveness of the human H7N9 virus to NAIs, thereby resulting in resistance to the treatment potencies of the NAIs. Previous studies have investigated the consequences of introducing or altering amino acid residues on the responsiveness and susceptibility of the human H7N9 virus on NAIs [29,30].

Jing et al. studied the avian influenza H7N9 virus' replicability and susceptibility potentials to NAIs when some amino acid residues were substituted, such as Arg292 to Lys292 (R292K), and Glu 119 to Val119 (E119V). The result showed that the neuraminidase inhibitor-resistant mutation in H7N9 could only reduce the susceptibility of neuraminidase inhibitors while the replicability remained unaffected [31]. The single mutation, E119V, has clinically been reported in oseltamivir, an analogue of peramivir. However, the molecular dynamics and conformational alterations resulting from E119V substitution on peramivir is yet to be investigated. Therefore, it is imperative to further study the effects of this mutation on peramivir, an analogue of oseltamivir at the intermolecular level [14,32,33]. The focus of this present study is to computationally investigate the intermolecular mechanisms

of E119V-substituted NA on peramivir. We employed conventional molecular dynamic simulations MD of 250 nanoseconds on the wildtype (WT) and the E119V mutation, and carried out subsequent post-MD analyses, such as root mean square deviation (RMSD), root mean square fluctuation (RMSF), hydrogen bond analysis, binding free energy calculations and the radius of gyration and principal component analysis (PCA) [34,35]. This study promises to offer contributory insight and additional knowledge to enhance future drug designs and help in the fight targeted at controlling the avian influenza H7N9 virus.

2. Materials and Methods

2.1. System Preparation

The X-ray crystallographic structure of neuraminidase–peramivir (wildtype) complex was retrieved from RCSB protein data bank with PDB ID 4MWV. The chimera software was applied in the mutation of arginine to valine (E119V), as well as in the ligand and protein preparations. The ligand was separated from the receptor and hydrogen and charges were added to it. The ligand was saved as mols. The other nonstandard residues and water were removed from the receptor, which was saved as PDB.

2.2. Molecular Dynamic Simulations

Molecular dynamic simulations provide a resemblance of possible real time situations, used in predicting the probability of ligand–protein or protein–protein interactions in a time period. It involves the computation of Newton's laws of motion and quantum physics in predicting the way atoms behave in three-dimensional space [36]. Molecular dynamic simulations of 250 ns were performed on both the wildtype of the peramivir–neuraminidase complex and the E119V mutant. An Amber 18 graphic processing unit (GPU) particle mesh Ewald molecular dynamic (PMEMD) was employed in the MD simulations. The force-field-related parameters and protein description were handled with FF14SB [37,38]. LEAP module implementation of Amber18 was utilised in the addition of hydrogen atoms to the neuraminidase (protein) and subsequent counter-ions additions to neutralise the system [39]. The systems were restrained in TIP3P water box, having the protein atoms situated at eight angstrom (8 Å) distance away to the end of the water box [40]. The system employed the periodic boundary conditions and the handling of the long-range electrostatics, using PMEMD in Amber18 with twelve angstrom (12 Å) van der Walls cut off. The initial minimisation was conducted using a restrained potential of 500 kcal/mol/Å^2 in 1000 steepest descent steps and 1000 conjugate gradient steps on the solute [41]. This was followed by 1000 steps unrestrained conjugate gradient minimisation for the entire system. A gradual heating (0 K to 300 K) used NVT canonical ensemble and a harmonic restraint of 5 kcal/mol/Å^2 for the solute atoms with a one pico-second random collision frequency. An unrestrained equilibration of the system, using NPT ensemble at 1 bar and 300 K, was performed [42]. A molecular dynamics simulation production run of 250 ns was conducted using an isothermal isobaric (NPT) ensemble and a Berendsen barostat [43]. The coordinates were saved at intervals after each stage and the trajectories were analysed. The post-MD analyses were carried out with Amber18 implemented modules, PTRAJ and CPPTRAJ. The plots were conducted using origin software, while the visualisations were conducted with chimera molecular modelling [44]. We measured system stability through the root mean square deviation (RMSD) calculation.

3. Results and Discussion

The results of the post-MD analyses, such as root mean square deviation (RMSD), root mean square fluctuation (RMSF), radius of gyration (RoG), solvent accessible surface area (SASA), hydrogen bond analysis, binding free energy calculations and principal component analysis (PCA), which were calculated for holistic knowledge on the effects of mutations on binding and the conformational terrain of the complex (peramivir-neuraminidase, are briefly discussed below).

3.1. Root Mean Square Deviations (RMSDs)

The root mean square deviation trajectory of the protein backbone alpha carbon (Cα) was produced using the CPPTRAJ module [45]. The standard deviation of the interatomic distance between the Cα backbone atoms of two amino acids were determined based on Equation (1):

$$RMSD(v,w) = \sqrt{\frac{1}{n}\sum_{i=1}^{n}||v_i - w_i||^2} \quad (1)$$

where n is the number of atoms, v_i is the coordinate vector for target atom I, and w_i is the coordinate vector for reference atom i. RMSD measures how the target coordinate set deviates from the reference coordinate sets. The root mean square deviation measures the similarities of the structures of biomolecular compounds and their dynamism. The root mean square deviation of backbone C-α atoms was evaluated (Figure 2), and the conformation's stability was analysed for peramivir wildtype and E119V mutant systems. We also observed the alignment of all the protein frames using the wildtype complex as the reference frame backbone. This provides insight and additional information into the root mean square deviation evolutionary trend of the protein's structural conformation during the simulation run. Figure 2 depicts the evaluated root mean square deviation values calculated for the two systems. We observed relative stability in both complexes, from 10 ns to 115 ns, with the mutant complex exhibiting higher stability. However, the mutant complex showed unusual higher values of 2.5 Å to 2.7 Å (at 115–149 ns), which could be due to the system exhibiting lower binding affinity at this time frame. Subsequently, the two complexes maintained good stability, with the wildtype complex displaying higher values from 150 ns to the end of the simulation time frame.

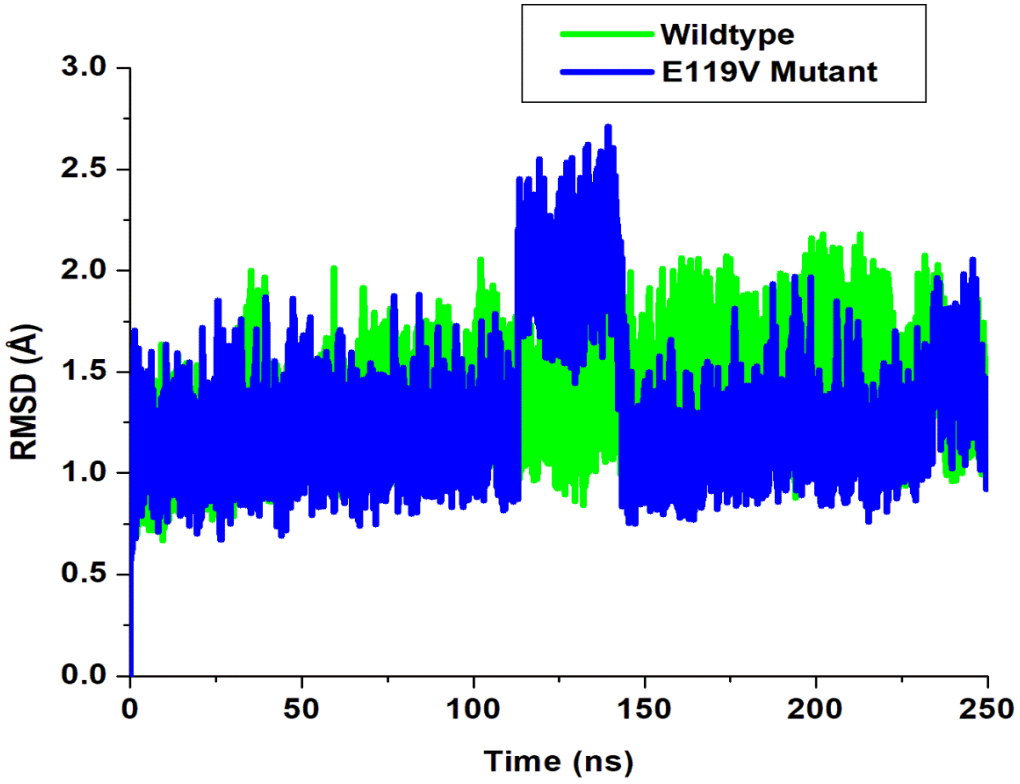

Figure 2. A plot of root mean square deviation.

These results suggested an overall stable molecular dynamics trajectory, occurring in an acceptable range during the simulation's timeframes for the studied systems. We hereby infer that the mutation induced a more stable conformational structure on the neuraminidase protein.

3.2. Root Mean Square Fluctuation (RMSF)

The root mean square fluctuation (RMSF) is calculated to predict the changes in a protein 's conformations based on each residues contribution. In RMSF Equation (2) below, $x_{i(j)}$ is the i-th Cα atom position in the j-th model structure, and (x_i) represents the averaged location of the i-th Cα backbone atom in all models.

$$RMSF = \sqrt{\frac{1}{n}\sum_{j}^{n}|x_{i(j)} - (x_i)|^2} \quad (2)$$

In any given protein, each amino acid residue shares a common backbone which is made up of alpha carbon, carboxyl and amine moiety. These amino acids differ due to the different side chains that take varied sizes and atomic conformations. When a ligand molecule is in a complex with the protein, it restricts the movement of the side chains within the active site region. This differs from the root mean square deviation, averaged over time with specific values for each residue. The root mean square fluctuations were evaluated for Cα atoms of each amino acid of the two complexes (Figure 3a). We observed conformational flexibility with a similar trend in both the wildtype and the mutant complexes. However, the wildtype complex showed higher fluctuations from the beginning to the end of the simulations, while the mutant complex maintained a lower fluctuation during the entire simulation period. This suggests that the Val119 mutation induces higher stability to the peramivir–neuraminidase complex and further confirms the root mean square deviation results.

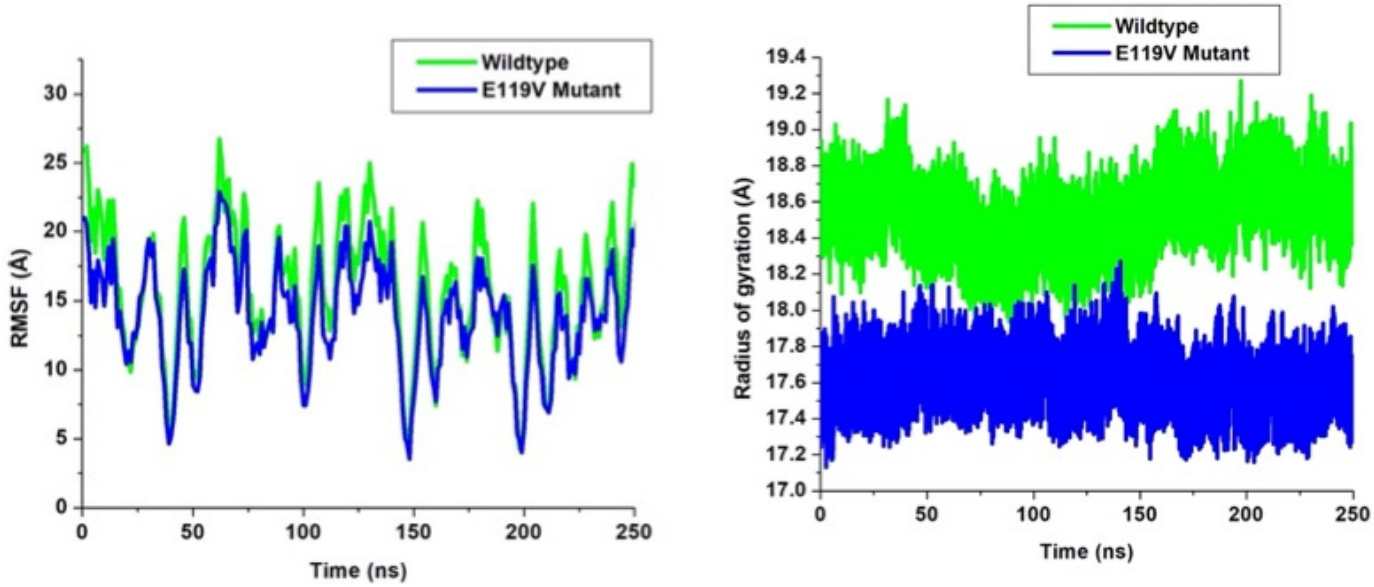

(**a**) (**b**)

Figure 3. (**a**) Plots of root mean square fluctuation and (**b**) radius of gyration.

3.3. Radius of Gyration (RoG)

The radius of gyration is associated with compound stability and connected with the secondary structure of biomolecular systems [46]. It quantitatively measures the compactness, shape and folding of biomolecular compounds during molecular dynamic simulations. It is the moment of inertia of atoms from their centre of mass, which quantifies the molecular rigidity [47]. The radius of gyration is the square root of the inertia moment of atoms (Equation (3)), where n is the number of atoms, r_i depicts the atomic position and r_m represents the mean position of all atoms. Herein, we evaluated the RoG of peramivir

wildtype and E119V mutant complexes, as depicted in Figure 4, using CPPTRAJ within the AMBER 18 suite [48].

$$RoG = \sqrt{\frac{1}{n}\sum_{n}^{i=0}(r_i - r_m)^2} \quad (3)$$

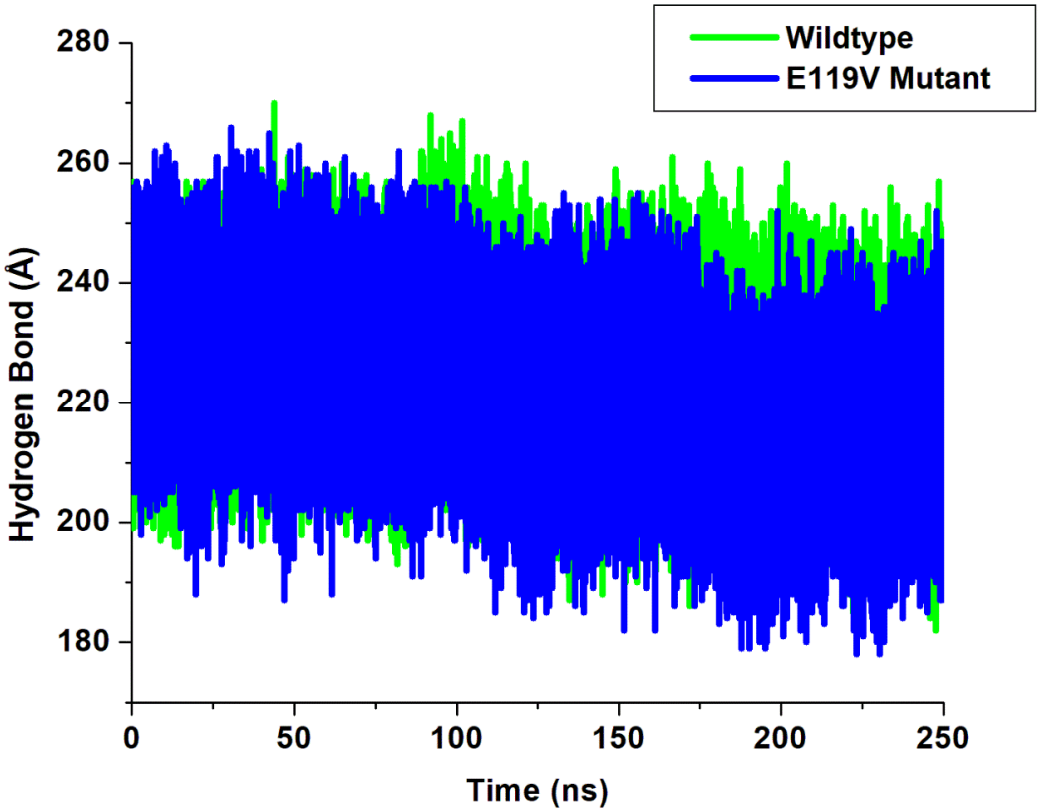

Figure 4. Plot of H-bond formation.

The plot (3b) depicts that the wildtype exhibited significantly higher values from the beginning to the end of the 250 ns simulations. Conversely, the E119V mutant complex maintained lower values and consequently good compactness throughout the simulations. The substitution of the amino acid glutamate by valine in the E119V mutant resulted in more compactness and good folding in the peramivir neuraminidase complex.

3.4. Hydrogen Bond Analysis

Hydrogen bonds perform essential roles in molecular recognition and the overall stability of the protein structure. The formation of hydrogen bonds between amino acid residues is vitally essential in maintaining the structural conformation of proteins. When proteins undergo mutation, the hydrogen bonds are usually altered around the mutation site. The plot (Figure 4) depicts an apparent loss in hydrogen bond formation from 80 ns to 250 ns in the E119V mutant complex, thereby resulting in a distortion in the conformation of the wildtype complex.

To further investigate the impact of peramivir binding on the wildtype and E119V mutant systems, the evolution of hydrogen bond distances and the percentage occupancy of each intermolecular hydrogen bond were monitored between amino acid residues interacting with wildtype and E119V in the active site for 250-ns simulations (Table 1). The primary residues constituted hydrogen bonds Glu 119, Asp 151, Glu 213, Glu 278, Arg 371 and Tyr 406. Such amino acids were identified as key residues for neuraminidase–peramivir binding. The more vital interaction between peramivir and these residues plays an essential role in the peramivir's potency.

Table 1. Percentage (%) occupancy and average distance (Å) between the peramivir (PERA) and prominent active site residues were calculated over simulation time.

Complexes	Acceptor	DonorH	Donor	Frames	Percentage Occupancy	Average Distance
Wildtype	PERA@O14	Glu119@HH11	Glu119@NH1	123148	79.26	2.8135
	PERA@O7	ARG371@HH22	ARG371@NH2	122459	68.21	2.8329
	GLU278@OE2	PERA@H25	PERA@N25	81010	52.40	2.8470
	TYR406@OH	PERA@H25	PERA@N25	27630	41.05	2.8491
	ASP151@OD1	PERA@H272	PERA@N27	6595	12.64	2.8949
E119V	PERA@O8	ARG371@HH12	ARG371@NH1	147426	99.06	2.7693
	TYR406@OH	PERA@H25	PERA@N25	142609	97.13	2.8687
	PERA@O14	VAL119@HH21	VAL119@NH2	117978	87.36	2.7971
	GLU278@OE2	PERA@H271	PERA@N27	121895	88.83	2.8190
	GLU213@OE2	PERA@H271	PERA@N27	55786	62.35	2.8874

The findings in Table 1 agree with the ligand–protein amino acid interaction at the active site in Figure 4, showing the atoms responsible for the hydrogen bond interactions. The mutant Glu 119–peramivir complex (87.36%) exhibited a high hydrogen bond percentage occupancy when compared to the wildtype Val 119–peramivir complex (79.26%) throughout the simulation. The mutant Glu 278–peramivir complex (88.83%) also indicated a high hydrogen bond percentage occupancy compared to the wildtype Glu 278–peramivir complex (52.40%). The E119V mutant Tyr 406–peramivir complex (97.13%) showed a high hydrogen bond percentage occupancy compared to the wildtype Tyr 406–peramivir complex (41.05%). These results suggest a strong interaction between E119V mutant active site residue atoms and peramivir compared to the wildtype. This could imply that interactions of E119V mutant amino acids with peramivir could be significant for high-affinity binding and relative stability of the peramivir–neuraminidase complex.

3.5. Principal Components Analysis (PCA)

The principal components analysis (PCA) makes the atomic dimensions of data from molecular dynamic simulation's trajectories more concise, making it possible to visualise and analyse them while comparing the detected dynamic movements during the MD run. It diagonalises positions of the covariance matrix while identifying the orthogonal group of eigenvectors (modes) that describe the path of maximal variation in the detected conformational distributions. Therefore, slow alterations in conformations are detected when these prevalent modes are projected back to the original trajectory data [49,50]. Preceding the molecular dynamic simulation's trajectory data analysis for PCA, solvents and ions were removed (stripped) from the PTRAJ Amber18 module, thereafter aligning the trajectories against a complete minimised structure. The principal component1 (PC1) and principal component2 (PC2) were analysed (Figure 5) while generating covariance matrices for the two systems (wildtype and E119V mutant) using origin software [46]. Figure 5 depicts a scattered plot for the two complexes, showing remarkable differences between the peramivir wildtype and E119V mutant complexes. The two systems displayed a conformational distribution in space. However, the E119V mutant complex exhibited slightly lower conformational changes than the wildtype.

3.6. MM/GBSA Binding Free Energy Calculation

The binding free energy analysis involves the endpoint energy calculations, which provide useful details about the ligand–protein complex association. In spontaneous processes, ligand–protein complexes occur when the change in Gibbs free energies (ΔG) of the given systems are negative and result when the systems reach equilibrium states at constant pressures and temperatures. Given that the ligand–protein association are subject to the magnitude of the negative ΔG, it is suggested that ΔG controls the stability of any given ligand–protein complex [44,46]. Therefore, the binding free energy is determined by

the states of a system and, as thus, ΔG is determined by the initial and final thermodynamic states, irrespective of the pathway linking these states. The binding free energies of neuraminidase–peramivir wildtype and E119V mutant were computed using the molecular mechanics/generalized Born surface area method. The following equations, therefore, summarise the binding free energy:

$$\Delta G_{bind} = G_{complex} - G_{receptor} - G_{ligand} \quad (4)$$

$$\Delta G_{bind} = E_{gas} + G_{sol} - T\Delta S \quad (5)$$

$$E_{gas} = E_{int} + E_{vdW} + E_{ele} \quad (6)$$

$$G_{sol} = G_{GB} + G_{SA} \quad (7)$$

$$G_{SA} = \gamma SASA \quad (8)$$

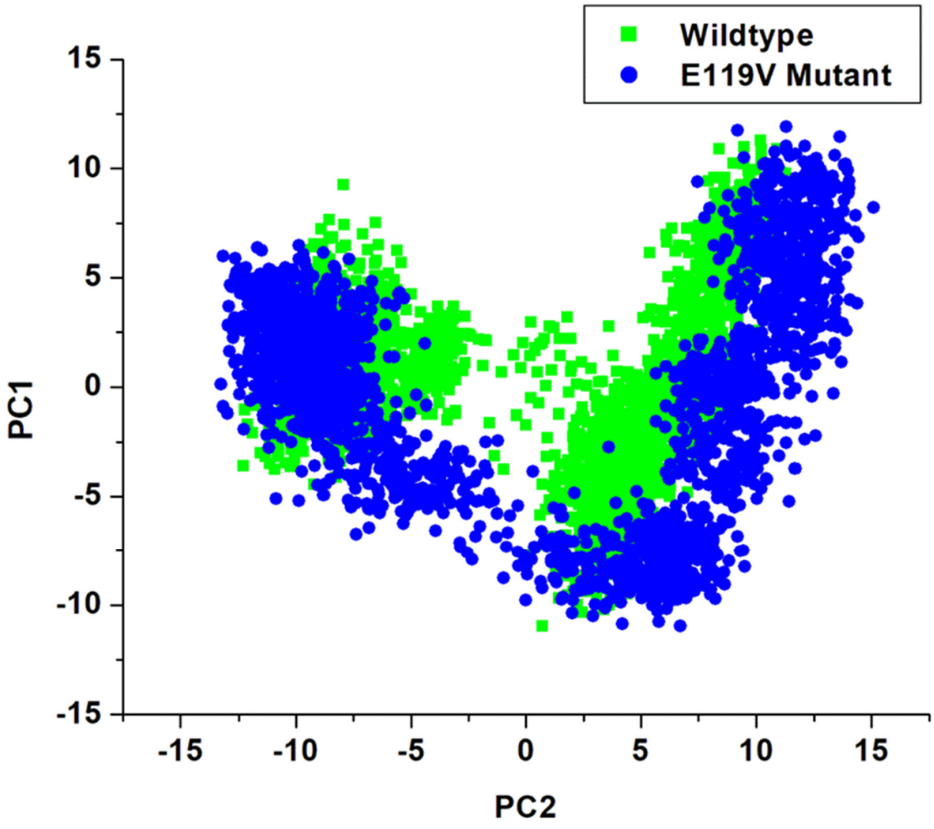

Figure 5. PCA scatter plot projection of C-α atoms motion of the first two principal components, PC1 and PC2.

3.7. MM/GBSA Binding Free Energy Calculation

Table 2 depicts the predicted MMGBSA binding energies for peramivir-wildtype (WT) and E119V mutant, respectively. The calculated total binding energy (ΔG_{bind}) for peramivir–wildtype was -49.09 ± 0.13 kcal/mol, while the E119V mutant was -58.55 ± 0.15 kcal/mol. This difference is puzzling since atomistic modelling of these complexes in the gas phase (ΔG_{gas}) show that WT is slightly energetically favoured than E119V. The decomposition of the binding energies into van der Waals, electrostatics, nonpolar and polar components enable us to identify the parameters driving the binding (Table 2) of the two complexes. We trace the solubility (ΔG_{sol}) difference to the polar nature of the WT with glutamate over the hydrophobic valine of the mutant with ΔG_{pol} values, 151.11 ± 0.26 and 139.56 ± 0.24 kcal/mol, respectively. Additionally, the van der Waals binding energy contribution of -29.19 ± 0.08 kcal/mol slightly drives the higher calculated binding en-

ergy in the E119V mutant. Our calculation revealed the impact of explicit solvation on protein dynamics, energy prediction and overall remodification of the protein behaviour, mimicking an ideal system [51].

Table 2. Calculated MMGBSA binding free energy for peramivir–wildtype and the E119V mutant.

Complexes	ΔG_{vdv}	ΔE_{ele}	ΔE_{bind}	ΔE_{gas}	ΔG_{sol}	ΔG_{pol}	ΔG_{nonpol}
Wildtype	−26.86 ± 0.08	−168.21 ± 0.35	−49.09 ± 0.13	−195.07 ± 0.33	145.99 ± 0.26	151.11 ± 0.26	−5.12 ± 0.00
E119V	−29.19 ± 0.08	−163.77 ± 0.37	−58.55 ± 0.15	−192.96 ± 0.35	134.41 ± 0.24	139.56 ± 0.24	−5.15 ± 0.00

ΔG_{bind}—binding free energy; ΔE_{ele}—electrostatic interaction; ΔE_{vdW}—van der Waals forces; ΔG_{gas}—gas–phase interaction; ΔG_{sol}—solvation energy; ΔG_{pol}—polar salvation energy; ΔG_{nonpol}—nonpolar salvation energy.

3.8. Per-Residue Contribution to Binding Free Energies

We further broke down the calculated binding energies for each active site residue to ascertain their significant intermolecular interacting contributions to the peramivir wildtype and E119V complexes. The active site residue total energies, electrostatic interactions, and the van der Waals energy contributions in kcal/mol are given in Figure 6A,C, respectively. Figure 6B,D also show the ligand interactions at the active site. In both systems, Arg 371 displayed the highest electrostatic contributions of −29.8 kcal/mol (wildtype) and −30.6 kcal/mol (mutant), respectively. There is a significant decrease in the electrostatic contribution in Glu 119 from −16.0 kcal/mol for the wildtype to −3.5 kcal/mol for the mutant. However, the electrostatic and van der Waal contributions from other residues in the mutant complex displayed significantly higher energies than in the wildtype. The overall higher van der Waal contribution and favourable higher hydrogen bond occupancy are suggested to be responsible for the higher compactness and stability in the mutant complex.

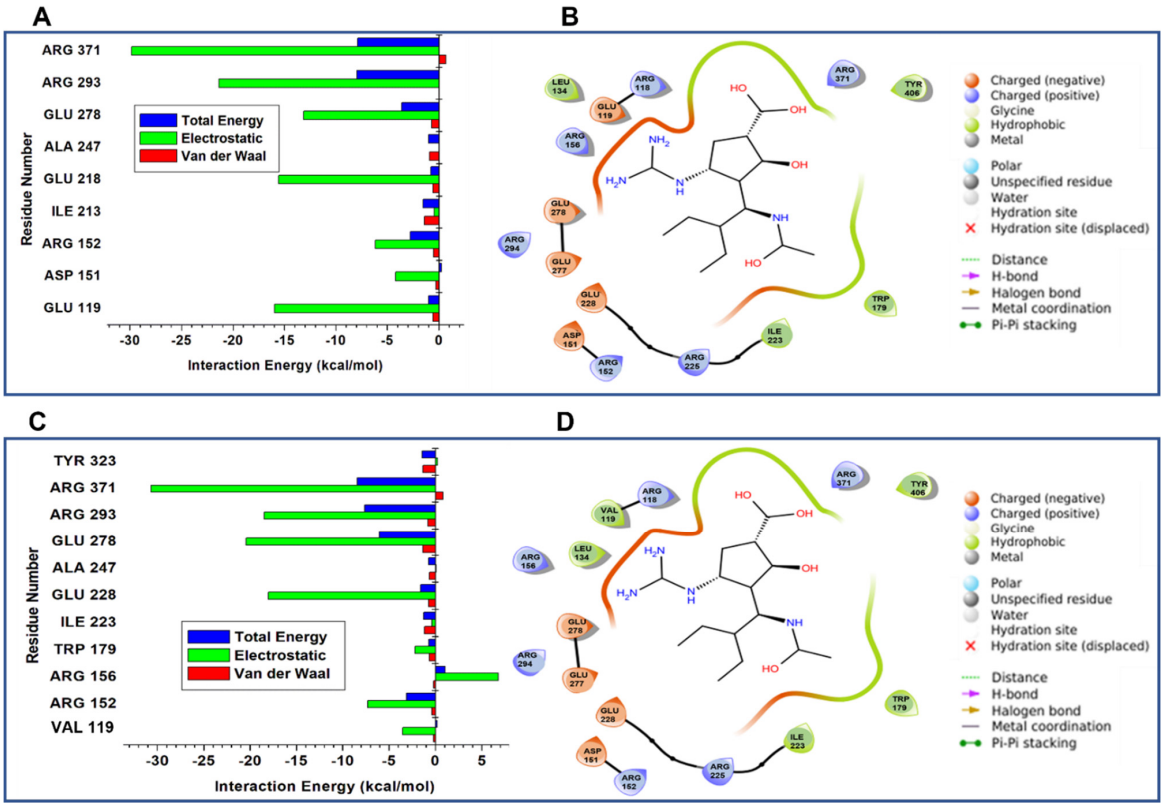

Figure 6. The electrostatic plots of van der Waals and the total energy per residue contributions for the wildtype (**A**) and the E119V mutant (**C**) complexes. The residues interacting at the active sites are also represented in (**B**,**D**).

4. Conclusions

We investigated the intermolecular mechanism and dynamism of avian influenza virus H7N9 susceptibility to E119V-substituted peramivir–neuraminidase complex. The study employed the post-molecular dynamic simulation analysis in proffering multidimensional insights on the effects of the substituted 119V towards peramivir. The analysed total binding energy, PCA, RMSD, RMSF, RoG and hydrogen bond formation alludes to the fact that the E119V mutation conferred relative stability to the peramivir–neuraminidase complex. Our investigation shows that the effects of the substituted 119V amino acid residue increased the peramivir binding energy by -9.46 ± 0.02 kcal/mol. This increase in the total binding energy of the peramivir–neuraminidase wildtype from -49.09 ± 0.13 kcal/mol to -58.55 ± 0.15 kcal/mol, and the significantly increased hydrogen occupancy of the E119V, could be responsible for the consistent higher stability of the mutant complex, as shown in the different post analyses plots and diagrams. This study promises to proffer contributory insight and additional knowledge that would enhance future drug designs and help in the fight targeted at controlling the avian influenza H7N9 virus. Therefore, we suggest the need for an experimentalist to always collaborate with computational chemists, as we have carried out in our previous studies. This promises to save time and resources.

Author Contributions: Conceptualization, S.E.M. and S.C.U.; methodology, All; software, All; validation, S.E.M., S.C.U., B.H.A., M.L.N. and H.M.K.; formal analysis, S.E.M. and S.C.U.; investigation, S.E.M.; resources, H.M.K.; data curation, All; writing—original draft preparation, S.E.M.; A.G.M.; and S.C.U.; writing—review and editing, All; visualisation, All; supervision, H.M.K.; project administration, H.M.K.; funding acquisition, H.M.K. All authors have read and agreed to the published version of the manuscript.

Funding: This research received no external funding.

Institutional Review Board Statement: Not applicable.

Informed Consent Statement: Not applicable.

Data Availability Statement: The data presented in this study are available on request from the corresponding author.

Acknowledgments: The authors acknowledge the UKZN School of Health Sciences and the Center for High-Performance Computing (CHPC, http://www.chpc.ac.za, accessed on 13 December 2021) for computational resources.

Conflicts of Interest: The authors declare no conflict of interest.

Sample Availability: Not applicable.

References

1. Gubareva, L.; Mohan, T. Antivirals Targeting the Neuraminidase. *Cold Spring Harb. Perspect. Med.* **2020**, *12*, a038455. [CrossRef] [PubMed]
2. Noshi, T.; Kitano, M.; Taniguchi, K.; Yamamoto, A.; Omoto, S.; Baba, K.; Hashimoto, T.; Ishida, K.; Kushima, Y.; Hattori, K.; et al. In vitro characterization of baloxavir acid, a first-in-class cap-dependent endonuclease inhibitor of the influenza virus polymerase PA subunit. *Antiviral Res.* **2018**, *160*, 109–117. [CrossRef]
3. Krammer, F.; Palese, P. Advances in the development of influenza virus vaccines. *Nat. Rev. Drug Discov.* **2015**, *14*, 167–182. [CrossRef]
4. Kalil, A.C.; Thomas, P.G. Influenza virus-related critical illness: Pathophysiology and epidemiology. *Crit. Care* **2019**, *23*, 258. [CrossRef]
5. Sunayana Shyam Jandhyala, B. Investigation of Influenza B Virus Replication Potential in Swine Primary Respiratory Epithelial Cells and Phylodynamic Analysis of Equine Influenza a H3n8 Viruses. Master's Thesis, South Dakota State University, Brookings, SD, USA, 2020.
6. Krammer, F.; Smith, G.J.D.; Fouchier, R.A.M.; Peiris, M.; Kedzierska, K.; Doherty, P.C.; Palese, P.; Shaw, M.L.; Treanor, J.; Webster, R.G.; et al. Influenza. *Nat. Rev. Dis. Prim.* **2018**, *4*, 3. [CrossRef]
7. Costa, T.; Chaves, A.J.; Valle, R.; Darji, A.; van Riel, D.; Kuiken, T.; Majó, N.; Ramis, A. Distribution patterns of influenza virus receptors and viral attachment patterns in the respiratory and intestinal tracts of seven avian species. *Vet. Res.* **2012**, *43*, 28. [CrossRef]

8. Richard, M.; van den Brand, J.M.A.; Bestebroer, T.M.; Lexmond, P.; de Meulder, D.; Fouchier, R.A.M.; Lowen, A.C.; Herfst, S. Influenza A viruses are transmitted via the air from the nasal respiratory epithelium of ferrets. *Nat. Commun.* **2020**, *11*, 1–11. [CrossRef]
9. Lee, J.; Ye, Y. The Roles of Endo-Lysosomes in Unconventional Protein Secretion. *Cells* **2018**, *7*, 198. [CrossRef] [PubMed]
10. Traving, C.; Schauer, R. Structure, function and metabolism of sialic acids. *Cell. Mol. Life Sci. C* **1998**, *54*, 1330–1349. [CrossRef] [PubMed]
11. Recherche, U.O. Research: Investigation of a Trimeric Hemagglutinin Stem Domain from Influenza B for a Universal Vaccine. Ph.D. Thesis, University of Ottawa, Ottawa, ON, Canada, 2018.
12. Madsen, A.; Dai, Y.N.; McMahon, M.; Schmitz, A.J.; Turner, J.S.; Tan, J.; Lei, T.; Alsoussi, W.B.; Strohmeier, S.; Amor, M.; et al. Human Antibodies Targeting Influenza B Virus Neuraminidase Active Site Are Broadly Protective. *Immunity* **2020**, *53*, 852–863.e7. [CrossRef]
13. Holmes, E.C.; Hurt, A.C.; Dobbie, Z.; Clinch, B.; Oxford, J.S.; Piedra, P.A. Understanding the impact of resistance to influenza antivirals. *Clin. Microbiol. Rev.* **2021**, *34*, 1–13. [CrossRef]
14. Bai, Y.; Jones, J.C.; Wong, S.-S.; Zanin, M. Antivirals Targeting the Surface Glycoproteins of Influenza Virus: Mechanisms of Action and Resistance. *Viruses* **2021**, *13*, 624. [CrossRef]
15. La Frazia, S.; Piacentini, S.; Riccio, A.; Rossignol, J.F.; Santoro, M.G. The second-generation thiazolide haloxanide is a potent inhibitor of avian influenza virus replication. *Antiviral Res.* **2018**, *157*, 159–168. [CrossRef]
16. Smee, D.F.; Hurst, B.L.; Wong, M.H.; Tarbet, E.B.; Babu, Y.S.; Klumpp, K.; Morrey, J.D. Combinations of oseltamivir and peramivir for the treatment of influenza A (H1N1) virus infections in cell culture and in mice. *Antiviral Res.* **2010**, *88*, 38–44. [CrossRef] [PubMed]
17. Wester, A.; Shetty, A.K. Peramivir injection in the treatment of acute influenza: A review of the literature. *Infect. Drug Resist.* **2016**, *9*, 201–214. [CrossRef]
18. Babu, Y.S.; Chand, P.; Bantia, S.; Kotian, P.; Dehghani, A.; El-Kattan, Y.; Lin, T.H.; Hutchison, T.L.; Elliott, A.J.; Parker, C.D.; et al. BCX-1812 (RWJ-270201): Discovery of a novel, highly potent, orally active, and selective influenza neuraminidase inhibitor through structure-based drug design. *J. Med. Chem.* **2000**, *43*, 3482–3486. [CrossRef] [PubMed]
19. Bantia, S.; Arnold, C.S.; Parker, C.D.; Upshaw, R.; Chand, P. Anti-influenza virus activity of peramivir in mice with single intramuscular injection. *Antiviral Res.* **2006**, *69*, 39–45. [CrossRef]
20. Mineno, T.; Miller, M.J. Stereoselective total synthesis of racemic BCX-1812 (RWJ-270201) for the development of neuraminidase inhibitors as anti-influenza agents. *J. Org. Chem.* **2003**, *68*, 6591–6596. [CrossRef]
21. Castillo, R.; Holland, L.E.; Boltz, D.A. Peramivir and its use in H1N1 influenza. *Drugs Today* **2010**, *46*, 399–408. [CrossRef] [PubMed]
22. Zhang, D.; Du, A.; Zhang, L.; Ma, J.; Meng, L.; Deng, M.; Xu, J.; Liu, H. Pharmacokinetics of peramivir after single intravenous doses in healthy Chinese subjects. *Xenobiotica* **2015**, *45*, 239–243. [CrossRef]
23. Sato, M.; Ito, M.; Suzuki, S.; Sakuma, H.; Takeyama, A.; Oda, S.; Watanabe, M.; Hashimoto, K.; Miyazaki, K.; Kawasaki, Y.; et al. Influenza viral load and peramivir kinetics after single administration and proposal of regimens for peramivir administration against resistant variants. *Antimicrob. Agents Chemother.* **2015**, *59*, 1643–1649. [CrossRef]
24. Hsieh, Y.H.; Dugas, A.F.; LoVecchio, F.; McBryde, B.; Ricketts, E.P.; Saliba-Shaw, K.; Rothman, R.E. Intravenous peramivir vs oral oseltamivir in high-risk emergency department patients with influenza: Results from a pilot randomized controlled study. *Influenza Respir. Viruses* **2021**, *15*, 121–131. [CrossRef] [PubMed]
25. Yen, H.-L.; Hoffmann, E.; Taylor, G.; Scholtissek, C.; Monto, A.S.; Webster, R.G.; Govorkova, E.A. Importance of Neuraminidase Active-Site Residues to the Neuraminidase Inhibitor Resistance of Influenza Viruses. *J. Virol.* **2006**, *80*, 8787–8795. [CrossRef] [PubMed]
26. Du, W.; de Vries, E.; van Kuppeveld, F.J.M.; Matrosovich, M.; de Haan, C.A.M. Second sialic acid-binding site of influenza A virus neuraminidase: Binding receptors for efficient release. *FEBS J.* **2021**, *288*, 5598–5612. [CrossRef] [PubMed]
27. Mtambo, S.E.; Amoako, D.G.; Somboro, A.M.; Agoni, C.; Lawal, M.M.; Gumede, N.S.; Khan, R.B.; Kumalo, H.M. Influenza Viruses: Harnessing the Crucial Role of the M2 Ion-Channel and Neuraminidase toward Inhibitor Design. *Molecules* **2021**, *26*, 880. [CrossRef]
28. Minchin, S.; Lodge, J. Understanding biochemistry: Structure and function of nucleic acids. *Essays Biochem.* **2019**, *63*, 433–456. [CrossRef] [PubMed]
29. Lampejo, T. Influenza and antiviral resistance: An overview. *Eur. J. Clin. Microbiol. Infect. Dis.* **2020**, *39*, 1201–1208. [CrossRef] [PubMed]
30. Prachanronarong, K.L.; Canale, A.S.; Liu, P.; Somasundaran, M.; Hou, S.; Poh, Y.-P.; Han, T.; Zhu, Q.; Renzette, N.; Zeldovich, K.B.; et al. Mutations in Influenza A Virus Neuraminidase and Hemagglutinin Confer Resistance against a Broadly Neutralizing Hemagglutinin Stem Antibody. *J. Virol.* **2019**, *93*, e01639-18. [CrossRef]
31. Tang, J.; Zhang, J.; Zhou, J.; Zhu, W.; Yang, L.; Zou, S.; Wei, H.; Xin, L.; Huang, W.; Li, X.; et al. Highly pathogenic avian influenza H7N9 viruses with reduced susceptibility to neuraminidase inhibitors showed comparable replication capacity to their sensitive counterparts. *Virol. J.* **2019**, *16*, 1–7. [CrossRef]

32. Tang, J.; Zhang, S.X.; Zhang, J.; Li, X.Y.; Zhou, J.F.; Zou, S.M.; Bo, H.; Xin, L.; Yang, L.; Liu, J.; et al. Profile and generation of reduced neuraminidase inhibitor susceptibility in highly pathogenic avian influenza H7N9 virus from human cases in Mainland of China, 2016–2019. *Virology* **2020**, *549*, 77–84. [CrossRef]
33. Takashita, E.; Daniels, R.S.; Fujisaki, S.; Gregory, V.; Gubareva, L.V.; Huang, W.; Hurt, A.C.; Lackenby, A.; Nguyen, H.T.; Pereyaslov, D.; et al. Global update on the susceptibilities of human influenza viruses to neuraminidase inhibitors and the cap-dependent endonuclease inhibitor baloxavir, 2017–2018. *Antiviral Res.* **2020**, *175*, 104718. [CrossRef]
34. Akachar, J. The Computational Analyses, Molecular Dynamics of Fatty-Acid Transport Mechanism to the CD36 Receptor: The Outcomes of the Mutation K164A on the Binding Domain, Structure and Function. *Res. Sq.* **2021**, 1–15. [CrossRef]
35. Pereira, G.R.C.; Vieira, B.d.A.A.; de Mesquita, J.F. Comprehensive in silico analysis and molecular dynamics of the superoxide dismutase 1 (SOD1) variants related to amyotrophic lateral sclerosis. *PLoS ONE* **2021**, *16*, e0247841. [CrossRef] [PubMed]
36. Zhao, X.; Jin, H.; Chen, Y.; Ge, Z. Numerical study of H_2, CH_4, CO, O_2 and CO_2 diffusion in water near the critical point with molecular dynamics simulation. *Comput. Math. Appl.* **2021**, *81*, 759–771. [CrossRef]
37. Ben-Shalom, I.Y.; Lin, C.; Radak, B.K.; Sherman, W.; Gilson, M.K. Fast Equilibration of Water between Buried Sites and Bulk by MD with Parallel Monte Carlo Water Moves on GPUs. pp. 1–17. Available online: https://chemrxiv.org/engage/chemrxiv/article-details/6123cb101d1cc2684fcab40a (accessed on 13 December 2021).
38. Du, Q.; Qian, Y.; Xue, W. Cross-reactivity of two human IL-6 family cytokines OSM and LIF explored by protein-protein docking and molecular dynamics simulation. *Biochim. Biophys. Acta Gen. Subj.* **2021**, *1865*, 129907. [CrossRef]
39. Fakhar, Z.; Hejazi, L.; Tabatabai, S.A.; Munro, O.Q. Discovery of novel heterocyclic amide-based inhibitors: An integrative in-silico approach to targeting soluble epoxide hydrolase. *J. Biomol. Struct. Dyn.* **2021**, 1–15. [CrossRef] [PubMed]
40. Li, Y.; Wang, C.; Xu, T.; Pan, P.; Yu, Q.; Xu, L.; Xiong, X.; Hou, T.; Cui, S.; Sun, Y. Discovery of a small molecule inhibitor of cullin neddylation that triggers ER stress to induce autophagy. *Acta Pharm. Sin. B* **2021**, *11*, 3567–3584. [CrossRef]
41. Wolf, S.; Sohmen, B.; Hellenkamp, B.; Thurn, J.; Stock, G.; Hugel, T. Hierarchical dynamics in allostery following ATP hydrolysis monitored by single molecule FRET measurements and MD simulations. *Chem. Sci.* **2021**, *12*, 3350–3359. [CrossRef] [PubMed]
42. Panwar, A.; Kumar, A. In-silico Analysis and Molecular Dynamics Simulations of Lysozyme by GROMACS 2020.2. *Ann. Rom. Soc. Cell Biol.* **2021**, *25*, 9679–9685.
43. Jin, T.; Patel, S.J.; Lehn, R.C. Van Molecular simulations of lipid membrane partitioning and translocation by bacterial quorum sensing modulators. *PLoS ONE* **2021**, *16*, e0246187. [CrossRef]
44. Ugbaja, S.C.; Appiah-Kubi, P.; Lawal, M.M.; Gumede, N.S.; Kumalo, H.M. Unravelling the molecular basis of AM-6494 high potency at BACE1 in Alzheimer's disease: An integrated dynamic interaction investigation. *J. Biomol. Struct. Dyn.* **2020**, 1–13. [CrossRef]
45. Muralidharan, N.; Sakthivel, R.; Velmurugan, D.; Gromiha, M.M. Computational studies of drug repurposing and synergism of lopinavir, oseltamivir and ritonavir binding with SARS-CoV. *J. Biomol. Struct. Dyn.* **2020**, *39*, 2673–2678. [CrossRef] [PubMed]
46. Mhlongo, N.N.; Soliman, M.E.S. Single H5N1 influenza A neuraminidase mutation develops resistance to oseltamivir due to distorted conformational and drug binding landscape: Multiple molecular dynamics analyses. *RSC Adv.* **2015**, *5*, 10849–10861. [CrossRef]
47. Yamamoto, E.; Akimoto, T.; Mitsutake, A.; Metzler, R. Universal Relation between Instantaneous Diffusivity and Radius of Gyration of Proteins in Aqueous Solution. *Phys. Rev. Lett.* **2021**, *126*, 128101. [CrossRef]
48. Kumar, D.; Meena, M.K.; Kumari, K.; Kumar, R.V.; Bahadur, I.; Jain, P.; Singh, P. Exploring the effect of temperature on inhibition of non-structural protease 3 of Chikungunya virus using molecular dynamics simulations and thermodynamics parameters. *J. Mol. Liq.* **2021**, *335*, 116164. [CrossRef]
49. Liu, Z.; Qian, S.; Wang, Y.; Yan, Y.; Yang, T. Schrödinger principal-component analysis: On the duality between principal-component analysis and the Schrödinger equation. *Phys. Rev. E* **2021**, *104*, 025307. [CrossRef]
50. Huang, Y.; Ferguson, N. Principal component analysis of the cross-axis apparent mass nonlinearity during whole-body vibration. *Mech. Syst. Signal Process.* **2021**, *146*, 107008. [CrossRef]
51. Lai, J.K.; Ambia, J.; Wang, Y.; Barth, P. Enhancing Structure Prediction and Design of Soluble and Membrane Proteins with Explicit Solvent-Protein Interactions. *Structure* **2017**, *25*, 1758–1770.e8. [CrossRef]

Chapter 6

RESEARCH ARTICLE

molecules

MDPI

Article

In silico drug repurposing of FDA-approved drugs highlighting promacta as a potential inhibitor of H7N9 influenza virus

Sphamandla E. Mtambo, and Hezekiel M. Kumalo *

Drug Research and Innovation Unit, Discipline of Medical Biochemistry, School of Laboratory Medicine and Medical Science, University of KwaZulu-Natal, Durban 4000, South Africa; sphamtambo@gmail.com (S.E.M.)
* Correspondence: kumaloh@ukzn.ac.za; Tel.: +27-031-260-4940

Abstract: Influenza virus infections continue to be a significant and recurrent public health problem. Although vaccine efficacy varies, regular immunisation is the most effective method of suppressing the influenza virus. Antiviral drugs are available for influenza, although two of the four FDA-approved antiviral treatments have resulted in significant drug resistance. Therefore, new treatments are being sought to reduce the burden of flu-related illness. The time-consuming development of treatments for new and re-emerging diseases like influenza and the high failure rate is an increasing concern. In this context, we used an *in silico*-based drug repurposing method to repurpose FDA-approved drugs as potential therapies against the H7N9 virus. To find potential inhibitors, a total of 2,568 drugs were screened. Promacta, tucitanib and lurasidone were identified as promising hits in the DrugBank database. According to the calculations of MM-GBSA, tucitanib (-54.11 kcal/mol) and promacta (-56.20 kcal/mol) occupied the active site of neuraminidase with a higher binding affinity than the standard drug peramivir (-49.09 kcal/mol). Molecular dynamics (MD) simulation studies showed that the C-α atom backbones of the complexes of tucatinib and promacta neuraminidase were stable throughout the simulation period. According to ADME analysis, the hit compounds have a high gastrointestinal absorption (GI) and do not exhibit properties that allow them to cross the blood-brain barrier (BBB). According to the *in silico* toxicity prediction, promacta is not cardiotoxic, while lurasidone and tucatinib show only weak inhibition. Therefore, we propose to test these compounds experimentally against the influenza H7N9 virus. The investigation and validation of these potential H7N9 inhibitors would be beneficial to bringing these compounds into the clinical settings.

Keywords: Virtual Screening; Drug Repurposing; *In Silico* Method; Molecular Dynamics Simulations; Influenza A Virus; H7N9; FDA Approved Drugs.

Citation: : Mtambo, S.E.; Kumalo, H.M. In silico drug repurposing of FDA-approved drugs highlighting promacta as a potential inhibitor of influenza A (H7N9) virus. *Molecules* **2022**, *27*, x. https://doi.org/10.3390/xxxxx

Academic Editor: Firstname Lastname

Received: date
Accepted: date
Published: date

1. Introduction

In March 2013, avian influenza A (H7N9) virus infection in humans was discovered in East China. Since then, it has infected 1,565 people and killed approximately 39% of those who have been confirmed to have an Asian H7N9 virus infection [1,2] Some influenza A (H7N9) virus-infected humans developed pneumonia and acute respiratory distress syndrome, with high case fatality rates [3,4]. The influenza A virus (IAV) has two major surface glycoproteins that dominate the virus surface: neuraminidase (NA) and hemagglutinin (HA). The cleavage of α-(2-3 or 2-6)-ketosidic linkage between terminal sialic acid and adjacent surface glycoprotein is catalyzed by NA. Furthermore, this promotes the budding of newly formed viral particles from the infected cell, allowing progeny viruses to infect uninfected host cells and infect respiratory tract mucins [5,6].

HA is responsible for the attachment of the influenza virus to the sialic acid of the infected host cell surface glycoprotein's sialic acid. Avian virus HA proteins specifically recognize an α-2,3-linkage found on the epithelial cells of duck intestines. On the other

hand, human virus HA proteins prefer sialic acid linked to galactose *via* an α-2,6-linkage expressed on the surface of human respiratory epithelial cells [7–9]. The influenza A (H7N9) virus has a higher affinity for the human α-2,6-linked sialic acid host cell receptor and a lower affinity for the avian α-2,3-linked sialic acid host cell receptor [10]. Serological studies have found no pre-existing immunity to H7 subtype influenza viruses present in humans [8,11]. As a result, the influenza A (H7N9) virus should be closely monitored due to its potential to cause a pandemic. Research on the development of more potent anti-influenza drugs should be prioritized.

NA and adamantanes drugs are the two traditional classes approved for the treatment of IAV infection [6,12]. NA inhibitors are the only way to treat influenza infection in most countries due to the mutation and subsequent resistance to adamantane drugs (amantadine and rimantadine) [13]. There are three Food and Drug Administration (FDA) approved NA inhibitors for treating influenza infection: zanamivir, oseltamivir, and peramivir. At present, laninamivir is only licensed in Japan. [2,14,15]. The FDA recently approved a polymerase inhibitor baloxavir marboxil in Japan and the United States as a possible antiviral option against IAV and IBV infection [16,17].

The NA from IAVs is divided into two phylogenetic groups: group 1 (N1, N4, N5, and N8) and group 2 (N1, N4, N5, and N8) (N2, N3, N6, N7, and N9). NA is a homotetramer with an active site in each subunit [6,18]. In IAV and IBV, the active site forms a pocket composed of 19 highly conserved amino acid residues. The inner cavity contains 8 highly conserved enzymatic residues (N2 numbering) that interact directly with the sialic acids responsible for enzymatic activity (Arg118, Asp151, Arg152, Arg224, Glu276, Arg292, Arg371, and Tyr406) (Figure 1). Furthermore, the rim contains 11 highly conserved framework residues that stabilize the enzymatic binding pocket (Glu119, Arg156, Trp178, Ser179, Asp (or Asn in N7 and N9) 198, Ile222, Glu227, His274, Glu277, Asp294, and Glu425) [5,19].

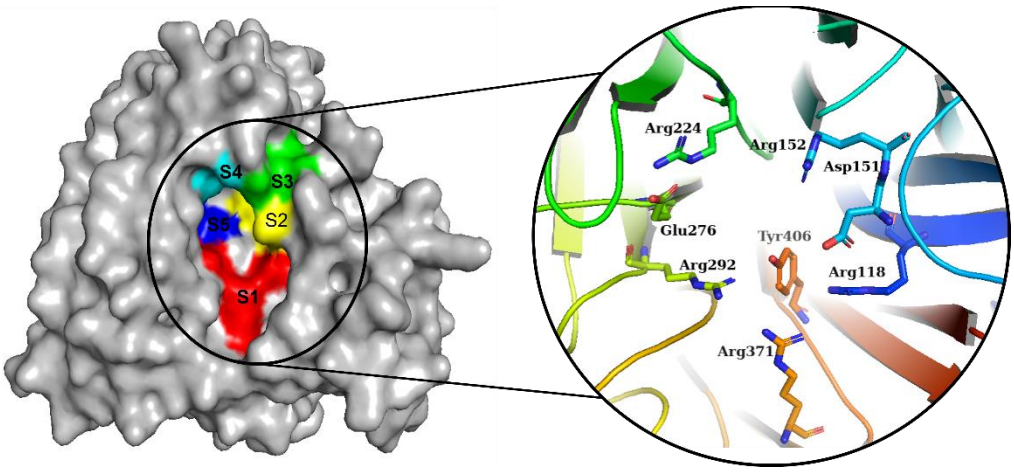

Figure 2. Diagram of the NA binding pocket showing inhibitory five binding subsites (S1 to S5) and conserved enzymatic residues.

While vaccination remains one of the primary prevention strategies, it may not provide adequate protection in some seasons [6]. As such, preventive and therapeutic agents, and antiviral drugs are critical to the control of seasonal influenza epidemics as well as the ongoing fight against a pandemic outbreak. Consequently, it is critical that more novel medical therapies be identified as soon as possible, both for preventive and therapeutic purposes. Developing novel therapeutic drugs, on the other hand, is a lengthy, time-consuming, and resource-intensive process that is plagued by more failures than successes [20].

In silico modeling is a useful approach for reducing the cost and time required for drug development [21]. The *in silico* technique has received a lot of attention as a tool for

finding new drug leads, understanding disease mechanisms, and researching drug-target interactions [22,23]. As a result, it has been recognized as a valuable tool in balanced planning and the discovery of potential novel drugs [24]. Virtual screening has improved drug discovery and is now one of the most promising *in silico* approaches for drug design and development [24].

Existing, licensed drugs could be repurposed to produce more therapeutic drugs faster. When compared to the process of generating a drug from scratch, drug repurposing has the potential to significantly reduce development time and cost. This is due to the availability of toxicity and safety data from previous clinical trial phases. In the current study, we used molecular docking studies to perform *in silico*-based repurposing of FDA-approved drugs against influenza A (H7N9). Peramivir was utilized as a control drug in the comparative investigations. The stability of hit compounds complexed with viral NA was investigated using molecular dynamics (MD) simulations. In addition, *in silico* approaches were employed to predict the pharmacokinetic and toxicological properties of the hit compounds.

2. Results and Discussion

2.1. Molecular Docking Analysis

DockRMSD server was used to evaluate the accuracy of AutoDock Vina docking for higher hit rates in our virtual screening. The RMSD (without considering hydrogen atoms) value of co-crystal bound peramivir and re-docked peramivir was found to be 1.78 Å, indicating the great reliability of the docking process [25]. The interaction profiles of the three highest-scoring docking poses were examined and compared to the peramivir binding profile (Table 1). The binding affinities of the hit compounds were found to be greater than those of the peramivir compound (-6.8 kcal/mol), with promacta having the greatest binding affinity (-9.9 kcal/mol), followed by lurasidone (-9.8 kcal/mol), and finally tucatinib (9.6 kcal/mol).

Table 1. Virtual screening results of the hit compounds.

DrugBank ID	Generic Name	Physicochemical Properties	Structures	Binding Residues	Binding Affinity (kcal/mol)	Function
DB06614	Peramivir	Mw = 328.41 LogP = 0.08 HBA = 5 HBD = 6	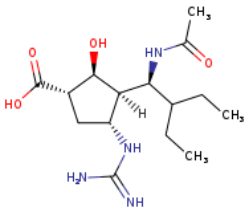	Glu119, Asp151, Trp178, Ile222, Arg227, Glu227 Ala246, Glu277, Arg292, Tyr406	-6.8	Treatment of influenza
DB08815	Lurasidone	Mw = 492.68 LogP = 4.22 HBA = 4 HBD = 0	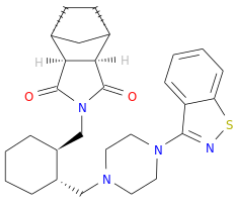	Asp151, Ala246, Glu277, Arg292, Arg371, Trp403, Tyr406, Ile427, Ly432	-9.9	Treatment of schizophrenia
DB11652	Tucitanib	Mw = 480.53 LogP = 3.77 HBA = 7 HBD = 2	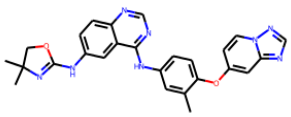	Ile149, Asp151, Arg152, Arg224, Ala246, Arg292, Asp294, Arg371, Ile427, Lys432, Pro431	-9.8	Treatment of metastatic breast cancer
DB06210	Promacta	Mw = 442.47 LogP = 3.74 HBA = 6 HBD = 3	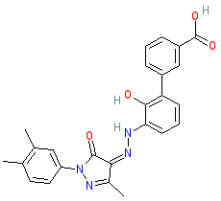	Arg118, Asp151, Ser179, Arg224, Arg292, Arg371, Ile427, Pro431, Lys432	-10.0	Treatment of thrombocytopenia or aplastic anemia

logP-partition coefficient; Mw-molecular weight; HBD-hydrogen bond donors; HBA-hydrogen bond acceptors.

2.2. Binding Pose Analysis

The NA binding site is made up of five sub-sites: S1, S2, S3, S4, and S5. The S1 site is made up of three positively charged arginine residues: Arg118, Arg292, and Arg371. The S2 site is a positively charged region composed of Glu119 and Glu227 residues, whereas the S3 site is a small hydrophobic region composed of Trp178 and Ile222 residues. The S4 site is a hydrophobic area that includes the residues Ile222, Arg224, and Ala246. Site S5 is a mixed polarity area composed of Glu276 and Ala246 residues. Our studies have demonstrated that promacta, tucitanib, and lurasidone interact with the NA protein and share the same binding pocket, with interaction profiles comparable to that of peramivir's binding pattern (Figure 2).

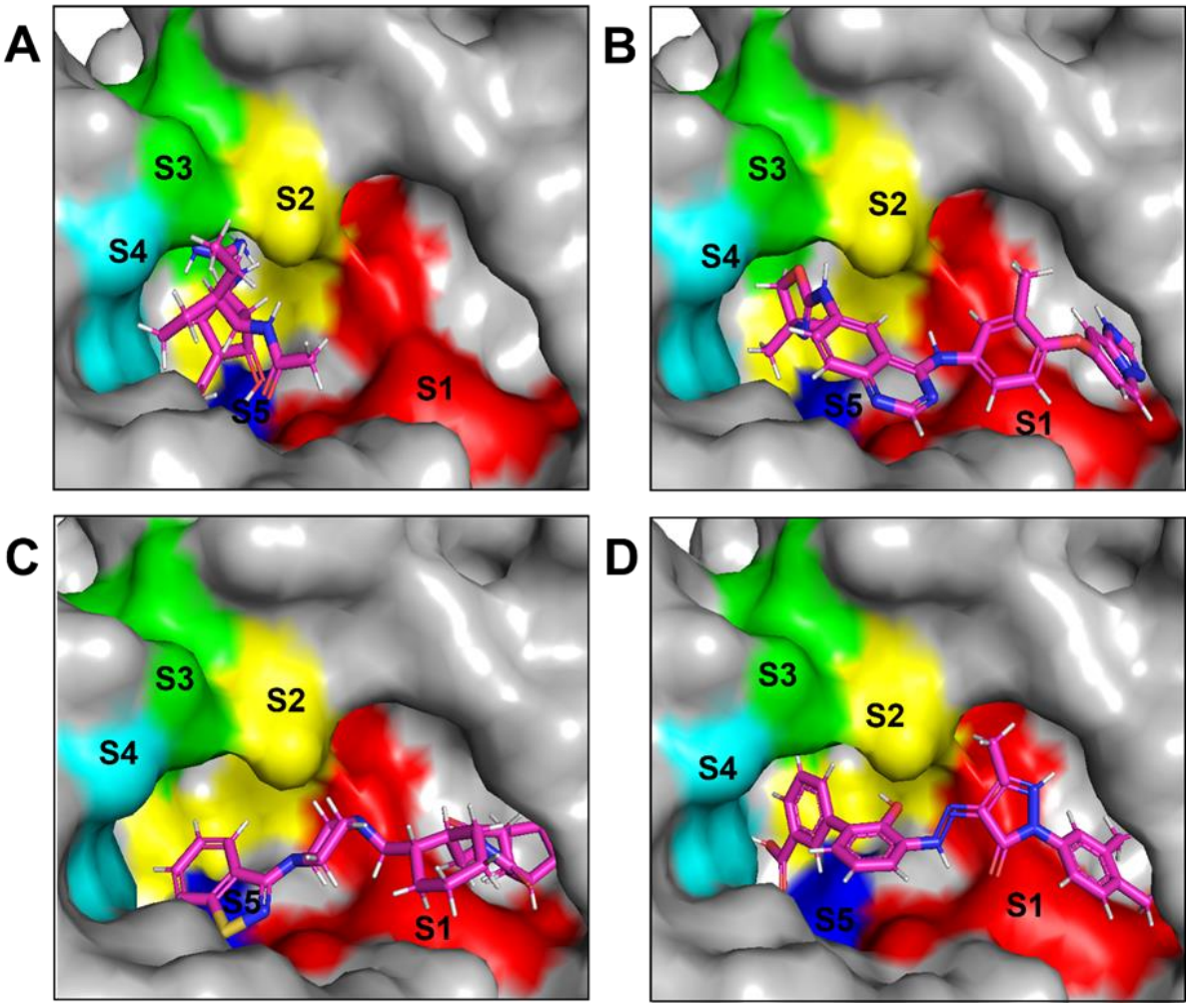

Figure 2. Binding modes of NA in complex with peramivir **(A)**, lurasidone **(B)**, tucitanib **(C)**, and promacta **(D)**.

When compared to other hit compounds, peramivir indicated the least favourable binding affinity of -6.8 kcal/mol. According to our findings, peramivir occupies the binding site and interacts with residues through hydrogen bonds and hydrophobic interactions. Our results suggest that peramivir accommodates in the S1, S2, S3, and S4 binding sub-sites (Figure 2A). Peramivir established hydrogen bonds with Trp178, Arg292, and Tyr406 in the framework amino acids Glu119, Asp151, Trp178, Ile222, Arg227, Glu227 Ala246, Glu277, Arg292, and Tyr406 (Figure 3A).

Lurasidone appears to accommodate more in S1 and S2 sub-sites of the binding pocket (Figure 2B). Lurasidone also interacted with enzymatic amino acid residues in the active site, including Asp151, Arg292, Arg371, Tyr406, and framework residues like Glu277. As seen in Figure 3B, the lurasidone compound formed hydrogen bonds with Arg292, Arg371, and Lys342 amino acids, showing potential good inhibitory activity (Figure 3B).

Tucatinib exhibited binding energy of -9.8 kcal/mol, which is more favourable when compared to peramivir (-6.8 kcal/mol). Our study showed that tucatinib interacts with Ile149, Asp151, Arg152, Arg224, Ala246, Arg292, Asp294, Arg371, Ile427, Lys432, and Pro431, where it formed hydrogen bonds with three of the active site residues, Asp151, Arg152, and Asp294 (Figure 3C). Tucatinib also showed interactions with enzymatic amino acid residues Asp151, Arg152, Arg224, Arg292, and Arg371 and a structural framework residue Asp294. These interactions appear throughout all sub-sites (S1, S2, S3, S4, and S5) located within the NA binding pocket (Figure 2C).

Promacta showed the most favorable binding energy of -10.0 kcal/mol in this study. It was found that promacta forms an interaction with conserved enzymatic residues such as Arg118, Asp151, Arg224, Arg292, and Arg 371 (Figure 3D). Along with these residues, interaction with the framework residue Ser179 was also found. Additionally, promacta formed hydrogen bonds with Arg371 and Ser179. Promacta appears to accommodate more in the binding pocket's S1, S2, and S4 sub-sites (Figure 2D). The interaction with these residues is the most critical determinant in the orientation and stability of the NA complex with promacta.

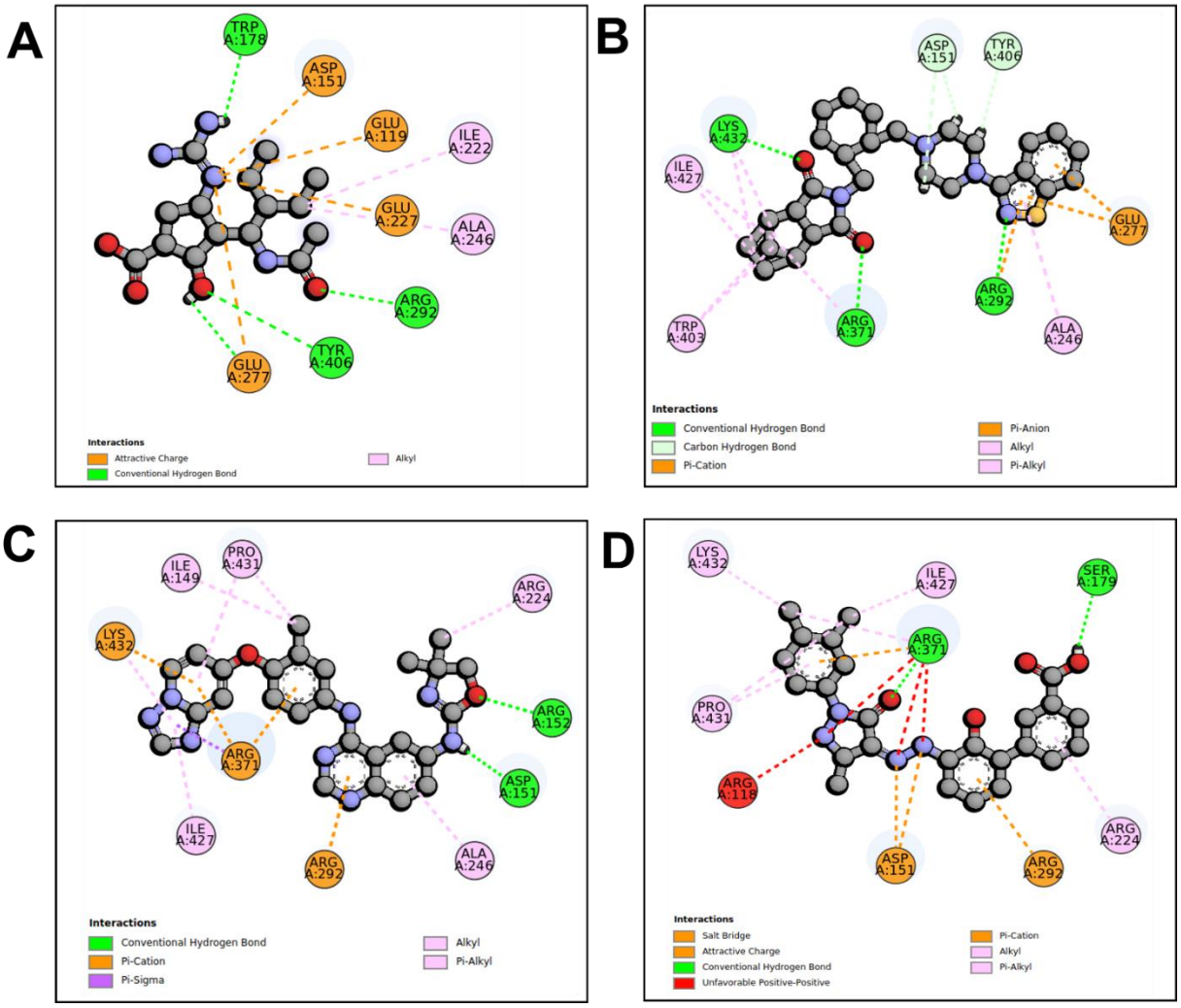

Figure 3. Molecular interaction profiles of NA with peramivir **(A)**, lurasidone **(B)**, tucitanib **(C)**, and promacta **(D).**

2.3. Molecular Dynamics Trajectory Analysis

To further evaluate the potential ability of lurasidone, tucatinib, and promacta to act as an efficient inhibitor of NA, MD simulations were performed. In addition, MD analyses were performed to analyze and compare the dynamic behaviours of NA complexes with lurasidone, tucatinib, promacta, and the reference ligand peramivir.

2.3.1. Root Mean Square Deviation (RMSD)

All four systems' stability was investigated using RMSD of the C-α atoms. We analyzed the structural stability of the docked compounds in the binding site and their effects on the overall system stability. During the simulations, the RMSD values of the entire system gradually converged and finally reached equilibrium at around 50 ns (Figure 4). The apo-enzyme showed an average RMSD value of 1.71 Å during the entire run. Lurasidone, tucatinib, and promacta as well as the reference ligand, peramivir, complexed with NA exhibited average RMSD values of 1.48 Å, 1.31 Å, 1.53 Å, and 1.17 Å, respectively, which are lower than that of apo-enzyme. This shows that the presence of a ligand stabilizes the structure of the NA protein. The average RMSD for all the systems was found to be 1.40 Å, which is lower than the ideal 2 Å RMSD value [26]. According to the findings, all three systems were stable, which could be due to strong hydrogen bond interactions between the protein-ligand complexes.

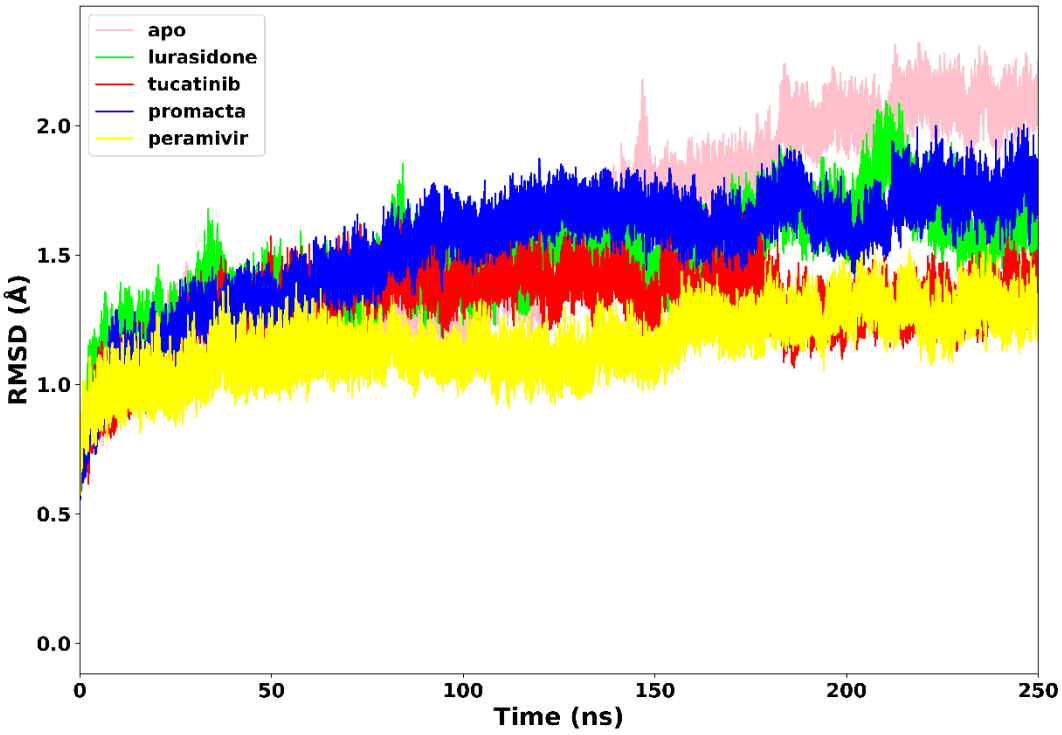

Figure 4. The RMSD trajectories of NA-ligand complexes during 250 ns simulations.

2.3.2. Root-Mean-Square Fluctuation (RMSF)

RMSF was used to measure the flexibility of the protein residues in terms of the C-α atom fluctuations throughout the MD simulation. As shown in Figure 5, the RMSF for individual amino acids correlates with the trend observed in the RMSD of complexes. The average RMSF was found to be 0.90 Å in the apo-enzyme, 0.78 Å in the lurasidone, 0.69 Å in the tucatinib, 0.67 Å in the promacta, and 0.67 Å in the reference peramivir NA complex. According to our findings, the presence of a ligand at the binding site reduces amino acid flexibility. In all systems, the pattern of residual flexibility is almost identical. Lower fluctuations were observed in the active site residues ranging from residues 110-120, 150-151, 152-160, 230-230, and 370-280, corresponding to S1, S2, S3, S4, and S5 binding sub-sites, respectively. These findings show that the target protein is stabilized by binding all three compounds docked against it.

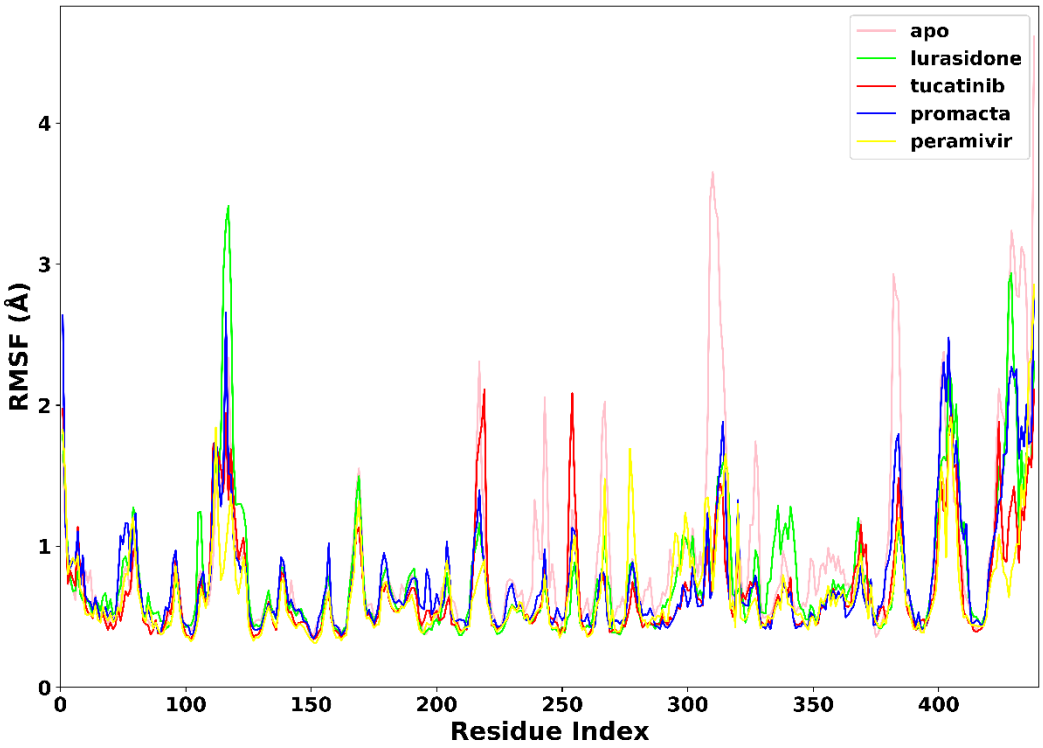

Figure 5. The RMSF trajectories of NA-ligand complexes during 250 ns simulations.

2.3.3. Radius of Gyration (RoG)

The RoG communicates information about the complex's stable and unstable folding behaviour during the interaction of a protein and a ligand. A high RoG value indicates low structural compactness, whereas a low RoG value indicates high structural compactness. RoG was therefore used to determine our system's compactness over simulation time. Figure 6 demonstrates that the apo-enzyme had a higher average RoG value of 20.1 Å across the 250 ns simulation period than the complexes. Peramivir, lurasidone, tucatinib, and promacta complexes exhibited average RoG values of 19.7 Å, 19.9 Å, 19.8 Å, and 19.8 Å, respectively. Contrary to lurasidone, the presence of peramivir, tucatinib, and promacta at the NA active site appears to exert conformational stability and compactness. The NA-lurasidone complex's higher fluctuations between 100 and 190 ns are assumed to be due to the binding and unbinding of lurasidone in the active site, thus affecting the overall compactness of the complex.

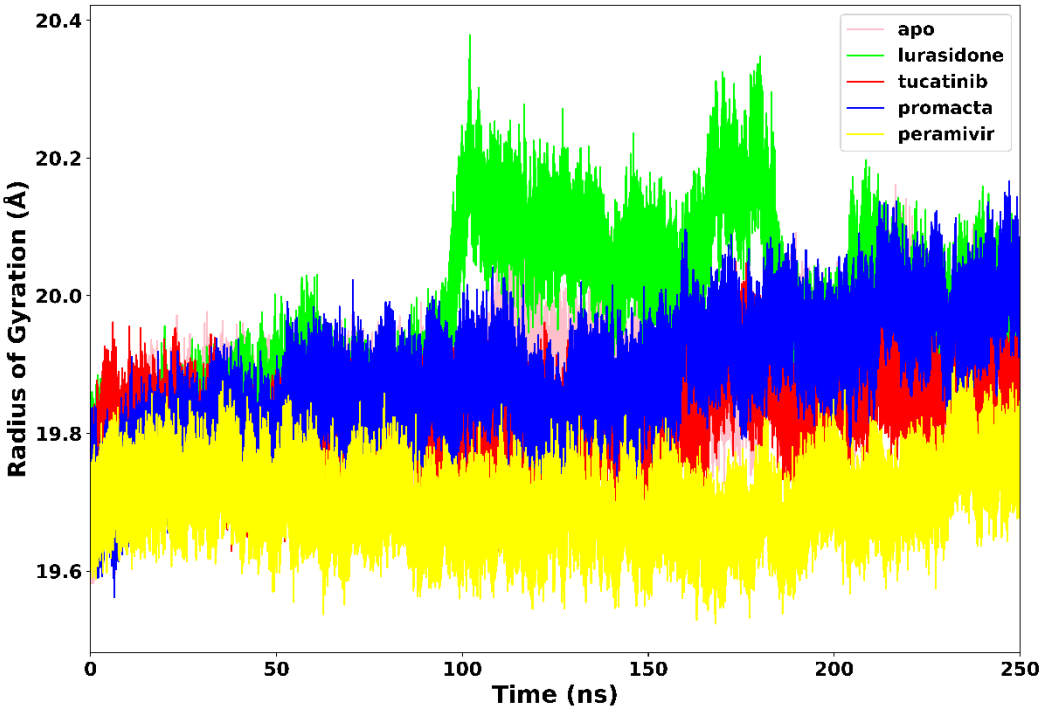

Figure 6. Radius of gyration trajectories of NA-ligand complexes during 250 ns simulations.

2.3.4. Hydrogen Bond Analysis

Hydrogen bonding between residues is an important metric for determining a protein's stability. A protein structure's stability may be increased by the presence of more intermolecular hydrogen bonds. Interactions at the binding site, such as hydrogen bonds, hydrophobic interactions, and ionic interactions, largely determine ligand binding affinity [27]. An average of 212 hydrogen bonds were consistently formed in the NA-lurasidone complex (Figure 7). In the cases of tucatinib and promacta NA-complexes, an average of 214 and 217 hydrogen bonds were consistently formed throughout the simulation period, respectively. Throughout the simulation, an average of 225 hydrogen bonds were formed with the reference ligand, peramivir. In comparison to lurasidone and tucatinib, our analysis revealed that promacta formed more hydrogen bonds with other amino acids over simulation time. This could be attributed to the NA-promacta complex's conformational stability, which could indicate a stronger binding affinity.

The phenomenon of hydrogen bonding was studied to determine which residues at the bonding site contribute to hydrogen bonding. For this purpose, the percentage occupancy of the hydrogen bonds was investigated. Throughout the 250 ns simulation time, the percentage of hydrogen bond occupancy (%) between the ligands and the active site residues was monitored (Figure 8). Based on our results, amino acid residues Arg118, Asp151, Arg152, Glu227, Glu277, Arg292, Asp344, Arg371 and Try406 were identified as the primary residues for hydrogen bonding between NA and the hit compounds, with the highest percentage occupancy, suggesting a significant contribution to system stabilisation. The interaction of the ligands with these primary residues has a significant impact on the efficacy of the ligand. As shown in Figure 6, the complexes of peramivir, promacta, lurasidone and tucatinib NA form hydrogen bonds with Arg118 at 78%, 40%, 30% and 32% occupancy throughout the simulation runs. Furthermore, Arg118 and Asp151 were found in nearly all complexes.

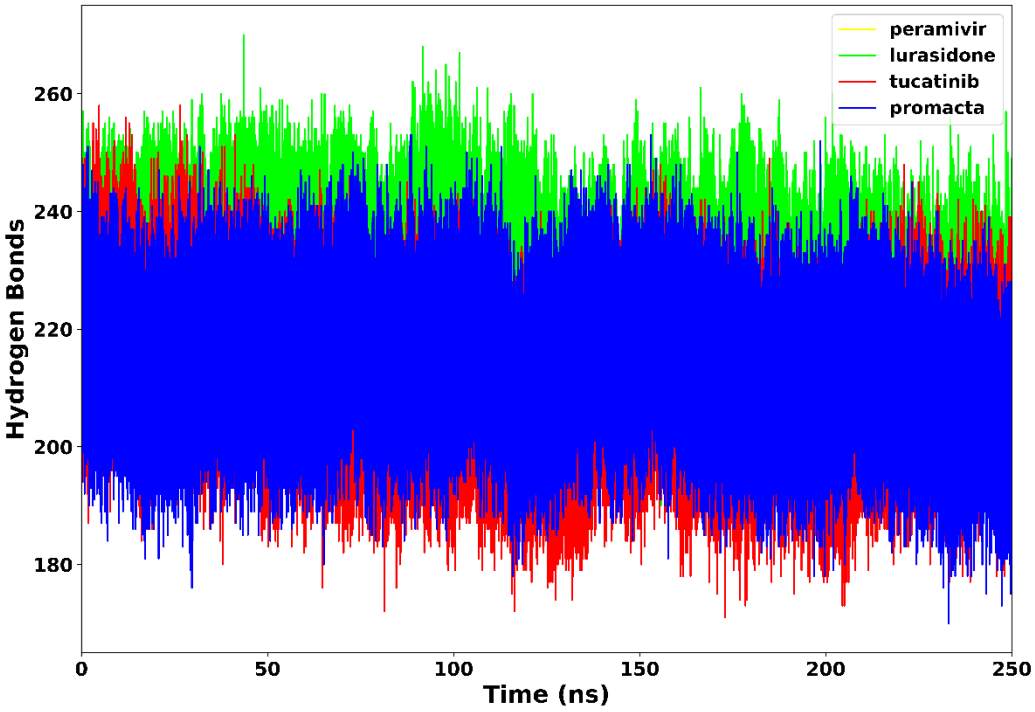

Figure 7. Hydrogen bond formation of NA-ligand complexes during 250 ns simulations.

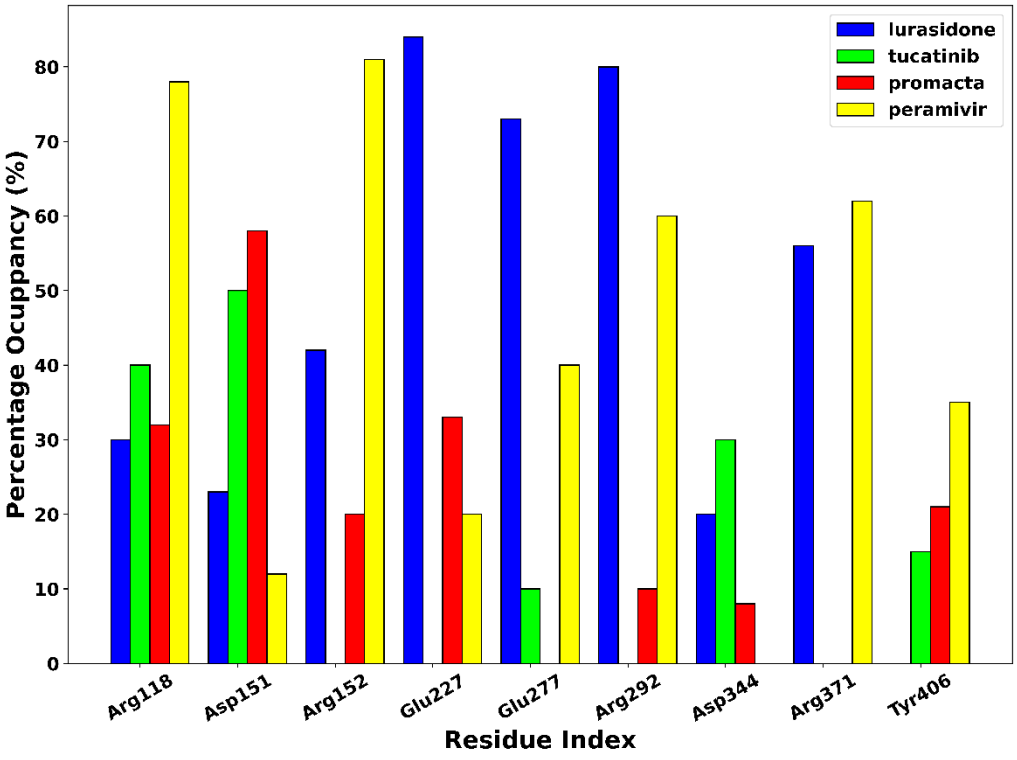

Figure 8. Hydrogen bond occupancy NA-ligand complexes during 250 ns simulations.

2.4. Binding Free Energy Analysis

The binding free energy contributions for NA-ligand complexes are shown in Table 2 over simulation time.

Table 2. Binding free energy contributions for NA-ligand complexes.

Complexes	ΔG_{bind}	ΔE_{vdw}	ΔE_{ele}	ΔG_{pol}	ΔG_{nonpol}
NA-lurasidone	-22.59 ± 0.14	-28.20 ± 0.09	-32.20 ± 0.51	41.27 ± 0.44	-3.33 ± 0.01
NA-tucitanib	-54.11 ± 0.11	-57.95 ± 0.09	-41.76 ± 0.25	51.50 ± 0.22	-5.91 ± 0.02
NA-promacta	-56.20 ± 0.19	-39.17 ± 0.12	-76.47 ± 0.43	65.07 ± 0.30	-5.66 ± 0.01
NA-peramivir	-49.09 ± 0.13	-28.86 ± 0.08	-128.21 ± 0.35	115.11 ± 0.26	-15.12 ± 0.00

ΔG_{bind}—binding free energy; ΔE_{ele}—electrostatic interaction; ΔE_{vdw}—van der Waals forces; ΔG_{pol} – polar salvation energy; ΔG_{nonpol} – nonpolar salvation energy.

Non-bond interactions, such as the van der Waal energy (ΔE_{vdw}) and the electrostatic energy (ΔE_{ele}), have a major impact on the estimation of the binding free energy (G_{bind}) in energy calculations. According to the binding free energy calculations, the compounds promacta and tucatinib have the highest binding affinity for NA with ΔG_{bind} of -54.11 ± 0.11 and -56.20 ± 0.19 kJ/mol, respectively, compared to the reference compound peramivir (-49.09 ± 0.13 kJ/mol). Compared to peramivir, the higher ΔE_{vdw} energy plays an essential role in the ΔG_{bind} binding energies of tucatinib and promacta. This is due to the presence of hydrophobic interactions between amino acid residues in the binding site, which contribute to stabilising the conformation of the promacta NA complex. According to our findings, tucatinib and promacta NA can effectively inhibit by binding to the active site and impeding catalytic activity. Therefore, we recommend that tucatinib and promacta be investigated for their potential use in the treatment of influenza virus infections.

2.5. Interaction Energy Decomposition Analysis

Interaction energy decomposition analysis was performed to gain insight into the contributions of individual amino acids to the total free energy of binding of protein-ligand complexes. As shown in Figure 9, the amino acids with the highest residual energy contributions were Arg118 (-3.12 kcal/mol) and Asp151 (-5.74 kcal/mol) in the NA-lurasidone, Arg118 (-29.74 kcal/mol), Arg152 (-13.21 kcal/mol), and Arg156 (-18.29 kcal/mol) in the NA-tucatinib complex, Arg118 (-14.47 kcal/mol), Arg225 (-16.83 kcal/mol) and Arg292 (-42.90 kcal/mol) in the NA-promacta complex, Arg119 (-15.91 kcal/mol), Arg292 (-24.47 kcal/mol), and Arg371 (-29.85 kcal/mol) in the reference compound peramivir.

The electrostatic interactions contributed much more to the total binding energy than the van der Waals interactions. These residues are thought to be important components of the protein-ligand binding pocket. Compared to the tucatinib and promacta complexes, the NA-lurasidone complex contributed the least residue energy. The thermodynamic stability and protein-ligand solid interactions in the tucatinib and promacta NA complexes are thought to be due to the overall higher electrostatic contribution and lower flexibility of the backbone C-α atoms. Furthermore, Arg118 was found in all complexes.

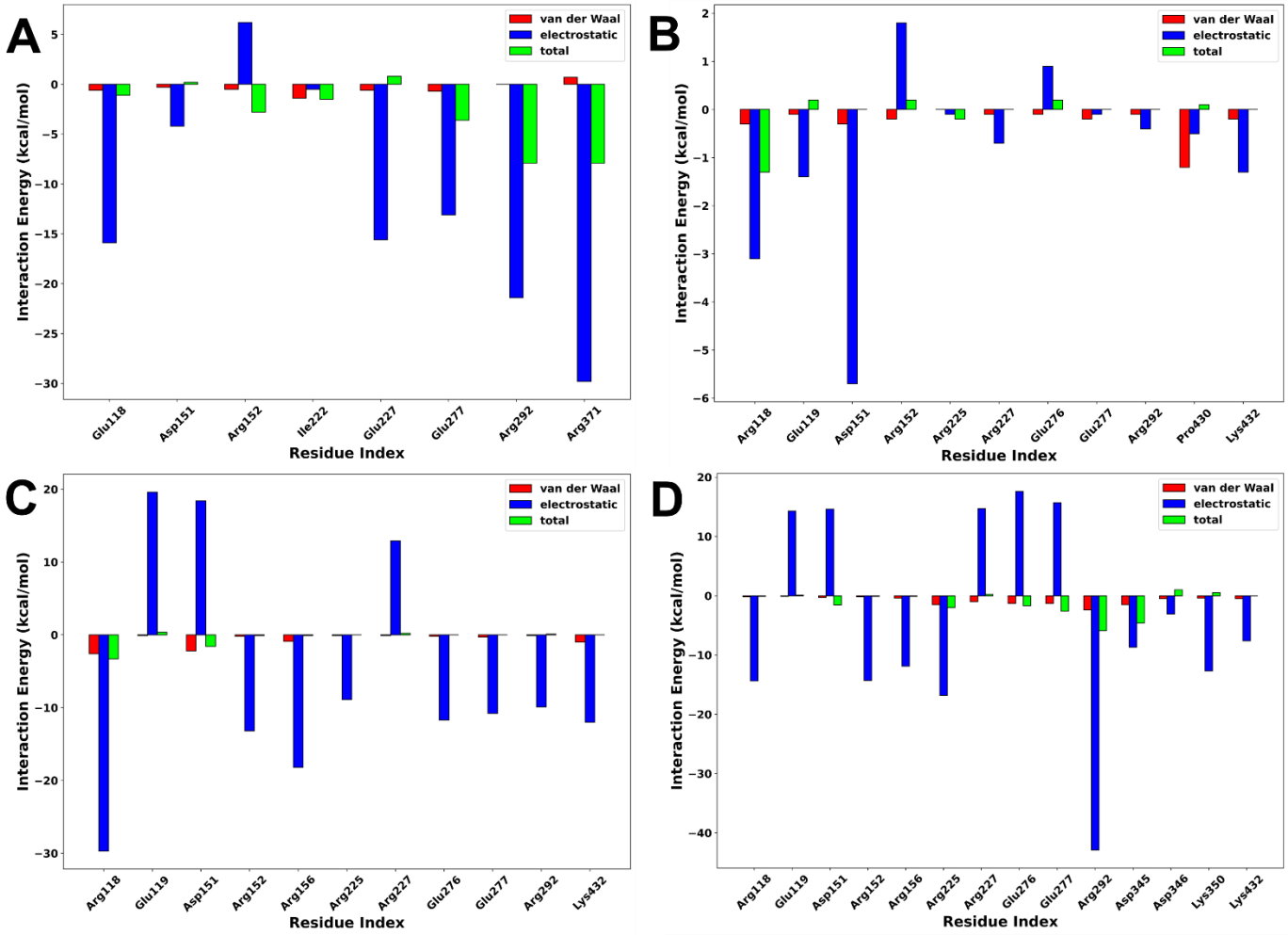

Figure 9. Interaction energy decomposition of NA complexed with peramivir **(A)**, lurasidone **(B)**, tucitanib **(C)**, and promacta **(D)**.

2.6. Pharmacokinetic analyses

An assessment of how an active ingredient is absorbed into the body, distributed, metabolised into its many components, and excreted from the body is very important for optimising the active ingredient during drug discovery. This section evaluates the absorption, distribution, metabolism and excretion (ADME) properties of hit compounds using an *in silico* Swiss-ADME server to understand pharmacokinetic properties.

Table 3. Comparative pharmacokinetics analyses.

Parameters	Lurasidone	Tucatinib	Promacta	Peramivir
GI absorption	High	High	High	Low
BBB permeant	No	No	No	No
P-gp substrate	No	Yes	No	Yes
CYP1A2 inhibitor	No	Yes	No	No
CYP2C19 inhibitor	Yes	Yes	No	No
CYP2C9 inhibitor	Yes	Yes	Yes	No
CYP2D6 inhibitor	No	Yes	No	No
CYP3A4 inhibitor	Yes	Yes	No	No

Table 3 shows that, unlike peramivir, all hit compounds have high gastrointestinal absorption (GI). The ability of a drug to cross the blood-brain barrier (BBB) is a prerequisite for a drug to have effects on the central nervous system. However, if the effect of the drug is needed in other tissues, passage through the BBB can have unfavourable consequences

[28]. In the case of hit substances, they lack properties that allow them to pass through the BBB and cause adverse effects.

Cellular efflux pumps like P-glycoprotein (P-gp) act as a first line of protection by transporting toxic xenobiotics and toxic substances out of the cell [29]. It is a substrate for many structurally varied therapeutics, and it prevents drug absorption, permeability, and retention, expels them out of the cells [30]. Notably, our analysis indicates that, in contrast to tucatinib, lurasidone and promacta are not P-gp substrates, suggesting the possibility of successful drug delivery. The drug metabolism of pharmaceuticals and other xenobiotics by cytochrome (CYP) enzymes produced variable results. All compounds demonstrated favourable ADME properties, indicating a high potential for use as lead compounds.

2.7. Toxicological analyses

In silico methodologies may now be used to determine the safety profiles of desired substances thanks to computerized technologies. These chemicals might damage humans and animals if they are not used properly. The server ProTox-I was used to analyze the safety profiles of our hit compounds (Table 4). According to the findings, tucatinib is the only compound with carcinogenic and immunotoxic adverse effects.

Table 4. Comparative toxicological analyses.

Parameters	Lurasidone	Tucatinib	Promacta	Peramivir
Carcinogenicity	No	Yes	No	No
Immunotoxicity	No	Yes	No	No
Mutagenicity	No	No	No	No
Cytotoxicity	No	No	No	No
LD_{50} (mg/kg)	660	3160	5000	1430
Class	4	5	5	4
hERG inhibition	Yes (weak)	Yes (weak)	No	No

Furthermore, all compounds show negative results for mutagenicity and cytotoxicity prediction. According to the ProTox-II server, tucatinib and promacta both belong to class 5, with LD_{50} ranging from 2000 to 5000 mg/kg and may be harmful when administered orally. The LD_{50} value for lurasidone was less than 2000 mg/kg, indicating that oral ingestion could be harmful, putting it in toxicity class 4.

Inhibition of human ether-a-go-go-related gene (hERG) channels is a widely accepted predictor of cardiotoxicity. Screening compounds in the early stages of discovery and development for their ability to inhibit the hERG channel has thus become an essential procedure in the pharmaceutical industry. The Pred-hERG server was used to predict the ability of the hit compounds to inhibit hERG, and the results show that promacta is non-cardiotoxic, while lurasidone and tucatinib only show weak inhibition.

3. Materials and Methods

3.1. Receptor and Ligand Preparation

The Protein Data Bank was used to obtain the X-ray crystal structure of the Anhui N9–peramivir (PDB code: 4MWV) complex. AutoDock Tools (ADT) v.1.5.6 was used to prepare the receptor for docking [31,32]. Water molecules, ions, and ligands were removed from the protein, which was then followed by the construction of missing side chain atoms, the addition of hydrogen atoms, and the protonation of individual residues. Following that, 1000 steps of receptor minimization were done with the conjugate gradient algorithm using MMFF94 force field, and the PDB file was translated to PDBPT file format using OpenBabel v.2.4.1[33].

A total of 2,568 FDA-approved drugs available for virtual screening were obtained from DrugBank database [34]. They were then filtered using Open Babel to select only drugs that meet Lipinski rule of five [35], filtering only 4 descriptors: Partition coefficient,

molecular weight, hydrogen bond donors and acceptors, yielding 1,597 drugs for virtual screening. The co-crystal bound peramivir, was used a reference compound. The SDF files were hydrogenated at pH 7.4, applied 1000 steps of a conjugate gradient algorithm using a MMFF94 force field and then converted to PDBPT format using OpenBabel.

3.2. Molecular Docking Based Virtual Screening

Molecular docking was carried out using AutoDock Vina v.1.1.2 [36]. ADT was used to calculate the grid, which includes the binding center and dimensions. A grid box centered at x = 63.17, y = 16.81, and z = -26.38 with the side lengths of x, y, and z set respectively at 50.0, 50.0, and 50.0 was positioned in the center of the receptor's binding site. Prior to conducting virtual screening with the selected compounds, AutoDock Vina was validated for its ability to reproduce the crystallographic pose of co-crystallized peramivir with NA. The RMSD values of docked peramivir and co-crystal bound peramivir were calculated using the DockRMSD server [25]. The docking data were evaluated and the top ten drug conformations with the highest scores were chosen for additional docking. Using an in-house bash script, these conformations were docked in triplicate to the binding site using 24 exhaustiveness. The top 3 docked compounds with the best binding affinity were visualized using Discovery Studio Visualizer version 20.1.0.19295 [37], and PyMol v.2.5 [38].

3.3. Pharmacokinetic and Toxicological Predictions

The Swiss-ADME server was utilized to collect information on the physicochemical and pharmacokinetic properties of the hit drugs in this study [39]. Assessment of toxicity was performed using the Pro-Tox II server [40]. The Pred-hERG server was used to predict the capacity of the ligands to inhibit hERG (Kv11.1) [41].

3.4. Molecular Dynamics Simulations

MD simulations of 250 ns were run with the best-scored poses of the screening complexes promacta, tucitanib, and lurasidone, as well as the reference ligand peramivir. Amber 18 graphic processing unit (GPU) Particle Mesh Ewald Molecular Dynamic (PMEMD) was employed in the MD simulations. The force field related parameters and protein description were handled with FF14SB [42,43]. LEAP module was used in the addition of hydrogen atoms to the protein and subsequent counter-ions addition [44]. The systems were enclosed in TIP3P water box , with a 10 Å distance between the system surface and box edge [45]. The system employed the periodic boundary conditions, while long range electrostatics was managed with 12 Å Van der Waals cut off. The initial minimization was performed using restrained potential of 500 kcal/mol/Å^2 in 1000 steepest descent steps and 1000 conjugate gradient steps on the solute [46]. This was followed by 1000 steps unrestrained conjugate gradient minimization for the entire system. A gradual heating from 0 to 300 K with 1 ps, 5 kcal/mol/Å^2 (collision frequency and harmonic restraints, respectively) settings using Langevin thermostat was applied to the system. An unrestrained equilibration of the system was performed using NPT ensemble at 300 K and 1 bar constant pressure [47]. MD simulation production run of 250 ns was done using an isothermal isobaric (NPT) ensemble and a Berendsen barostat [48]. The coordinates were saved at intervals after each stage and the trajectories were analysed.

3.5. Molecular Dynamics Trajectory Analyses

The Amber18 implemented modules, PTRAJ and CPPTRAJ, were used to perform post-MD trajectory studies such as root mean square deviation (RMSD) and root mean square fluctuations (RMSF), radius of gyration (RoG), number of hydrogen bonds, and hydrogen bond occupancy. All plots were created with Python custom scripts and the Pandas and Matplotlib libraries.

3.6. Binding Free Energy Calculation

The binding free energy profiles of the best docking poses of promacta, tucitanib, and lurasidone and also reference compound, peramivir, complexed with NA were computed using the Molecular Mechanics/Generalized Born Surface Area (MM/GBSA) approach [49–52]. The following equations provide a full description of how to calculate binding free energy:

$$\Delta G_{bind} = G_{complex} - G_{receptor} - G_{ligand} \quad (1)$$

$$\Delta G_{bind} = E_{gas} + G_{sol} - T\Delta S \quad (2)$$

$$E_{gas} = E_{int} + E_{vdW} + E_{ele} \quad (3)$$

$$G_{sol} = G_{GB} + G_{SA} \quad (4)$$

In this equation, ΔG_{bind} indicates total free binding energy, whereas others reveal the free energy of complex, the protein, and the ligand. The gas phase energy is denoted by E_{gas}, while internal energy is denoted by E_{int}. The temperature is represented by T, and the total solute entropy is represented by ΔS. Interactions between bonded, electrostatic, and van der Waals states are specified by $G_{bind,}$ E_{ele} and E_{vdw}, respectively. G_{GB} and G_{SA}, on the other hand, represent the polar and non-polar interaction to free energy. The MM/GBSA method was also utilized to calculate the energy contributions of individual amino acid residues to the overall binding free energy.

4. Conclusions

The newly developed drugs showed binding in the active site of NA in a highly specific binding pattern similar to that of peramivir with this in silico approach. According to our findings, some of the selected compounds occupied the active site of NA with an even higher binding affinity than peramivir. The MM-GBSA calculations showed that lurasidone and promacta had higher binding affinity than the standard drug peramivir (-49.09 kcal/mol), with ΔG_{bind} values of -54.11 kcal/mol and -56.20 kcal/mol, respectively. The MD simulation studies revealed that the backbone of C-α atoms in the complexes of tucatinib and promacta NA is stable throughout the simulation period and is not subject to significant fluctuations. In contrast, RoG analysis of the NA-lurasidone complex revealed higher fluctuations between 100 and 190 ns, affecting the complex's stability. The major amino acid residues with the highest energy contributions were identified, providing a solid basis for future research into novel and effective influenza virus inhibitors. According to ADME analysis, the hit compounds have a high GI and do not possess properties that allow them to overcome the BBB. *In silico* toxicity prediction revealed that all compounds tested negative for mutagenicity and cytotoxicity. In addition, promacta is not cardiotoxic, while lurasidone and tucatinib have only weak inhibition. Promacta and tucatinib could be used as lead compounds to combat the influenza A (H7N9) virus.

Author Contributions: Conceptualization, S.E.M. and H.M.K.; methodology, S.E.M.; software, S.E.M..; validation, S.E.M. and H.M.K.; formal analysis, S.E.M.; investigation, S.E.M.; resources, H.M.K.; data curation, All; writing—original draft preparation, S.E.M.; writing—review and editing, All; visualization, All; supervision, H.M.K.; project administration, H.M.K.; funding acquisition, H.M.K. All authors have read and agreed to the published version of the manuscript.

Funding: This research received no external funding.

Institutional Review Board Statement: Not applicable.

Informed Consent Statement: Not applicable.

Data Availability Statement: The data presented in this study are available on request from the corresponding author.

Acknowledgments: The authors acknowledge the UKZN School of Health Sciences and the Center for High Performance Computing (CHPC, http://www.chpc.ac.za, accessed on 14 March 2022) for computational resources.

Conflicts of Interest: The authors declare no conflict of interest.

References

1. World Health Organisation (WHO) Analysis of recent scientific information on avian influenza A(H7N9) virus. *https://www.who.int/influenza/human_animal_interface/avian_influenza/riskassessment_AH7N9_201702/en/* **2021**.
2. Gao, R.; Cao, B.; Hu, Y.; Feng, Z.; Wang, D.; Hu, W.; Chen, J.; Jie, Z.; Qiu, H.; Xu, K.; et al. Human Infection with a Novel Avian-Origin Influenza A (H7N9) Virus. *N. Engl. J. Med.* **2013**, *368*, 1888–1897, doi:10.1056/nejmoa1304459.
3. Gao, H.-N.; Lu, H.-Z.; Cao, B.; Du, B.; Shang, H.; Gan, J.-H.; Lu, S.-H.; Yang, Y.-D.; Fang, Q.; Shen, Y.-Z.; et al. Clinical Findings in 111 Cases of Influenza A (H7N9) Virus Infection. *N. Engl. J. Med.* **2013**, *368*, 2277–2285, doi:10.1056/nejmoa1305584.
4. Xiang, N.; Li, X.; Ren, R.; Wang, D.; Zhou, S.; Greene, C.M.; Song, Y.; Zhou, L.; Yang, L.; Davis, C.T.; et al. Assessing Change in Avian Influenza A(H7N9) Virus Infections During the Fourth Epidemic — China, September 2015–August 2016. *MMWR. Morb. Mortal. Wkly. Rep.* **2016**, *65*, 1390–1394, doi:10.15585/mmwr.mm6549a2.
5. Colman, P.M.; Varghese, J.N.; Laver, W.G. Structure of the catalytic and antigenic sites in influenza virus neuraminidase. *Nature* **1983**, *303*, 41–44, doi:10.1038/303041a0.
6. Mtambo, S.E.; Amoako, D.G.; Somboro, A.M.; Agoni, C.; Lawal, M.M.; Gumede, N.S.; Khan, R.B.; Kumalo, H.M. Influenza Viruses: Harnessing the Crucial Role of the M2 Ion-Channel and Neuraminidase toward Inhibitor Design. *Molecules* **2021**, *26*, doi:10.3390/molecules26040880.
7. Watanabe, T.; Kiso, M.; Fukuyama, S.; Nakajima, N.; Imai, M.; Yamada, S.; Murakami, S.; Yamayoshi, S.; Iwatsuki-Horimoto, K.; Sakoda, Y.; et al. Characterization of H7N9 influenza A viruses isolated from humans. *Nature* **2013**, *501*, 551–555, doi:10.1038/nature12392.
8. Zhou, J.; Wang, D.; Gao, R.; Zhao, B.; Song, J.; Qi, X.; Zhang, Y.; Shi, Y.; Yang, L.; Zhu, W.; et al. Biological features of novel avian influenza A (H7N9) virus. *Nature* **2013**, *499*, 500–503, doi:10.1038/nature12379.
9. Tharakaraman, K.; Jayaraman, A.; Raman, R.; Viswanathan, K.; Stebbins, N.W.; Johnson, D.; Shriver, Z.; Sasisekharan, V.; Sasisekharan, R. Glycan-Receptor Binding of the Influenza A Virus H7N9 Hemagglutinin. *NIH Public Access* **2013**, *153*, 1486–93, doi:10.1016/j.cell.2013.05.034.
10. Xiong, X.; McCauley, J.; Steinhauer, D. Receptor binding properties of the influenza virus hemagglutinin as a determinant of host range. *Curr. Top. Microbiol. Immunol.* **2014**, *385*, 63–91, doi:10.1007/82_2014_423.
11. Bai, T.; Zhou, J.; Shu, Y. Serologic Study for Influenza A (H7N9) among High-Risk Groups in China. *N. Engl. J. Med.* **2013**, *368*, 2339–2340, doi:10.1056/NEJMC1305865.
12. Aoki, F.Y. Antiviral Drugs for Influenza and Other Respiratory Virus Infections | Elsevier Enhanced Reader. *Mand. Douglas, Bennett's Princ. Pract. Infect. Dis.* **2014**, 531–545, doi:10.1016/B978-1-4557-4801-3.00044-8.
13. Samson, M.; Pizzorno, A.; Abed, Y.; Boivin, G. Influenza virus resistance to neuraminidase inhibitors. *Antiviral Res.* **2013**, *98*, 174–185, doi:10.1016/J.ANTIVIRAL.2013.03.014.
14. Zhang, F.; Y, B.; Wang, J.; Wong, G.; Shi, W.; Hu, F.; Yang, Y.; Yang, L.; Deng, X.; Jiang, S.; et al. Human infections with recently-emerging highly pathogenic H7N9 avian influenza virus in China. *J. Infect.* **2017**, *75*, 71–75, doi:10.1016/J.JINF.2017.04.001.
15. Li, Q.; Zhou, L.; Zhou, M.; Chen, Z.; Li, F.; Wu, H.; Xiang, N.; Chen, E.; Tang, F.; Wang, D.; et al. Epidemiology of Human Infections with Avian Influenza A(H7N9) Virus in China. *N. Engl. J. Med.* **2014**, *370*, 520–532, doi:10.1056/NEJMOA1304617.
16. Du, Z.; Nugent, C.; Galvani, A.P.; Krug, R.M.; Meyers, L.A. Modeling mitigation of influenza epidemics by baloxavir. *Nat. Commun.* **2020**, *11*, 1–6, doi:10.1038/s41467-020-16585-y.

17. Koshimichi, H.; Ishibashi, T.; Kawaguchi, N.; Sato, C.; Kawasaki, A.; Wajima, T. Safety, Tolerability, and Pharmacokinetics of the Novel Anti-influenza Agent Baloxavir Marboxil in Healthy Adults: Phase I Study Findings. *Clin. Drug Investig.* **2018**, *38*, 1189–1196, doi:10.1007/S40261-018-0710-9.
18. RJ, R.; LF, H.; DJ, S.; PJ, C.; YP, L.; GM, B.; AJ, H.; SJ, G.; JJ, S. The structure of H5N1 avian influenza neuraminidase suggests new opportunities for drug design. *Nature* **2006**, *443*, 45–49, doi:10.1038/NATURE05114.
19. Varghese, J.N.; Colman, P.M. Three-dimensional Structure of the Negraminidase of Influenza Virus A / Tokyo / 3 / 67 at 2-2 A Resolution receptor. *J. Mol. Biol.* **1991**, *221*, 473–486, doi:10.1016/0022-2836(91)80068-6.
20. Wouters, O.J.; McKee, M.; Luyten, J. Estimated Research and Development Investment Needed to Bring a New Medicine to Market, 2009-2018. *JAMA* **2020**, *323*, 844–853, doi:10.1001/JAMA.2020.1166.
21. Honarparvar, B.; Govender, T.; Maguire, G.E.M.; Soliman, M.E.S.; Kruger, H.G. Integrated approach to structure-based enzymatic drug design: Molecular modeling, spectroscopy, and experimental bioactivity. *Chem. Rev.* **2014**, *114*, 493–537, doi:10.1021/cr300314q.
22. Usha, T.; Shanmugarajan, D.; Goyal, A.K.; Kumar, C.S.; Middha, S.K. Recent Updates on Computer-aided Drug Discovery: Time for a Paradigm Shift. *Curr. Top. Med. Chem.* **2017**, *17*, 3296–3307, doi:10.2174/1568026618666180101163651.
23. Batool, M.; Ahmad, B.; Choi, S. A Structure-Based Drug Discovery Paradigm. *Int. J. Mol. Sci.* **2019**, *20*, 2783, doi:10.3390/IJMS20112783.
24. Maia, E.H.B.; Assis, L.C.; de Oliveira, T.A.; da Silva, A.M.; Taranto, A.G. Structure-Based Virtual Screening: From Classical to Artificial Intelligence. *Front. Chem.* **2020**, *8*, 343, doi:10.3389/FCHEM.2020.00343/BIBTEX.
25. Bell, E.W.; Zhang, Y. DockRMSD: An open-source tool for atom mapping and RMSD calculation of symmetric molecules through graph isomorphism. *J. Cheminform.* **2019**, *11*, 1–9, doi:10.1186/S13321-019-0362-7/FIGURES/5.
26. Xiang, Z.; Soto, C.S.; Honig, B. Evaluating conformational free energies: The colony energy and its application to the problem of loop prediction. *Proc. Natl. Acad. Sci. U. S. A.* **2002**, *99*, 7432–7437, doi:10.1073/PNAS.102179699/ASSET/68C5F447-6151-4C41-B267-D3266C07AE7B/ASSETS/GRAPHIC/PQ1021796002.JPEG.
27. Gomes, D.E.B.; Lins, R.D.; Pascutti, P.G.; Lei, C.; Soares, T.A. The Role of Non-Bonded Interactions in the Conformational Dynamics of Organophosphorous Hydrolase Adsorbed onto Functionalized Mesoporous Silica Surfaces. *J. Phys. Chem. B* **2010**, *114*, 531, doi:10.1021/JP9083635.
28. Pardridge, W.M. Drug transport across the blood–brain barrier. *J. Cereb. Blood Flow Metab.* **2012**, *32*, 1959, doi:10.1038/JCBFM.2012.126.
29. Gupta, P.; Garg, T.; Tanmay, M.; Arora, S. Polymeric Drug-Delivery Systems: Role in P-gp Efflux System Inhibition. *Crit. Rev. Ther. Drug Carrier Syst.* **2015**, *32*, 247–275, doi:10.1615/CRITREVTHERDRUGCARRIERSYST.2015011592.
30. Amin, M.L. P-glycoprotein Inhibition for Optimal Drug Delivery. *Drug Target Insights* **2013**, *7*, 27–34, doi:10.4137/DTI.S12519.
31. Morris, G.; Huey, R.; Lindstrom, W.; Sanner, M.; Belew, R.; Goodsell, D.; Olson, A. AutoDock4 and AutoDockTools4: Automated docking with selective receptor flexibility. *J. Comput. Chem.* **2009**, *30*, 2785–2791, doi:10.1002/JCC.21256.
32. Trott, O.; Olson, A.J. AutoDock Vina: improving the speed and accuracy of docking with a new scoring function, efficient optimization and multithreading. *J. Comput. Chem.* **2010**, *30*, 455–461, doi:10.1002/jcc.21334.
33. O'Boyle, N.M.; Banck, M.; James, C.A.; Morley, C.; Vandermeersch, T.; Hutchison, G.R. Open Babel: An Open chemical toolbox. *J. Cheminform.* **2011**, *3*, 1–14, doi:10.1186/1758-2946-3-33/TABLES/2.
34. Wishart, D.S.; Feunang, Y.D.; Guo, A.C.; Lo, E.J.; Marcu, A.; Grant, J.R.; Sajed, T.; Johnson, D.; Li, C.; Sayeeda, Z.; et al. DrugBank 5.0: a major update to the DrugBank database for 2018. *Nucleic Acids Res.* **2018**, *46*, D1074–D1082, doi:10.1093/NAR/GKX1037.
35. Lipinski, C.A.; Lombardo, F.; Dominy, B.W.; Feeney, P.J. Experimental and computational approaches to estimate solubility and permeability in drug discovery and development settings. *Adv. Drug Deliv. Rev.* **2001**, *46*, 3–26, doi:10.1016/S0169-

409X(00)00129-0.

36. Trott, O.; Olson, A.J. AutoDock Vina: improving the speed and accuracy of docking with a new scoring function, efficient optimization and multithreading. *J. Comput. Chem.* **2010**, *31*, 455, doi:10.1002/JCC.21334.
37. BIOVIA, D.S. Discovery Studio Modeling Environment, Release 2020 2020.
38. Schrödinger, L.; DeLano, W. PyMol 2021.
39. Daina, A.; Michielin, O.; Zoete, V. SwissADME: a free web tool to evaluate pharmacokinetics, drug-likeness and medicinal chemistry friendliness of small molecules. *Sci. Reports 2017 71* **2017**, *7*, 1–13, doi:10.1038/srep42717.
40. Banerjee, P.; Eckert, A.O.; Schrey, A.K.; Preissner, R. ProTox-II: a webserver for the prediction of toxicity of chemicals. *Nucleic Acids Res.* **2018**, *46*, W257, doi:10.1093/NAR/GKY318.
41. Braga, R.C.; Alves, V.M.; Silva, M.F.B.; Muratov, E.; Fourches, D.; Lião, L.M.; Tropsha, A.; Andrade, C.H. Pred-hERG: A Novel web-Accessible Computational Tool for Predicting Cardiac Toxicity. *Mol. Inform.* **2015**, *34*, 698–701, doi:10.1002/MINF.201500040.
42. Ben-shalom, I.Y.; Lin, C.; Radak, B.K.; Sherman, W.; Gilson, M.K. Fast Equilibration of Water between Buried Sites and Bulk by MD with Parallel Monte Carlo Water Moves on GPUs. 1–17.
43. Du, Q.; Qian, Y.; Xue, W. Cross-reactivity of two human IL-6 family cytokines OSM and LIF explored by protein-protein docking and molecular dynamics simulation. *Biochim. Biophys. Acta - Gen. Subj.* **2021**, *1865*, 129907, doi:10.1016/J.BBAGEN.2021.129907.
44. Fakhar, Z.; Hejazi, L.; Tabatabai, S.A.; Munro, O.Q. Discovery of novel heterocyclic amide-based inhibitors: an integrative in-silico approach to targeting soluble epoxide hydrolase . *J. Biomol. Struct. Dyn.* **2021**, *0*, 1–15, doi:10.1080/07391102.2021.1894987.
45. Li, Y.; Wang, C.; Xu, T.; Pan, P.; Yu, Q.; Xu, L.; Xiong, X.; Hou, T.; Cui, S.; Sun, Y. Discovery of a small molecule inhibitor of cullin neddylation that triggers ER stress to induce autophagy. *Acta Pharm. Sin. B* **2021**, doi:10.1016/J.APSB.2021.07.012.
46. Wolf, S.; Sohmen, B.; Hellenkamp, B.; Thurn, J.; Stock, G.; Hugel, T. Hierarchical dynamics in allostery following ATP hydrolysis monitored by single molecule FRET measurements and MD simulations. *Chem. Sci.* **2021**, *12*, 3350–3359, doi:10.1039/D0SC06134D.
47. Panwar, A.; Kumar, A. In-silico Analysis and Molecular Dynamics Simulations of Lysozyme by GROMACS 2020.2. *Ann. Rom. Soc. Cell Biol.* **2021**, *25*, 9679–9685.
48. Jin, T.; Patel, S.J.; Lehn, R.C. Van Molecular simulations of lipid membrane partitioning and translocation by bacterial quorum sensing modulators. *PLoS One* **2021**, *16*, e0246187, doi:10.1371/JOURNAL.PONE.0246187.
49. Kollman, P.A.; Massova, I.; Reyes, C.; Kuhn, B.; Huo, S.; Chong, L.; Lee, M.; Lee, T.; Duan, Y.; Wang, W.; et al. Calculating structures and free energies of complex molecules: combining molecular mechanics and continuum models. *Acc. Chem. Res.* **2000**, *33*, 889–897, doi:10.1021/ar000033j.
50. Massova, I.; Kollman, P.A. Combined molecular mechanical and continuum solvent approach (MM-PBSA/GBSA) to predict ligand binding. *Perspect. Drug Discov. Des.* **2000**, *18*, 113–135, doi:10.1023/A:1008763014207.
51. Hou, T.; Wang, J.; Li, Y.; Wang, W. Assessing the performance of the MM/PBSA and MM/GBSA methods. 1. The accuracy of binding free energy calculations based on molecular dynamics simulations. *J. Chem. Inf. Model.* **2011**, *51*, 69–82, doi:10.1021/ci100275a.
52. Xu, L.; Sun, H.; Li, Y.; Wang, J.; Hou, T. Assessing the performance of MM/PBSA and MM/GBSA methods. 3. The impact of force fields and ligand charge models. *J. Phys. Chem. B* **2013**, *117*, 8408–8421, doi:10.1021/jp404160y.

Chapter 7

CONCLUSION

7. CONCLUSION

7.1 CONCLUSION AND RECOMMENDATION

Influenza causes high illness and death by means of seasonal flu and global pandemics [1]. Influenza infections are primarily prevented and treated using vaccines and anti-influenza drugs [2–4]. New, extremely virulent influenza strains can emerge unpredictably due to antigenic drift or shift and generate novel epidemics or pandemics. As a result, influenza viruses mutate rapidly, making vaccinations insufficient to manage the spread of the virus [5,6]. Humans are most at risk from the subtypes H5 and H7 of avian influenza, both of which cause serious infections when introduced into poultry [7,8]. According to serological studies, no human population has pre-existing immunity to influenza viruses of the H7 subtype [9–12]. In view of this, avian influenza H7N9 virus is of concern as a possible cause of a pandemic. It should continue to be monitored, and more effective anti-viral agents should be developed.

In the current thesis, CADD approaches were used to unravel the mechanism of inhibition of some therapeutic targets in treating human avian influenza H7N9 virus infections. Moreover, the drug-target interaction dynamics and mechanisms of actions presented in this thesis play a vital role in the drug discovery process by influencing new drugs' overall therapeutic effectiveness. As a result, these interactions dynamics offer valuable insights that might lead to the development of new compounds for biological targets or to the improvement of existing compounds for therapeutic purposes. In light of this, the domains of this research were divided into two. The research in this thesis began with a comprehensive review of the latest research on the bio-molecular fundaments of influenza viruses, with emphasis on the structure, function, and mechanisms of action of the M2-ion channel and neuraminidase as possible targets for anti-viral drug. The review outlined the progress made in the development of anti-viral treatments that target M2-ion channel and neuraminidase as alternatives to current anti-viral drugs. Subsequently, possible therapeutic approaches for designing new anti-viral inhibitors that would be able to inhibit resistant strains of influenza were outlined.

Studies presented in the first domain of the research aimed to provide a comprehensive and detailed understanding of the impact of the R292K mutation on peramivir resistance to H7N9. In the first research domain, we analyzed how mutation affected peramivir's binding ability to the R292K mutant in the H7N9 virus. This was done using different computational methods. These methods, which included MD simulations, principal components analysis, radius of gyration, and solvent-accessible surface area helped improve our understanding of the peramivir resistance effect of R292K mutation. The highly flexible RMSD and RMSF of peramivir in the mutant complex indicated decreased peramivir binding affinity due R292K mutation when compared to the wildtype. The larger radius of gyration resulted in reduced interaction between neighboring amino acid residues, resulting in decreased receptor-ligand interactions, as well as an increase in water accessibility nearby the K292 amino acid and the carboxylate group of peramivir, which caused peramivir binding to become distorted.

According to these results, zanamivir and laninamivir with their hydrophilic bulky groups are likely to be potent neuraminidase inhibitors with their hydrophobic pentyl ether side chains. During this study it was shown that peramivir binding affinity is reduced by 17.28 kcal/mol due to the R292K mutation, which also alters the orientation of the ligand in the binding site and affects the overall optimal conformation of the protein-ligand complex. Furthermore, the R292K mutation altered the hydrogen bonding network between the mutant and peramivir.

In the second domain influenza H7N9 containing E119V substitution was studied for its intermolecular mechanism and dynamics against peramivir. We performed post-molecular dynamic simulations to offer multi-directional understandings into the susceptibility of peramivir to the E119V mutant. Based on analyses of total binding energy, principal components analysis, root-mean-square deviation, root-mean-square fluctuations, radius of gyration, and hydrogen bond formation, the peramivir-E119V mutant complex demonstrated relative stability. By substituting the amino acid 119V, peramivir's binding free energy (ΔG_{bind}) increased by -9.46 ± 0.02 kcal/mol. As such, the binding free energy of the peramivir-wildtype complex increased from -49.09 ± 0.13 360 kcal/mol to -58.55 ± 0.15 kcal/mol and an increase in the hydrogen bond occupancy in the peramivir-mutant was noted. These factors may account for the consistently higher stability of the E119V mutant complex as indicated by different post-molecular dynamic simulations analysis. The findings of this study will assist in the development of new anti-influenza drugs and the control of the avian influenza H7N9 virus.

An *in silico*-based drug repurposing method was used to repurpose FDA-approved drugs as potential therapies against the H7N9 virus. A total of 2,568 drugs were virtually screened in order to find potential inhibitors. We observed that some compounds occupied the active site of NA with an even stronger affinity than peramivir. Lurasidone and promacta had higher binding affinity than the standard drug peramivir (-49.09 kcal/mol), with ΔG_{bind} values of -54.1 kcal/mol and -56.20 kcal/mol, respectively, according to the MM-GBSA calculations. The MD simulation studies revealed that the backbone of C-α atoms in tucatinib and promacta NA complexes is stable throughout the simulation period and does not fluctuate significantly. According to ADME analysis, the hit compounds have a high GI and lack properties that would allow them to overcome the BBB. *In silico* toxicity prediction revealed that all compounds were not mutagenic or cytotoxic. Additionally, promacta is not cardiotoxic, whereas lurasidone and tucatinib have only weak inhibitory effects. Promacta and tucatinib may be used as lead compounds in the fight against the H7N9 influenza virus.

The study provided valuable insight into the structural and conformational molecular outlooks that could be potentially applied when designing and developing new drugs to treat avian influenza H7N9 infections. We suggest the use of quantum-mechanical (QM) methods such as density functional theory (DFT) and hybrid quantum mechanics/molecular mechanics (QM/MM) in studying the effect of mutation on neuraminidase inhibitors. We also recommend the exploration of multi-target drug approach for effective design and development of neuraminidase inhibitors.

7.2 REFERENCES

1. Paget, J.; Spreeuwenberg, P.; Charu, V.; Taylor, R.J.; Iuliano, A.D.; Bresee, J.; Simonsen, L.; Viboud, C. Global mortality associated with seasonal influenza epidemics: New burden estimates and predictors from the GLaMOR Project. *J. Glob. Health* **2019**, *9*, 1–12, doi:10.7189/jogh.09.020421.

2. Das, K. Antivirals targeting influenza A virus. *J. Med. Chem.* **2012**, *55*, 6263–6277, doi:10.1021/JM300455C.

3. Hampson, A.W.; Mackenzie, J.S. The influenza viruses. *Med. J. Aust.* **2006**, *185*, doi:10.5694/J.1326-5377.2006.TB00705.X.

4. Bai, Y.; Jones, J.C.; Wong, S.-S.; Zanin, M.; Russell, C.J.; Govorkova, E.A.; Org, J.J. Antivirals Targeting the Surface Glycoproteins of Influenza Virus: Mechanisms of Action and Resistance. *Viruses 2021, Vol. 13, Page 624* **2021**, *13*, 624, doi:10.3390/V13040624.

5. Kim, H.; Webster, R.G.; Webby, R.J. Influenza Virus: Dealing with a Drifting and Shifting Pathogen. *Viral Immunol.* **2018**, *31*, 174–183, doi:10.1089/VIM.2017.0141.

6. Lowen, A.C. Constraints, Drivers, and Implications of Influenza A Virus Reassortment. *Annu. Rev. Virol.* **2017**, *4*, 105–121, doi:10.1146/ANNUREV-VIROLOGY-101416-041726.

7. Proença-Módena, J.L.; Macedo, I.S.; Arruda, E. H5N1 avian influenza virus: an overview. *Brazilian J. Infect. Dis.* **2007**, *11*, 125–133, doi:10.1590/S1413-86702007000100027.

8. Li, Y.T.; Linster, M.; Mendenhall, I.H.; Su, Y.C.F.; Smith, G.J.D. Avian influenza viruses in humans: lessons from past outbreaks. *Br. Med. Bull.* **2019**, *132*, 81, doi:10.1093/BMB/LDZ036.

9. Bai, T.; Zhou, J.; Shu, Y. Serologic study for influenza A (H7N9) among high-risk groups in China. *N. Engl. J. Med.* **2013**, *368*, 2339–2340, doi:10.1056/NEJMC1305865.

10. Zhou, J.; Wang, D.; Gao, R.; Zhao, B.; Song, J.; Qi, X.; Zhang, Y.; Shi, Y.; Yang, L.; Zhu, W.; et al. Biological features of novel avian influenza A (H7N9) virus. *Nature* **2013**, *499*, 500–503, doi:10.1038/nature12379.

11. Liu, W.J.; Xiao, H.; Dai, L.; Liu, D.; Chen, J.; Qi, X.; Bi, Y.; Shi, Y.; Gao, G.F.; Liu, Y. Avian influenza A (H7N9) virus: from low pathogenic to highly pathogenic. *Front. Med. 2021 154* **2021**, *15*, 507–527, doi:10.1007/S11684-020-0814-5.

12. Wang, W.; Chen, X.; Wang, Y.; Lai, S.; Yang, J.; Cowling, B.J.; Horby, P.W.; Uyeki, T.M.; Yu, H. Serological Evidence of Human Infection With Avian Influenza A(H7N9) Virus: A Systematic Review and Meta-analysis. *J. Infect. Dis.* **2022**, *226*, 70–82, doi:10.1093/INFDIS/JIAA679.